Acta morphologica et anthropologica 24 (1–2)

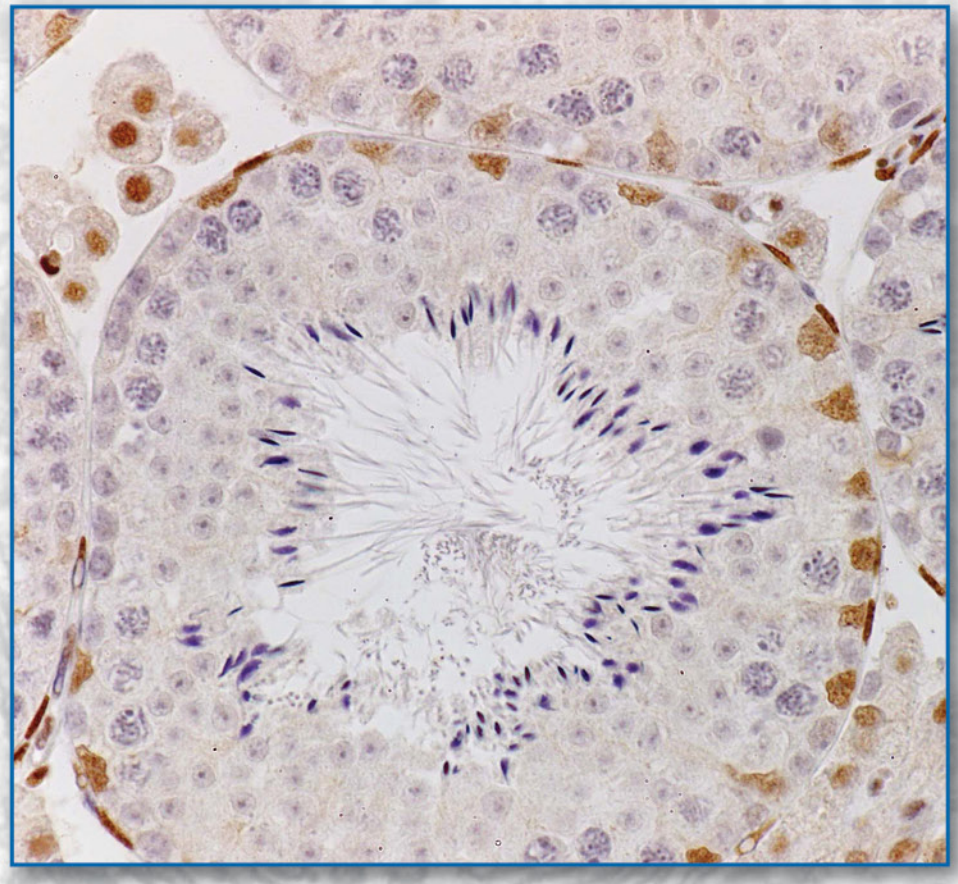

Prof. Marin Drinov Publishing House
of Bulgarian Academy of Sciences

Acta morphologica et anthropologica

is the continuation of
Acta cytobiologica et morphologica

Editorial Correspondence
Institute of Experimental Morphology, Pathology and Anthropology with Museum
Bulgarian Academy of Sciences
Acta Morphologica et Anthropologica
Acad. Georgi Bonchev Str., Bl. 25
1113 Sofia
Bulgaria
e-mail: iempam@bas.bg
Tel.: +359 2 979 2311

Prof. Marin Drinov Academic Publishing House
Bulgaria, 1113 Sofia, Acad. Georgi Bonchev Str., Bl. 6

Графичен дизайнер Даниела Мицева
Формат 70×100/16 печ. коли 6

Печатница на Издателство на БАН „Проф. Марин Дринов“
1113 София, ул. „Акад. Георги Бончев“, бл. 5

ISSN 1311-8773 (print)
ISSN 2535-0811 (online)

Acta morphologica et anthropologica 24

24 (1-2) ● Sofia ● 2017
Institute of Experimental Morphology, Pathology and Anthropology with Museum
Bulgarian Anatomical Society

Contents

Institute of Experimental Morphology, Pathology and Anthropology with Museum
Bulgarian Anatomical Society

Acta morphologica et anthropologica, 24 (1-2)
Sofia ● 2017

Morphology

Morphological Disorder Progression in Rat High-Fat, High-Carbohydrate Diet Induced Metabolic Syndrome

Petar Hrischev[1], *Pepa Atanassova*[2], *Nadya Penkova*[2*], *Gorana Rancic*[3], *Penka Angelova*[1], *Katya Georgieva*[1]

[1]*Department of Physiology, Medical University – Plovdiv, Bulgaria*
[2]*Department of Anatomy, Histology and Embryology, Medical University – Plovdiv, Bulgaria*
[3]*Department of Histology, Medical Faculty - Nis, Serbia*

* Corresponding author: e-mail: nadja_penkova@abv.bg

High-fat-carbohydrate intake correlates with the epidemic rise in obesity and metabolic syndrome and related diseases. The aim of our work was to study the liver and mesenteric adipose tissue in rats with metabolic syndrome induced by high-fat-high-carbohydrate diet (HFHCD). Wistar rats (n = 10) were fed with HFHCD for 16 weeks. Control rats (n = 10) were on a normal diet. Metabolic control was determined by measuring BMI, adiposity, plasma parameter. Histopathological study was performed on the mesenteric adipose tissue and liver using PAS-reaction and Sudan-III-staining. Results: HFHCD increased body weight, BMI, adiposity, decreased HDL-cholesterol. Mesenteric adipose tissue was with larger adipocytes, liver steatosis and an increase in glycogen storage was also observed in the HFHCD group. In conclusion, nutritional stress caused by HFHCD promotes oxidative stress as evident by increased lipid peroxidation products and de novo lipogenesis which contributed to fat accumulation in the adipose tissue and the liver and to the development of non-alcoholic liver disorders.

Key words: metabolic syndrome, male rats, hepatic steatosis

Introduction

Obesity is a major health problem in the world. It is associated with the risk of cardiovascular disease, cancers, hyperlipidemia, and liver steatosis development [4]. Obesity constitutes a risk factor for contributing to the development of type 2 diabetes [11]. Sprague-Dawley rats were fed a high fat and high cholesterol diet demonstrated diet-induced non-alcoholic fatty liver disease [3]. High fat diet increases body and liver

weight, fasting blood glucose, serum aminotransferase (ALT) and lipid accumulation in the liver [3]. High fat diet administered to Prague hereditary hypertriglyceridemic (HTG) rats can induce signs of metabolic syndrome [5]. The increased consumption of high-fructose corn syrup may contribute to the worldwide epidemic of fatty liver [9]. High fats and sugars rich diets also induce obesity and other metabolic disorders. They lead the body to a pro-inflammatory pattern, which may affect the proper functioning of many tissues, including adipose tissue and liver. During the expansion of adipose tissue, a number of functions such as activation and release of cytokines and hormones may be affected [10]. After eight weeks high fat, high carbohydrates diet, body weights increased 2.4-fold, hepatic-triglyceride content increased progressively [1]. Most of the experimental animal models use male rats for studying these processes. Few of them use female rats [2]. Relatively little is known about gender-dependent susceptibility to obesity and hepatic injury induced by nutritional factors. Such is the work of Pektas et al. (2017) who investigated dietary fructose-induced hepatic degeneration in male and female rats [8]. Dietary fructose activates both insulin signaling and inflammatory pathway in the adipose tissues of male and female rats proposing no correlation between the tissue insulin signaling and inflammation [7].

The aim of our study was to detect morphological changes in the liver and adipose tissue of male and female rats with diet induced metabolic syndrome with high-fat, high-carbohydrate diet.

Materials and Methods

Male and female Wistar rats (n = 10) were fed with high-fat, high-carbohydrate diet (HFHCD) for 16 weeks. Control male and female rats (n = 10) were fed a normal diet for the same period of time. Metabolic control was determined by measuring body weight, BMI, adiposity, plasma biochemical parameter - total cholesterol, HDL and LDL cholesterol. Two-way ANOVA statistic analysis was used. Sections of the liver lobe and visceral mesenteric adipose tissue were fixed in 10% buffered formalin. Histopathological study was performed on the visceral mesenteric adipose tissue and liver (glycogen and lipid content) using routine staining with hematoxylin-eosin and histochemical PAS reaction and Sudan III staining.

Results

The obtained results show that dietary manipulated rats (male and female) began to increase their weight of the 11th week onwards, which was maintained until the end of the experiment (**Fig. 1**). Male and female dietary-manipulated rats had a higher weight at the end of the experiment (**Fig. 2**).

At the end of the experiment dietary-manipulated rats had a higher BMI as compared to the control rats (0.69 ± 0.02 g/cm^2 vs 0.63 ± 0.02 g/cm^2, $p < 0.01$). At the end of the experiment the diet had significant main effect on the total cholesterol plasma level, as it was significantly higher in dietary-manipulated rats compared to the controls (2.00 ± 0.09 mmol/l vs 1.67 ± 0.10 mmol/l, $p < 0.05$). The rats from the dietary-manipulated groups had lower concentrations of HDL-cholesterol compared to the control groups (1.11 ± 0.05 mmol/l vs 1.31 ± 0.05 mmol/l, $p = 0.01$).

No gender differences were noticed in the morphology of the liver of the dietary-manipulated rats. HFHCD leads to accumulation of a lot of lipid cytoplasmic inclusions in the hepatocytes of the experimental rats. These extensive lesions in the liver showed

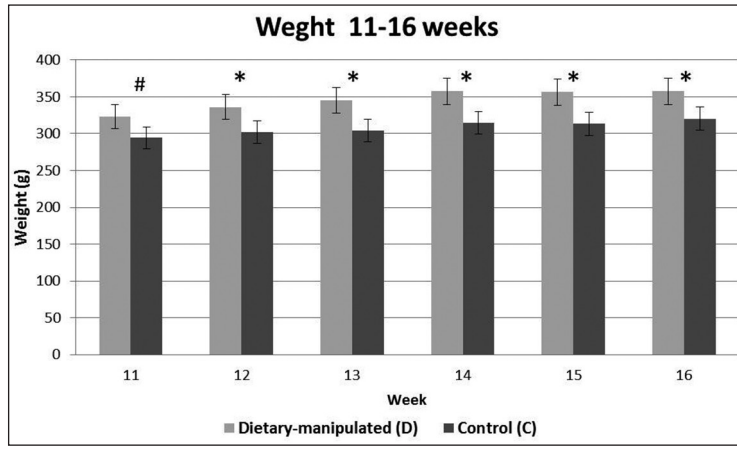

Fig. 1. Weight (g) of dietary-manipulated and control groups from the 11th week until the end of the experiment #P = 0.078, *p < 0.05 dietary-manipulated vs controls

Group	Weight (g) 16th week
Male control group	371.50 ± 54.01
HFHCD male rats	394.50 ± 42.81
Female control group	269.33 ± 31.61
HFHCD female rats	320.17 ± 37.95

Fig. 2. Weight (g) of male and female rats: control and dietary-manipulated groups at the end of the experiment (16th week)

advanced lipodystrophy. Steatosis changes were observed in two areas - the periphery of the liver lobules and around the central vein (**Fig. 3A**). In the cytoplasm of the cells of these areas liposomes of various sizes were observed (**Fig. 3B**). Other cells had more severe dystrophic damage - microvesicles around the nucleus and large vacuoles in the periphery of the cytoplasm. There were also hepatocytes with irreversible lesions - presence of lipid cysts formed after rupture of the cell membrane and extracellular lipid droplets (**Fig. 3C**). Lipid inclusions stained with Sudan III were not observed in the hepatocytes of the control group (**Fig. 3D**).

Increased carbohydrate intake in the experimental group rats leads to the accumulation of glycogen inclusions in the liver hepatocytes. PAS-reaction was positive – a large number of cells equally scattered in the liver (**Fig. 4A**). Glycogen granules were accumulated to a greater degree in the hepatocytes, which do not have lipid inclusions (**Fig. 4B**). Cysts of extracted lipid droplets were seen (**Fig. 4C**). Hepatocytes of the control rats had a moderate amount of glycogen granules equally distributed in the cytoplasm of cells (**Fig. 4D**).

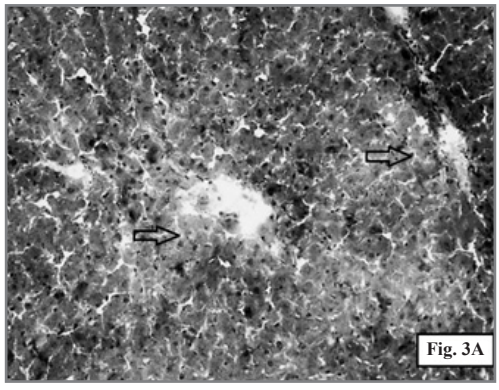

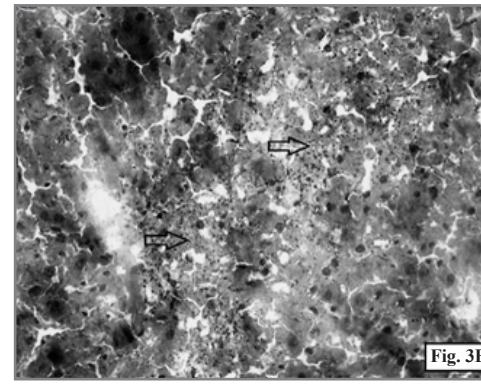

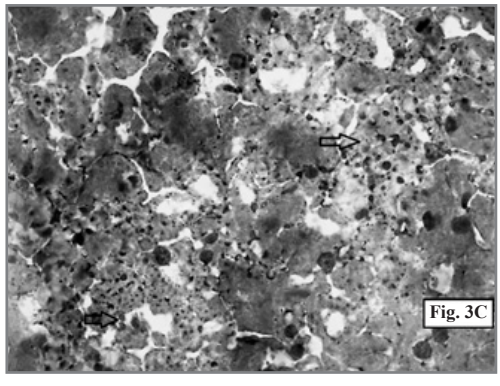

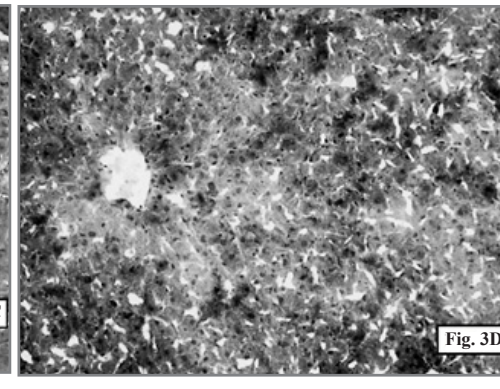

Fig. 3. A. HFHCD male rats' liver. Hepatic lobules with dystrophic processes around the central vein and periportal areas. Sudan III stainingp × 100; **B.** HFHCD male rats' liver. Wide area of hepatocytes with presence of large numbers of lipid droplets. Sudan III staining, × 200; **C.** HFHCD female rats' liver. Rounded hepatocytes with various degrees of lipodystrophy: lipid microvesicles, lipid vacuoles and lipid cysts. Presence of lipid droplets in extracellular space. Sudan III staining, × 400; **D.** Liver of the control group. Liver lobules with normal structure. Without lipid inclusions in the hepatocytes. Sudan III staining. × 100

No gender differences were noticed in the morphology of the adipose tissue of the dietary-manipulated rats. HFHCD leads to accumulation of extreme level of lipid inclusions in the cells of the adipose tissue of the experimental group rats compared to the controls. This was particularly expressed in the visceral mesenteric adipose tissue (**Fig. 5A**). Adipocytes were enlarged, as a result of the large lipid droplets, which occupied the whole cytoplasm. These drops pushed the nuclei into the periphery of the cells. The amount of the lipid drops in the adipose tissue of the controls is smaller compared to the dietary-manipulated rats (**Fig. 5B**).

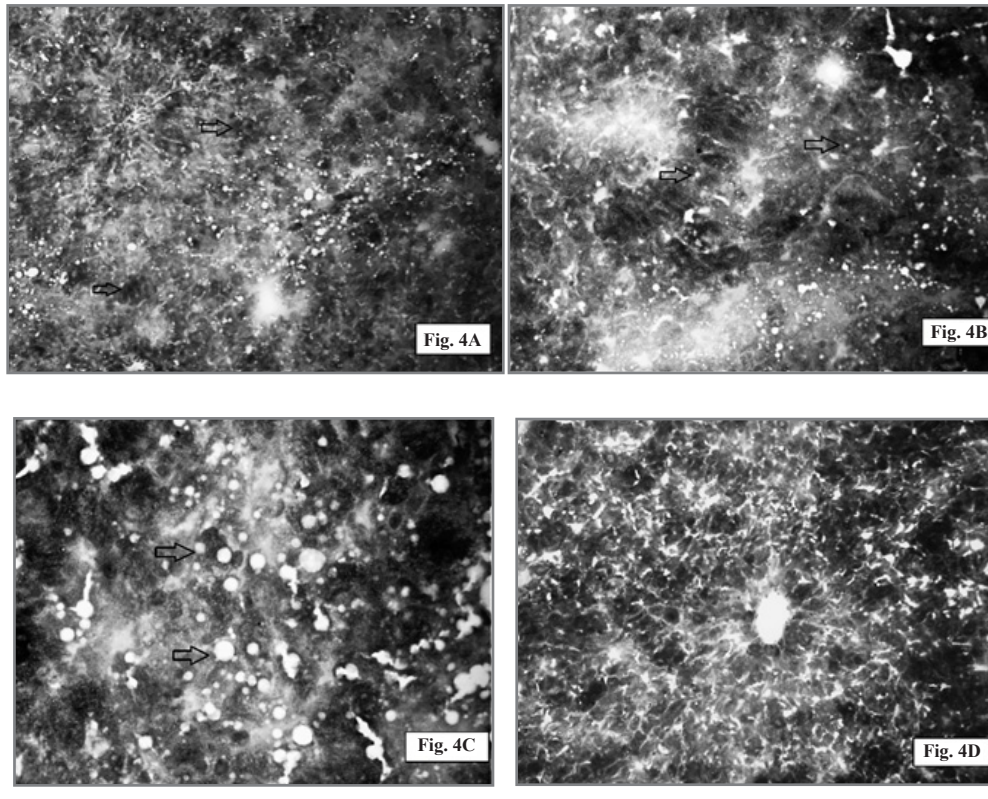

Fig. 4. A. Liver of HFHCD male rats. Drags of hepatocytes with raspberry-red glycogen granules in the cytoplasm. PAS–reaction, ×100; **B.** Liver of HFHCD male rats. Glycogen granules in hepatocytes without lipid inclusions. PAS–reaction, ×200; **C.** Liver of HFHCD female rats. Area a heavy dystrophy. Hepatocytes with glycogen and lipid inclusions, visualized by empty vesicles and vacuoles. PAS-reaction, × 400; **D.** Liver of control group. Hepatocytes with a uniform accumulation of glycogen granules in the cytoplasm. PAS-reaction, ×100

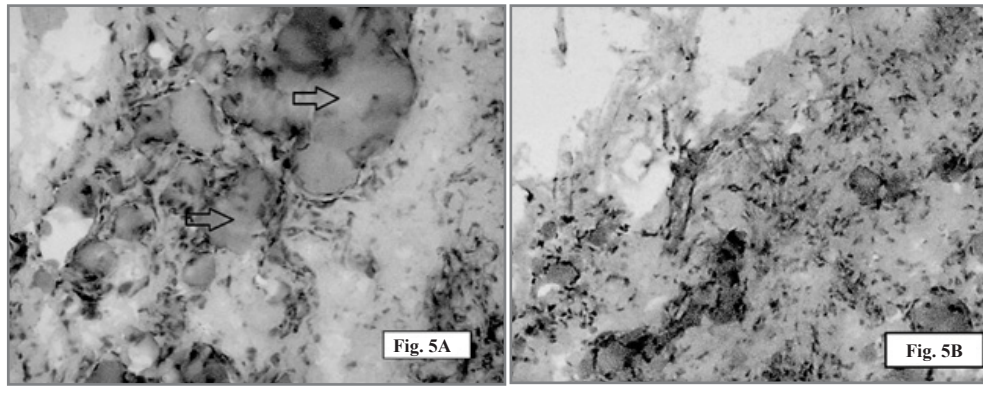

Fig. 5. A. HFHCD female rats' visceral mesenteric adipose tissue. Sudan III staining, × 400; **B.** Control group. Visceral mesenteric adipose tissue. Sudan III staining, × 100

Discussion

We found that HFHC diet consumption resulted in obesity development in both male and female rats. It is responsible for increased body weight, adiposity and liver steatosis. Increased body weight was accompanied by increased lipid plasma levels. We observed increased lipid deposition in the adipose tissue in both male and female HFHC diet fed rats. Lipid deposition was also seen in the liver of the same groups. Obesity increases the risk for non-alcoholic fatty liver disease through adipokine dysregulation and inflammation [2]. Our results were concomitant to a certain extent with other authors' data, regarding the effect of high-fructose diet [9], high-fat diet [5] or high-fat, high-carbohydrates diet [1] in rats. The increased consumption of high-fructose corn syrup increased triglyceride content and caused mild microvesicular steatosis in liver of male rats [9]. An increase in body and liver weight, fasting blood glucose, fasting insulin, serum aminotransferase (ALT) as well as lipid accumulation in the liver were documented in Sprague-Dawley rats fed with a high-fat and high-cholesterol diet [3]. Some of the works report that eight weeks of high fat, high carbohydrates diet caused 2.4-fold increase in body weights as well as hepatic-triglyceride content increased progressively and is enough for reaching obesity [1]. We think that a longer period of HFHC diet is more appropriate for this purpose, especially for the liver lipid dystrophy. Long-term fructose diet caused pronounced increase in body weight of males, but not of female rats [6]. Pektas et al. (2017) proved that long-term fructose diet caused parenchymal degeneration and hyperemia in liver of male and female rats and also led to increase in hepatic triglyceride content [8]. Some gender differences were found concerning body weight and plasma lipid levels. High-fructose diet increased plasma insulin, triglyceride and VLDL levels as well as omental weights in both genders [6]. But in another study, no gender-related differences, as a consequence of fructose consumption, were found by Pektas et al. (2017) [8]. In our study we also did not observed any gender-related differences in liver and adipose tissue disorders about the effects of HFHC diet in female and male rats.

Conclusion

We proved that diet rich in fats and carbohydrates is strongly associated with the development of obesity in male and female Wistar rats. It is also associated with liver steatosis. Intake of HFHCD establish the Wistar rats as an excellent experimental model for the study of metabolic and hepatic abnormalities resulting from obesity.

Acknowledgements: This study was financed by Medical University of Plovdiv - project SDP 09/2015.

References

1. **Alwahsh, S. M., B. J. Dwyer, S. Forbes, D. H. Thiel, P. J. Lewis, G. Ramadori.** Insulin Production and Resistance in Different Models of Diet-Induced Obesity and Metabolic Syndrome. – *Int. J. Mol. Sci*., **18**, 2017, 285.
2. **Bell, A., S. Korourian, H. Zeng, J. Phelps, R. Hakkak.** A diet containing a high- versus low-daidzein level does not protect against liver steatosis in the obese Zucker rat model. – *Food Funct*., **8**, 2017, 1293-1298.

3. **Gao, H, Z. Zeng, H. Zhang, X. Zhou, L. Guan, W. Deng, L. Xu.** The Glucagon-Like Peptide-1 Analogue Liraglutide Inhibits Oxidative Stress and Inflammatory Response in the Liver of Rats with Diet-Induced Non-alcoholic Fatty Liver Disease. – *Biol. Pharm. Bull*., **38**, 2015,694-702.
4. **Hakkak, R., A. Bell, S. Korourian.**Dehydroepiandrosterone (DHEA) Feeding Protects Liver Steatosis in Obese Breast Cancer Rat Model. – *Sci Pharm*., **85,** 2017; 13.
5. **Kaprinay, B., B. Lipták, L. Slovák, K. Švík, V. Knezl, R. Sotníková, Z. Gáspárová**. Hypertriglyceridemic rats fed high fat diet as a model of metabolic syndrome. – *Physiol. Res*., **65**, 2016, 515-518.
6. **Pektaş, M. B., G. Sadi, F. Akar.** Long-Term Dietary Fructose Causes Gender-Different Metabolic and Vascular Dysfunction in Rats: Modulatory Effects of Resveratrol. – *Cell Physiol. Biochem.*, **37**, 2015, 1407-20.
7. **Pektas, MB, HB Koca, G Sadi, F Akar.** Dietary Fructose Activates Insulin Signaling and Inflammation in Adipose Tissue: Modulatory Role of Resveratrol. – *Biomed. Res. Int*., **2016**, 2016, 8014252.
8. **Pektas, M. B., G. Yücel, H. B. Koca, G. Sadi, O. G Yıldırım, G. Öztürk, F. Akar.** Dietary Fructose-Induced Hepatic Injury in Male and Female Rats: Influence of Resveratrol. – *Drug Res.* (Stuttg)., **67**, 2017, 103-110.
9. **Sadi, G., V. Ergin, G. Yilmaz, M. B. Pektas, O. G. Yildirim, A. Menevse, F. Akar.** High-fructose corn syrup-induced hepatic dysfunction in rats: improving effect of resveratrol. – *Eur. J. Nutr*., **54**, 2015, 895-904.
10. **Ventura, L. L., N. C. Fortes, H. C. Santiago, M. V. Caliari, M. A. Gomes, D. R. Oliveira.** Obesity-induced diet leads to weight gain, systemic metabolic alterations, adipose tissue inflammation, hepatic steatosis, and oxidative stress in gerbils (Merionesunguiculatus). – *Peer J*., **5**, 2017, 2967.
11. **Vinothiya, K., N. Ashokkumar.** Modulatory effect of vanillic acid on antioxidant status in high fat diet-induced changes in diabetic hypertensive rats. – *Biomed. Pharmacother.*, **87**, 2017, 640-652.

Institute of Experimental Morphology, Pathology and Anthropology with Museum
Bulgarian Anatomical Society

Acta morphologica et anthropologica, 24 (1-2)
Sofia ● 2017

The Astrocytic Environment Differs among the Divisions of the Rat Striatum

Nikola Tomov[1*], *Lachezar Surchev*[1,2]

[1]*Department of Anatomy, Faculty of Medicine, Trakia University, Stara Zagora, Bulgaria*
[2]*Department of Anatomy, Histology and Embryology, Medical University of Sofia, Bulgaria*

[*]Corresponding author. e-mail: tomovmd@gmail.com

The current concept of the structure of the striatum is that it consists of a dorsolateral, sensorimotor, and a ventromedial, limbic part. This division is backed up by studies of the neuronal population of the striatum. In this investigation we aim to elucidate the morphological basis of the different striatal areas by studying their glial environment. For this purpose, we employed immunohistochemistry for GFAP for visualization of astrocytes, followed by image analysis for quantitative assessment of astroglia in different areas of the striatum. Our results show that the astroglial parameters in the dorsolateral division of the striatum are considerably greater than in the ventromedial one. This peculiarity of the glial environment hints towards the notion that astroglia is differentially regulated according to local characteristics of synaptic activity and density in different divisions of the striatum.

Key words: striatum, astrocytes, astroglia, GFAP

Introduction

The striatum of the rat is a relatively large structure, which occupies much of the volume of the telencephalic hemispheres [9]. It has been subdivided into a dorsal (or dorsolateral) and ventral (or ventromedial) portion. The dorsal part is usually accepted to include the caudate-putamen complex, while the ventral part is associated with the nucleus accumbens and the olfactory tubercle [12]. However, no sharp boundary between the two divisions exists, neither histologically nor immunohistochemically [10].

The main cellular population of the striatum are the medium spiny neurons, which, through their intricate dendritic tree, are the target of extrinsic afferents [2]. The source of these afferents might be regarded as the most reliable criterion for dividing the striatum. Projections from the cortex, amygdala and thalamus reach the neurons in different parts of the striatum [4, 5, 11]. Thus, the dorsolateral part of striatum is integrated in the sensorimotor circuitry, the ventromedial is visceral-related, and areas lying between these extremes receive associational information [10].

Despite the knowledge about the neuronal connections of the divisions of the striatum, little has been described about their glial environment. It is well known that as-

troglial cells are intimately associated with synapses. They are stimulated by increased synaptic activity, and can regulate synaptic transmission themselves [3, 8]. Therefore, information about the astroglia of the striatum can shed light on some functional aspects of this brain structure, and the regulation of the activity in its divisions.

Aim

In the present study we aim to investigate the astrocytic population of the rat striatum, comparing the dorsal and the ventral part, by means of a quantitative assessment of an immunohistochemical staining.

Materials and Methods

We used 9 adult male Sprague-Dawley rats, kept in cages under standard conditions, with free access to food and water. After terminal anaesthesia with ketamine and xylazine, the animals were fixed to a styrofoam board and perfused transcardially with 300 ml ice-cold 4% solution of paraformaldehyde in phosphate-buffered saline. Following perfusion, brains were removed and postfixed in the same fixative overnight. Upon cryoprotection in 20% sucrose the brains were sectioned in 40 μm sections on a freezing microtome and processed for immunohistochemistry.

The resulting free-floating sectioned were incubated for 30 min in a solution containing 3% H_2O_2 for quenching the endogenous peroxidase activity. Blocking of the non-specific immunoreactivity was obtained with incubation in 3% bovine serum albumin with addition of 0,3% Triton X-100. Antibody against GFAP (rabbit; Abcam, ab7779) was used as a primary antibody in a 1:800 dilution. The sections were incubated with the primary antibody for 12 h. After washing, the sections were incubated with the secondary antibody (anti-rabbit biotinilated IgG; Dako, E0432) for 2 h. Vectastain ABC HRP Kit was used per manufacturer's directions and 3,3-diaminobenzidyne was employed as a chromogen for visualization of the reaction. The free-floating sections were mounted on glass slides, air-dried, dehydrated and coverslipped. In order to evaluate the specificity of the immunohistochemical reaction, sections were processed in control experiments in which the primary antibody was omitted, the secondary antibody was omitted, the ABC-reagent was omitted, or non-immune antiserum was used in place of the anti-GFAP antiserum.

Digital images were obtained using a Leica DM1000 microscope coupled with a standard camera. Care was taken that light conditions and exposure time did not vary between frames. The obtained images were analyzed using the software package ImageJ (NIH, USA). For the analysis only zones, clearly belonging to either the dorsal or the ventral division of the striatum were used; zones from intermediate areas were avoided. Cell density was determined by manually counting cell bodies in a given zone. Immunopositive area was calculated as a percentage of pixels of all pixels in the same zone. Pixels were considered immunopositive when they had gray values above a threshold obtained according to the algorithm of Otsu [7]. Statistical analysis was performed using GraphPad Prism 9. Student's t-test was applied, $p<0.05$ was considered statistically significant.

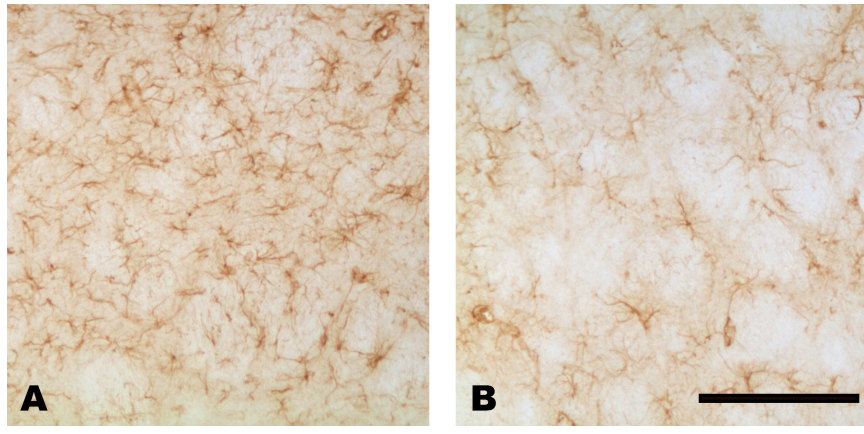

Fig. 1. Representative images of GFAP-stained astrocytes of the dorsal (A) and ventral (B) striatum. Scale bar = 100 μm

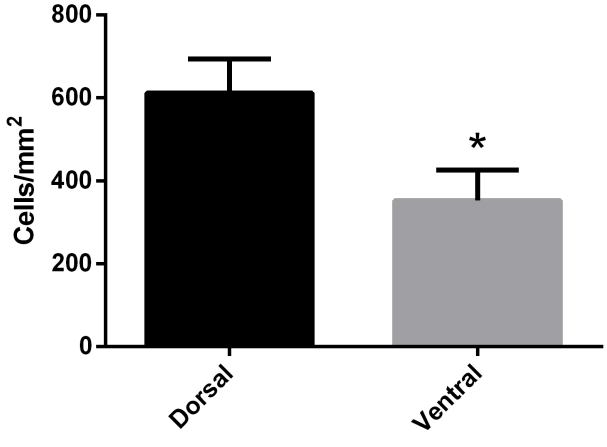

Fig. 2. Comparison between the density of GFAP+ cells per mm^2 area in the dorsal and ventral striatum. Data represents average values ±SD. Student's t-test. Asterisk indicates $p < 0.05$

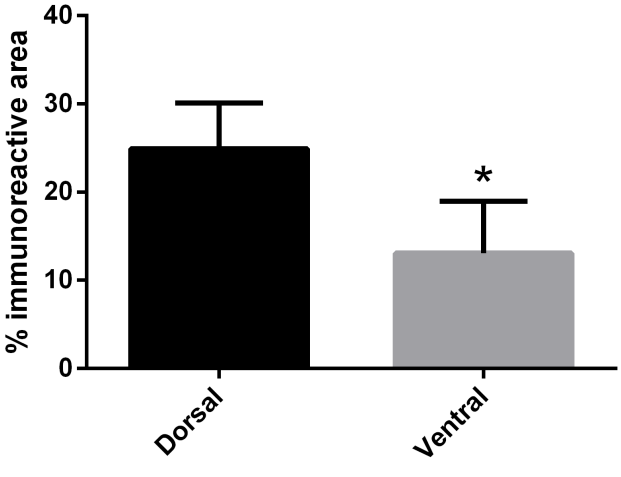

Fig. 3. Comparison between GFAP-immunopositive area in the dorsal and ventral striatum. Data represents average values ±SD. Student's t-test. Asterisk indicates $p < 0.05$

Results

Astrocytes were visualized throughout the striatum. They were seen extending their processes in all directions, covering a territorial domain in the gray matter. In some areas, processes of neighboring cells were seen overlapping and crossing, but no cellular clustering could be demonstrated. Some astrocytes wrapped their bodies and processes around the fibers of the internal capsule. GFAP+ elements were seen wrapping around blood vessels of different caliber, running in different directions in all parts of the striatum.

A clear-cut boundry between any of the divisions of the striatum could not be established. However, a gradient of the amount of stained elements was evident. The zones in the most dorsal part of the striatum, immediately below corpus callosum, showed a dense cell population (Fig. 1A). Contrary, astrocytes in the most ventral parts were scarce and divided by large zones of immunonegative tissue (Fig. 1B).

The quantitative assessment confirmed this finding. The dorsal division of the striatum contained significantly more cells (Fig. 2), and the immunoreactive area was larger, compared to the ventral division (Fig 3).

Discussion

Our findings generally confirm the notion, that the striatum is a structure relatively scarcely populated by astrocytes [6]. When stained for GFAP, the striatum looks relatively pale compared to the neighboring structures. This can be partially explained by the fact, that despite the numerous neuronal population, the synaptic density is not as great, or at least nor all synapses are active at the same time [6]

The astrocytes are not uniformly distributed in all parts of the striatum. Despite this, no unambiguous delineation between dorsal and ventral striatum can be made solely by their distribution. It is clear however, that different divisions of the striatum posses different astrocytic populations. This can be interpreted in the context of neuron-glia interaction. Astrocyte-rich environment could correlate with greater synaptic activity [3]. Therefore, this study presents an indirect evidence for differences in synaptic density and/or activity in different parts of the striatum.

Moreover, the possible differences of the capacity for glial scarring should be taken into account. It is widely known that injection of substances/cells in the striatum may produce different results, depending on the exact coordinates used [1]. The extent of astrocytic activation in such experimental models should be considered.

Conclusion

The rat striatum is a heterogeneous structure, despite the very subtle histological differences. Astrocytes are not uniformly distributed in the tissue of the different divisions of the striatum. This could have functional implications, considering neuron-glia interactions.

References

1. **Deumens, R., A. Blokland, J. Prickaerts.** Modeling Parkinson's disease in rats: an evaluation of 6-OHDA lesions of the nigrostriatal pathway. – *Exp. Neurol*., **175**(2), 2002, 303-317.
2. **Gerfen, C. R**. The neostriatal mosaic: multiple levels of compartmental organization. – *Trends Neurosci*., **15**(4), 1992, 133-139.
3. **Hirrlinger, J., S. Hülsmann, F. Kirchhoff.** Astroglial processes show spontaneous motility at active synaptic terminals in situ. – *Eur. J. Neurosci*., 2004, **20**, 2235-2239.
4. **McGeorge, A. J., R. M. Faull.** The organization of the projection from the cerebral cortex to the striatum in the rat. – *Neuroscience*, **29**, 1989, 503-537.
5. **Namba, M.** Cytoarchitektonische Untersuchungen am Striatum. – *J. Brain Res*., **3**, 1957, 24-48.
6. **Oorschot, D.** Cell types in the different nuclei of the basal ganglia. – In: *Handbook of Basal Ganglia Structure and Function* (Ed. H.Steiner and K.Y. Tseng), Elsevier, San Diego, 2010, 99-117.
7. **Otsu, N.** A threshold selection method from gray-level histogram. – *IEEE Trans. Sys*., *Man., Cyber*., **9**(1), 1979, 62-66.
8. **Pankratov Y., U. Lalo, A. Verkhratsky, R. A. North.** Vesicular release of ATP at central synapses. – *Pflugers Arch*., **452**, 2006, 589-597.
9. **Paxinos. G., C. Watson.** *The Rat Brain in Stereotaxic Coordinates*. London: Academic Press Limited, 1997, 18.
10. **Voorn, P., L. J. M. J. Vanderschuren, H. J. Groenewegen, T. W. Robbins, C. M. A. Pennartz.** Putting a spin on the dorsal-ventral divide of the striatum. – *Trends Neurosci*., **27**, 2004, 468-474.
11. **Willuhn, I., W. Sun, H. Steiner**. Topography of cocaine-induced gene regulation in the rat striatum: relationship to cortical inputs and role of behavioural context. – *Eur. J. Neurosci*., **17**, 2003, 1053-1066.
12. **Zaborszky, L., G. F. Alheid, M. C. Beinfeld, L. E. Eiden, L. Heimer, M. Palkovits**. Cholecystokinin innervation of the ventral striatum: a morphological and radioimmunological study. – *Neuroscience*, **14**, 1985, 427-453.

Institute of Experimental Morphology, Pathology and Anthropology with Museum
Bulgarian Anatomical Society

Acta morphologica et anthropologica, 24 (1-2)
Sofia ● 2017

Punctate Staining as Indirect Evidence for Microglial Ramification

Nikola Tomov[1*], *Lachezar Surchev*[1,2]

[1]*Department of Anatomy, Faculty of Medicine, Trakia University, Stara Zagora, Bulgaria*
[2]*Department of Anatomy, Histology and Embryology, Medical University of Sofia, Sofia, Bulgaria*

[*]Corresponding author: e-mail: tomovmd@gmail.com

Microglia are finely ramified cells, uniformly distributed in the tissue of brain and spinal cord. Upon activation, they migrate towards the activating stimulus, dramatically changing their morphology. Their fine processes disappear, and the cells become ameboid. In the present study we demonstrate that in an immunohistochemical staining for microglia, the areas between activated cells become lighter, compared to the noticeable presence of immunoreactive puncta around quiescent cells. This can be interpreted as an evidence for the presence of extremely fine microglial processes around resting cells, which are lost following activation.

Key words: microglia, cell processes, activation, immunohistochemistry

Introduction

Microglia are a population of cells of mesodermal origin, distributed all over the central nervous system. They constitute the intrinsic defense system of the nervous tissue and can act as macrophages and antigen-presenting cells [1]. Through intricate ramifications, each of the microglial cells occupies its own territory [2]. In this territory, microglial cells actively interact with synapses depending on their activity [5].

Following trauma of the nervous tissue, microglial cells are among the first cells to react. They direct their processes towards the site of the lesion, and can actively move their cell body through the tissue. When microglial cells are phagocytic, they alter their morphology by becoming ameboid, rather than ramified [2].

Aim

The present study aims to illustrate the morphological transformation of activated microglia by demonstrating changes in the immediate vicinity of the cells. These changes can be indirectly related to the arborization of their processes.

Materials and Methods

We used male adult Sprague-Dawley rats, which were kept in cages under standard conditions. The animals were inhalatory anaesthetized with isoflurane and fixed to a stereotactic frame. Following a punctiform craniotomy using a high speed drill, a 26G steel cannula was lowered into the parietal cortex at the following coordinates, relative to bregma: AP: +0.2, L:-3.5 [3], retained for 5 minutes, and retracted. Extracranial soft tissues were sutured and the animals were left to recover. 7 days after surgery, following terminal anesthesia with ketamine and xylazine, the animals were perfused transcardially with 300 ml ice-cold 4% solution of paraformaldehyde in phosphate-buffered saline. Following perfusion, brains were removed and postfixed in the same fixative overnight. They were transferred to a 20% sucrose solution for cryoprotection and sectioned in 40 µm sections on a freezing microtome. The resulting free-floating sections were processed for immunohistochemistry following a standard protocol. Anti-Iba1 (rabbit; Wako, 019-19741) was used as a primary antibody in a 1:700 dilution. After overnight incubation and washing, the sections were incubated with the secondary antibody (anti-rabbit biotinilated IgG; Dako, E0432). Vectastain ABC HRP Kit was used per manufacturer's directions and 3,3-diaminobenzidyne was employed as a chromogen. The sections were then mounted on glass slides, air-dried, dehydrated and coverslipped.

For evaluation of the specificity of the immunohistochemical reaction, sections were processed in control experiments, in which the anti Iba1-antibody was omitted, the secondary antibody was omitted, the ABC reagent was omitted, or non-immune serum was used instead of anti-Iba1 antiserum.

Results

Immunoreactive microgliocytes with radiating processes were seen in all brain structures. Intermingled with them, immunoreactive puncta could also be observed, without being properly associated with individual cell bodies or processes (**Fig. 1**).

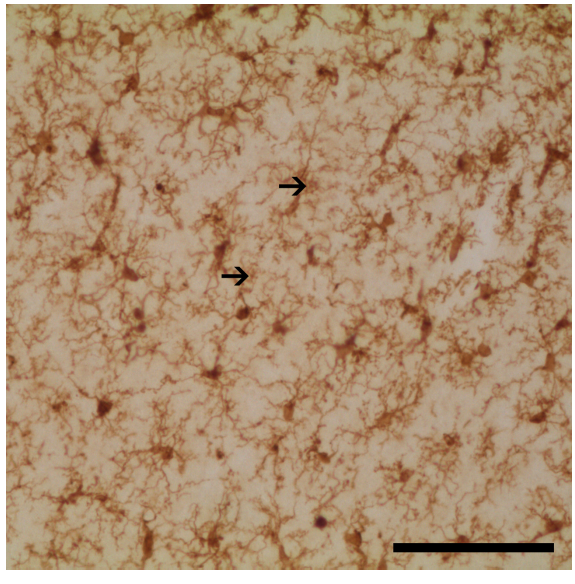

Fig. 1. Normal cortical Iba1+ microglia. Microgliocytes with typical radiating processes are evident. Arrows point to some of the existing immunoreactive puncta. Scale bar = 50 µm

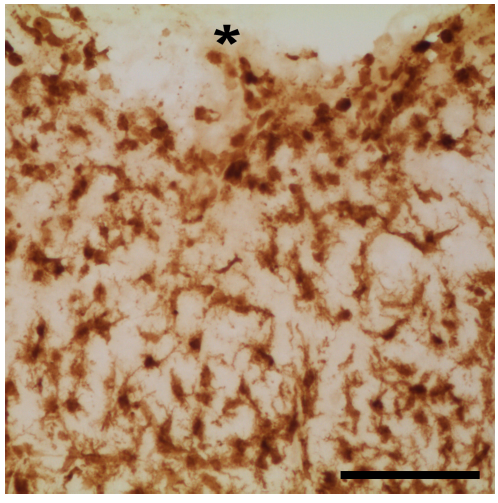

Fig. 2. Ameboid Iba1+ microglia adjacent to the cortical impact site (asterisk). Scale bar = 50 µm

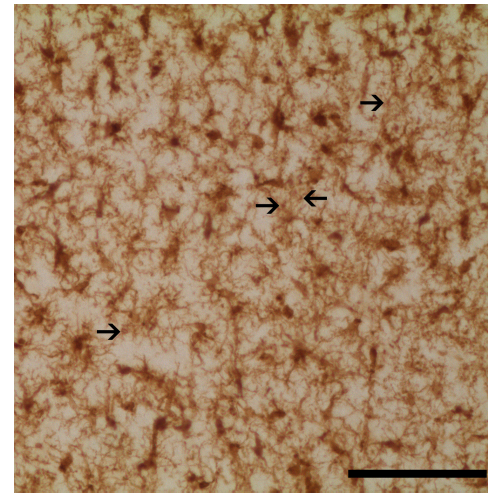

Fig. 3. Ramified Iba1+ microglia close to the cortical impact site. Note the intensive punctate background staining (arrows). Scale bar = 50 µm

The cortical impact site of the cannula on the brain surface was seen as a concavity, lined with microglia. The cannula tract itself was visualized as an intensively immunopositive band, crossing dorso-ventrally through the cortex at the coordinates used. The cannula tract was infiltrated with round and ameboid microglia, having a considerable density. In the proximity of the tissue defect ameboid microglial cells were almost exclusively present. Moving away from the site of mechanical influence, ameboid cells were gradually replaced with ramified ones.

Interestingly, the immediate vicinity of the ameboid cells adjacent to the cortical impact site, was almost not stained (**Fig. 2**). The cells were separated by zones without the characteristic immunoreactive puncta, seen between cells close to the impact site (**Fig. 3**) or in the normal cortical tissue, further away (**Fig. 1**).

Discussion

The present study is based on observations of immunoreactivity of microglia and their alterations following stimulation. Here we attempt for the first time to analyze the nature of the immunoreactive puncta, visible around microgliocytes. Furthermore, we demonstrate these details of the immunohistochemical staining for the first time using Iba1 as a microglial marker.

We interpret our observation of loss of immunoreactive puncta as an evidence for the existence of very fine, delicate ramifications of microglial cells. Despite the considerable thickness of the sections and the good quality of staining, those ramifications cannot be visualized, even under a high magnification. Those extremely thin ramifications can be considered the morphological basis of the extreme sensitivity of microglial cells in their territorial domains [2]. Even though a similar loss of immunoreactivity has been previously reported, a morphological explanation has not yet been provided [4]. Therefore, the present study seems to give new knowledge regarding visual interpretation of microglial immunoreactivity on histological slides.

Conclusion

Microglial cells, in their quiescent state, are extremely well ramified. Light microscopy, however, cannot demonstrate the finest arborizations of their processes. Despite this limitation, the loss of immunoreactive puncta following activation is an indirect sign for the presence of such arborizations.

References

1. **Ginhoux, F., M. Prinz**. Origin of microglia: current concepts and past controversies. – *Cold Spring Harb. Perspect. Biol*., **7**, 2015, a02053. doi: 10.1101/cshperspect.a020537.
2. **Nimmerjahn, A., F. Kirchhoff, F. Helmchen**. Resting microglial cells are highly dynamic surveillants of brain parenchyma in vivo. – *Science*, **308**, 2005, 1314-1318.
3. **Paxinos, G.**, **C. Watson**. *The Rat Brain in Stereotaxic Coordinates*. Academic Press Limited, London, 1997, 18.
4. **Schlichter, L. C., V. Kaushal, I. Moxon-Emre, V. Sivagnanam, C. Vincent**. The Ca2+ activated SK3 channel is expressed in microglia in the rat striatum and contributes to microglia-mediated neurotoxicity in vitro. – *J. Neuroinflammation*, **7**, 2010, 4. doi: 10.1186/1742-2094-7-4.
5. **Wake, H., A. J. Moorhouse, S. Jinno, S. Kohsaka, J. Nabekura**. Resting microglia directly monitor the functional state of synapses in vivo and determine the fate of ischemic terminals. – *J. Neurosci*., **29**, 2009, 3974-3980.

Institute of Experimental Morphology, Pathology and Anthropology with Museum
Bulgarian Anatomical Society

Acta morphologica et anthropologica, 24 (1-2)
Sofia ● 2017

A Comparative Analysis of Capillary Density in the Myocardium of Normotensive and Spontaneously Hypertensive Rats

Alexandar Iliev[1*], *Georgi Kotov*[1], *Boycho Landzhov*[1], *Lazar Jelev*[1], *Iva N. Dimitrova*[2], *Lina Malinova*[1], *Dimka Hinova-Palova*[1]

[1]*Department of Anatomy, Histology and Embryology, Medical University of Sofia, Bulgaria*
[2]*Department of Cardiology, University Hospital "St. Ekaterina", Medical University of Sofia, Bulgaria*

[*]Corresponding author: e-mail: dralexiliev@abv.bg

Changes in the vessels of the myocardium are of particular interest during its morphological development both under physiological conditions and conditions of hypertrophy. Measuring the morphometric parameter capillary density is a method for statistically significant assessment of capillary growth. The aim of the present study was to measure capillary density in the left and right ventricle of normotensive and spontaneously hypertensive rats and to conduct a comparative analysis of the received values between the two species of rats. A total of 15 male normotensive Wistar rats and 6 spontaneously hypertensive rats (SHR) were used for this study. Throughout the whole postnatal period capillary density decreased steadily and uniformly in both ventricles. The comparative analysis of corresponding age groups of Wistar rats and SHR revealed that changes occurred at a younger age in SHR. In conclusion, as age advanced, we established an inversely proportional correlation between cardiomyocytic hypertrophy and capillary density.

Key words: capillary density, myocardium, comparative analysis, rat

Introduction

Cardiac hypertrophy, regardless of the initiating event, is a structural consequence of one or more factors. These factors include the increase of the number and/or size of cardiomyocytes, the quantity of connective tissue elements and the blood vessel density, or a combination of some or all of the above-mentioned. Spontaneously hypertensive rats (SHR) represent an often analysed model of essential hypertension in humans, where the relation between hypertension and cardiac hypertrophy can be influenced and often interrupted [7, 22]. Changes in the vessels of the myocardium are of particular interest during its morphological development. These take place during the postnatal development of both normotensive and spontaneously hypertensive rats. Wearn [27], as well as Roberts and Wearn [21] were the first to show that increase in the weight of the myo-

cardium due to a higher workload leads to a significant decrease in capillary density. These and several later studies consider that capillary proliferation does not represent a primary response to hypertrophy by the myocardium [5, 9, 14, 19, 20]. Other studies state that the decrease in capillary density which takes place as hypertrophy develops is in fact reversed after the process of hypertrophy becomes more stable [24, 25].

There are three main morphometric markers for assessment of the capillary network, which are used to evaluate capillary proliferation under conditions of physiological and induced myocardial growth: the ratio between capillary and cardiomyocytic profiles [15, 16]; capillary density [1, 14, 26]; total length of the capillaries within the entire wall of the ventricle [1, 16]. Measuring capillary density is a method for statistically significant assessment of capillary growth. If this parameter increases together with myocardial growth, this is an unequivocal sign of capillary proliferation, since such change in the parameter can only result from addition of new capillary units per square millimetre of tissue. Cardiomyocytic hypertrophy leads to lateral displacement of the adjacent capillaries, which is also reflected in an increase in the surface area of the transverse section of the cardiac muscle cells [4]. Capillary proliferation in the myocardium of the left ventricle in SHR has been observed in a number of studies during different stages of the postnatal development both through quantitative and qualitative studies [12, 25].

The aim of the present study was to measure the morphometric parameter capillary density in the left and right ventricle of normotensive and spontaneously hypertensive rats and conduct a comparative analysis of the received values between the two species of rats.

Materials and Methods

In the present study, we used histological material from the hearts of male normotensive Wistar rats (WR) and SHR. The total number of WR was 15, divided into five age groups, each containing three animals: two-week-old; one-month-old; three-month-old; six-month-old; twelve-month-old. The SHR were distributed in two age groups, each containing three animals: one-month-old (young) and six-month-old (adult). The animals were anaesthetised with ether and cervical dislocation was performed. The hearts were removed from the chest cavity and were placed in physiological saline in order to rinse the blood in the cardiac cavities. After a short fixation in 10% neutral buffered formalin, a transverse incision was performed through the middle of the heart, a little below the level of the cardiac valves. The hearts were then placed again in 10% neutral buffered formalin for immersion fixation. Afterwards, they were fixed in paraffin blocks, from which we prepared 7 μm wide paraffin tissue slides, which were stained with haematoxylin and eosin.

The morphometric analysis was performed on five slides from the heart of each animal. Quantitative data were obtained with a computerised system for image analysis NIS-Elements Advanced Research (Ver. 2.30). The areas of interest in each slide were first found on low magnifications (×100, ×200), taking into account the respective age group. Afterwards, at magnification ×400 we marked a zone with surface area of 0.04 mm^2 (400 μm^2). The contours of the capillaries within the zone were outlined. In order to make a good comparison of the data, it was decided that the marked zone should include these capillaries which are adjacent, on the inside or outside, to two perpendicular contours and, respectively, should not include capillaries which are adjacent, on the inside or outside, to the other two borders. After outlining the borders, we automatically obtained the values of the morphometric parameter capillary density – calculated as number of capillaries per unit of surface area of the slide (number of capillaries/mm^2).

The obtained quantitative data were demonstrated with diagrams and were statistically evaluated through a Student's t test. Statistically significant differences were read in the case of $p < 0.05$. Microsoft Office Excel 2010 was used to process the data and to demonstrate the obtained results in an adequate way.

Results

The quantitative data, as well as the comparative analysis of the morphometric parameter capillary density in the free wall of the left and right ventricle during different periods of the postnatal development of normotensive Wistar rats and SHR were obtained through analyzing randomly selected areas of the myocardium without large or massive ruptures resulting from the processing of the material.

Throughout the whole postnatal period the values of the parameter capillary density decrease steadily and uniformly in both ventricles. Changes in the dynamic of this parameter were inversely proportional to changes in the transverse section of the cardiac muscle cells in all age groups. We established a directly proportional correlation between the morphometric index cardiomyocytic density in the left and right ventricle and capillary density. These comparative characteristics indicate that the development of the capillary network during the postnatal period of development in rats falls significantly behind the increase in the surface area of cardiac muscle cells both in left and right ventricle (**Fig. 1**; **Table 1**).

The comparative analysis of representative diagrams of capillary density demonstrated that in young (1-month-old) SHR the values of the parameter for both left and right ventricle are identical to those obtained for young (1-month-old) normotensive Wistar rats. A deviation from this correlation was observed both between adult (6-month-old) SHR and respective age groups of normotensive Wistar rats, as well as between adult (6-month-old) SHR and senescent (12-month-old) normotensive Wistar rats. The decrease in the values in adult (6-month-old) SHR constitutes approximately

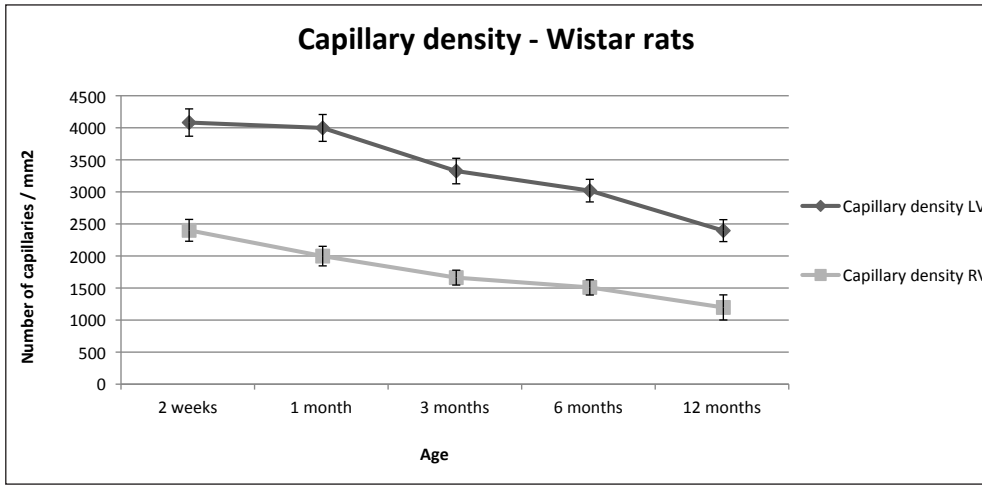

Fig. 1. Graphic representation of the changes in capillary density in the left and right ventricle. LV – left ventricle; RV – right ventricle

Table 1. Numerical representation of the changes in capillary density in the left and right ventricle

	Left ventricle		Right ventricle		
WR	**Number of capillaries/mm²**		**Number of capillaries/mm²**		
Age	**Mean value**	**SD**	**Mean value**	**SD**	**T-test**
2 weeks	4081.6	213.1	2400.1	170.3	p<0.001
1 month	3997.6	209.5	1998.1	152.6	p<0.001
3 months	3325.1	198.9	1662.3	115.9	p<0.001
6 months	3019.4	176.1	1509.8	118.8	p<0.001
12 months	2395.5	171.1	1197.3	195.9	p<0.001

Note: WR – Wistar rats.

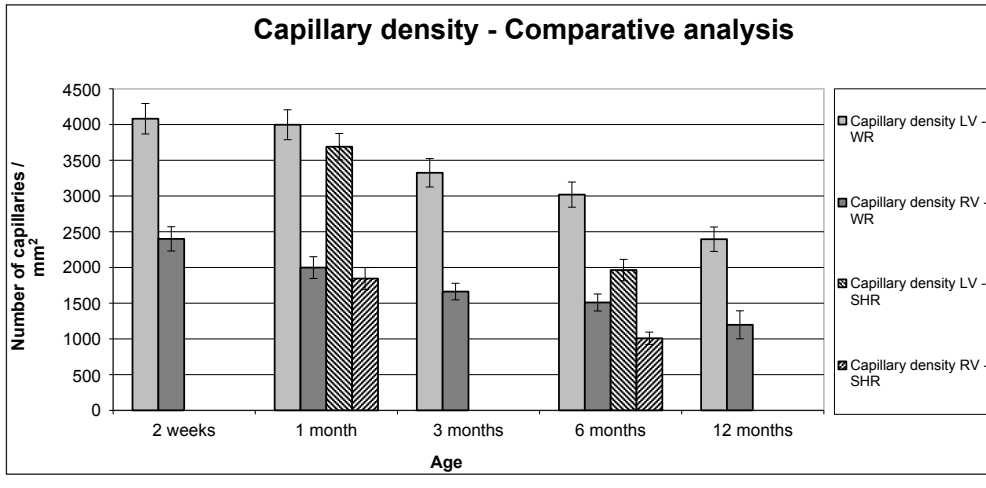

Fig. 2. Comparative analysis of the changes in capillary density in the left and right ventricle between Wistar rats and spontaneously hypertensive rats. LV – left ventricle; RV – right ventricle; WR – Wistar rats; SHR – spontaneously hypertensive rats

Table 2. Numerical representation of the changes in capillary density in the left and right ventricle and comparison between Wistar rats and spontaneously hypertensive rats

	Left ventricle			Left ventricle		
WR	**Number of capillaries/mm²**		**SHR**	**Number of capillaries/mm²**		
Age	**Mean value**	**SD**	**Age**	**Mean value**	**SD**	**T-test**
2 weeks	4081.6	213.1				
1 month	3997.6	209.5	1 month	3689.6	185.2	p<0.001
3 months	3325.1	198.9				
6 months	3019.4	176.1	6 months	1963.7	149.4	p<0.001
12 months	2395.5	171.1				

	Right ventricle			Right ventricle		
WR	**Number of capillaries/mm²**		**SHR**	**Number of capillaries/mm²**		
Age	**Mean value**	**SD**	**Age**	**Mean value**	**SD**	**T-test**
2 weeks	2400.1	170.3				
1 month	1998.1	152.6	1 month	1844.6	154.3	$p<0.05$
3 months	1662.3	115.9				
6 months	1509.8	118.8	6 months	1008.8	86.6	$p<0.001$
12 months	1197.3	195.9				

Note: WR – Wistar rats; SHR – spontaneously hypertensive rats.

one third of the values in adult (6-month-old) normotensive Wistar rats, and these values are lower even than the corresponding values for the two ventricles in senescent (12-month-old) normotensive Wistar rats (**Fig. 2**; **Table 2**).

Discussion

During the initial development of cardiac hypertrophy in SHR and normotensive rats (1- to 6-month-old), capillary density decreases significantly due to the increase in the transverse section of cardiomyocytes [6]. Our data show similar results. The decrease in capillary density demonstrates that compensatory neovascularisation does not take place during this period or, to say the least, is insignificant to sustain a normal vascular profile in SHR. Anversa et al. [4] describe various structural compensatory mechanisms in SHR aged under 2 months. During this period capillary proliferation in SHR exceeds the one in normotensive Wistar rats, despite capillary density remaining unchanged. This shows that the shortage of capillaries observed in 6-month-old SHR occurs after the second month, with Tomanek and Hovanec [25] reporting that decreased capillary density is observed in SHR aged 2-5- and 7-month-old. Together with the insufficient neovascularisation in SHR, the increasing size of cardiomyocytes leads to an increase in the mean diffusion distance. While at age 1 month the mean diffusion distance in both SHR and normotensive rats is similar, in 6-month-old SHR it increases to an extent that it does not differ substantially from the mean diffusion distance in 24-month-old normotensive Wistar rats. Insufficient revascularisation during ventricular remodeling in SHR as part of the development of cardiac hypertrophy can lead to a decrease in the cardiac output and ventricular necrosis, which has been observed in advanced age [17]. The data obtained in the present study for the period 1-6 months in normotensive Wistar rats and young SHR show a decrease in the capillary density which is more pronounced in the group of SHR.

During the full stage of development of hypertrophy (6-12 months) capillary density shows a similar degree of decrease in both ventricles [6]. The part of the left ventricle, occupied by cardiomyocytes in SHR remains significantly vast, with the amount of interstitial tissue being markedly decreased. Over the same period, the cardiac muscle cells in normotensive Wistar rats occupy a significantly smaller portion of the wall of the left ventricle, while the amount of interstitial tissue markedly increases [6]. This clearly demonstrates that during the full stage of development of hypertrophy, the increased surface area of the muscle fibres in SHR significantly exceeds the capacity of the neovascularisation and worsens the already advancing heart failure [6].

It is well known that the working potential of the muscle tissue depends on the blood supply which is a function of capillary density. The ratio between capillary and cardiomyocytic profiles in transverse sections of the myocardium increases 5 times in the left ventricle and 4 times in the right ventricle [18]. On the eleventh day after birth the capillary density in the myocardium is comparable to that observed in adults. These data are based on morphometric [1] and in vivo microscopic techniques [10, 11]. Together with the subsequent increase of the surface area of cardiomyocytes there is an almost directly proportional proliferation of capillaries [1, 13]. Similar data based on a comparative morphometric analysis between different age groups of normotensive Wistar rats and SHR were obtained in the present study. At a structural level, a decrease in capillary density is observed in the aging myocardium [23, 28]. The quantitative analysis of the structural features of capillaries shows a linear increase in capillary density as age advances, which helps maintain the number of capillaries per unit area of cardiomyocytes [2]. The rising afterload in senescent rats induces the development of concentric ventricular hypertrophy with an increase in the thickness of the free wall without an increase of the ventricular chamber [8]. The results obtained in the present study demonstrated a decrease in capillary density in rat ventricles as age advanced.

The changes observed during the comparative analysis of capillary density correlated with a more clearly pronounced hypertrophy, predominantly noted in the free wall of the left ventricle as age advanced in the group of SHR. Changes were more dynamic in the left ventricle due to the fact that the rising arterial pressure in the systemic circulation affects predominantly the afterload in the left ventricle. It should be noted that age-related hypertrophy was observed in normotensive Wistar rats as well. The development of hypertrophy had a profound effect on the parameter capillary density (the values of which showed a pattern of gradual decrease). The comparative analysis of corresponding age groups of Wistar rats and SHR revealed that changes occurred at a younger age in SHR.

Conclusion

Capillary proliferation observed in SHR exceeds the one in normotensive control animals, which indicates that myocardial hypertrophy induced by hypertension is related to an accelerated capillary growth in relatively young animals [4]. In that aspect, literature data correspond to a more dynamic rate of growth of the capillary network during postnatal development [16, 18, 20]. According to other data [3, 16, 18, 20] confirmed by the present study, the mechanism for increase of the capillary network under conditions of hypertrophy due to a rise in the afterload is inherent in young but not in senescent animals.

References

1. **Anversa, P., A. V. Loud, F. Giacomelli, J. Wiener.** Absolute morphometric study of myocardial hypertrophy in experimental hypertension. II. Ultrastructure of myocytes and interstitium. – *Lab. Invest*., **38**, 1978, 597-609.
2. **Anversa, P., B. Hiler, R. Ricci, G. Guideri, G. Olivetti.** Myocyte cell loss and myocyte hypertrophy in the aging rat heart. – *J. Am. Coll. Cardiol*., **8**, 1986, 1441-1448.
3. **Anversa, P., G. Olivetti, A. V. Loud.** Morphometric study of early postnatal development in the left and right ventricular myocardium of the rat. – *Circ. Res*., **46**, 1980, 495-502.
4. **Anversa, P., M. Melissari, C. Beghi, G. Olivetti.** Structural compensatory mechanisms in rat heart in early spontaneous hypertension. – *Am. J. Physiol*., **246**, 1984, H739-H746.

5. **Breisch, E. A., F. C. White, C. M. Bloor.** Myocardial characteristics of pressure overload hypertrophy. A structural and functional study. – *Lab. Invest*., **51**, 1985, 333-342.
6. **Engelmann, G., C. John, G. Ross.** Morphometric analysis of cardiac hypertrophy during development, maturation and senescence in spontaneously hypertensive rats. – *Circ. Res*., **60**, 1987, 487-494.
7. **Frohlich, E. D., R. C. Tarazi.** Is arterial pressure the sole factor responsible for hypertensive cardiac hypertrophy? – *Am. J. Cardiol*., **44**, 1979, 959-963.
8. **Grossman, W., D. Jones, L.P. McLaurin.** Wall stress and pattems of hypertrophy in the human left ventricle. – *J. Clin. Invest*., **56**, 1975, 56-64.
9. **Harrison, D. G., D. H. Barnes, L. F. Hiratzka, C. L. Eastham, R. E. Kerber, M. L. Marcus.** The effect of cardiac hypertrophy on the coronary collateral circulation. – *Circ*., **71**, 1985, 1135-1145.
10. **Henquell, L., C. R. Honig.** Intercapillary distances and capillary reserve in right and left ventricles: Significance for control of tissue Po2. – *Microvasc. Res*., **12**, 1976, 35-41.
11. **Henquell, L., C.L. Odoroff, C.R. Honig.** Intercapillary distance and capillary reserve in hypertrophied rat heart beating in situ. – *Circ. Res*., **41**, 1977, 400-408.
12. **Imamura, K.** Ultrastructural aspect of left ventricular hypertrophy in spontaneously hypertensive rats: A qualitative and quantitative study. – *Jpn. Circ. J*., **49**, 1978, 979-1002.
13. **Katzberg, A. A., B. B. Fanner, R. A. Harris.** The predominance of binucleation in isolated rat heart myocytes. – *Am. J. Anat*., **149**, 1977, 489-500.
14. **Lund, D. D., R. J. Tomanek.** Myocardial morphology in spontaneously hypertensive and aortic constricted rats. – *Am. J. Anal*., **152**, 1978, 141-152.
15. **McElroy, C. L., S. A. Gissen, M. C. Fishbein.** Exercise inducted reduction in myocardial infarct size after coronary artery occlusion in the rat. – *Circ*., **57**, 1978, 958-962.
16. **Olivetti, G., P. Anversa, M. Melissari, A. V. Loud.** Morphometric study of early postnatal development of the thoracic aorta in the rat. – *Circ. Res*., **47**, 1980, 417-424.
17. **Pfeffer, J.M., M.A. Pfeffer, M.C. Fishbein, E.D. Frolich.** Cardiac function and morphology with aging in the spontaneously hypertensive rat. – *Am. J. Physiol*., **237**, 1979, H461-H468.
18. **Rakusan, K., J. Jelinek, B. Korecky, M. Soukupova, O. Poupa.** Postnatal development of muscle fibers and capillaries in the rat heart. – *Physiol. Bohemoslov*., **14**, 1965, 32-37.
19. **Rakusan, K., O. Poupa.** Changes in the diffusion distance in the rat heart muscle during development. – *Physiol. Bohemoslov*., **12**, 1963, 220-227.
20. **Rakusan, K., W. DuMesnilde-Rochemont, W. Braasch, H. Tschopp, R. J. Bing.** Capacity of the terminal vascular bed during normal growth, in cardiomegaly, and in cardiac hypertrophy. – *Circ. Res*., **21**, 1967, 209-215.
21. **Roberts, J.R., J.I. Wearn.** Quantitative changes in the capillarymuscle relationship in human hearts during normal growth and hypertrophy. – *Am. Heart J*., **21**, 1941, 617-633.
22. **Sen, S.** Regression of cardiac hypertrophy. Experimental animal model. – Am. J. Med., **75**, 1983, 87-93.
23. **Tomanek, R. J.** Effects of age and exercise on the extent of the myocardial capillary bed. – *Anat. Rec*., **167**, 1970, 55-62.
24. **Tomanek, R. J., J. C. Searls, P. A. Lachenbruch.** Quantitative changes in the capillary bed during development, peak, and stabilized cardiac hypertrophy in the spontaneously hypertensive rat. – *Circ. Res*., **51**, 1982, 295-304.
25. **Tomanek, R. J., J. M. Hovanec.** The effects of long-term pressure overload and aging on the myocardium. – *J. Mol. Cell. Cardiol*., **13**, 1981, 471-488.
26. **Wallenstein, S., C.L. Zucker, J.L. Fleiss.** Some statistical methods useful in circulation research. – *Circ. Res*., **47**, 1980, 1-9.
27. **Wearn, J.T.** Alterations in the heart accompanying growth and hypertrophy. – *Bull. Johns Hopkins Hosp*., **68**, 1941, 363-374.
28. **Yin, F. C. P., H. A. Spurgeon, K. Rakusan, M. L. Weisfeldt, E. G. Lakatta.** Use of tibial length to quantify cardiac hypertrophy: Application in the aging rat. – *Am. J. Physiol*., **243**, 1982, H941-H947.

Institute of Experimental Morphology, Pathology and Anthropology with Museum
Bulgarian Anatomical Society

Acta morphologica et anthropologica, 24 (1-2)
Sofia ● 2017

Histomorphometric Studies of the Healing Process in Artificial Bone Defects in Rabbit Long Bones

Jermen Indjova[1*], *Khodor Fakih*[1], *Dimitar Sivrev*[2]

[1] *Department of Oral and Maxillo-Facial Surgery, Faculty of Dental Medicine, Medical University, Sofia, Bulgaria*
[2] *Department of Anatomy, Faculty of Medicine, Trakia University, St. Zagora, Bulgaria*

* Corresponding author: e-mail: indjovaj@yahoo.com

Histomorphometry was used for evaluation and quantitative measurement of the types of new bone formation in artificial defects created in long bones of rabbits. The aim of the study is monitoring the amounts of new woven and lamellar bone formed in artificial bone defects treated with various combinations of Bio Oss and Emdogain under guided bone regeneration. Forty bone defects were created in the hindlimbs of 10 rabbits. The amount of woven and lamellar bone increased between post treatment months 3 and 4 both after independent and combined application of both xenografts. The amount of lamellar bone was the greatest in natural healing with coagulum and after treatment with combination of Bio Oss+Emdogain. Bio Oss+Emdogain combination could be used to preserve the volume of alveolar bone and at the same time to create an environment for placing intraosseous dental implants when the available healing time was over 4 months.

Key words: experimental model, histomorphometry, Bio Oss, Emdogain

Introduction

The survival of dental implants is closely related to the achieved primary stability [9]. It is a function of the amount and quality of bone at the site of implantation and more specifically, the compact bone thickness and presence of lamellar bone [7]. For oral dental implants, the main structural elements relevant for the primary and later, for the secondary stability, are the newly formed woven and lamellar bone [10].

For evaluation of new bone formation, various techniques are used: quantitative computed tomography, histological and histomorphometric examinations [6].

Quantitative computed tomography has the disadvantage of providing no information about the ratio between bone components, e.g. for the fine bone structure. By means of histology, the type of the newly formed bone elements could be established although no data about quantitative ratios are available [6]. Histomorphometry allows

the determination of the amount and relative proportion of the new bone formation (woven and lamellar bone) and other structures (connective tissue, transplant materials) on histological specimens.

The reports with quantitative histomorphometric data are only few [9]. What is more, to the best of our knowledge, there are no data from histomophometrical assessment of defect healing with different combinations of Bio Oss and Emdogain of more than 4 months' duration.

The aim of the present study was to monitor the time course of quantitative parameters of bone defect healing in a rabbit experimental model, notably the relative proportions of formed woven and lamellar bone in groups treated with guided bone regeneration and different combinations of Bio Oss and Emdogain xenografts over 4 months.

Materials and Methods

Experimental animals. Ten New Zealand White rabbits were used as experimental subjects. The long bones of hindlimbs (femur and tibia) were used. Five rabbits were euthanised by the end of the 3rd month and the other five – by the end of the 4th month. The experiments were approved by the Research Ethics Committee at the Medical University – Sofia (permit No. 77/02. 05. 2012).

Experimental design. Bone defects were created with a bone cutters with outer diameter 4 mm, labelled at 5 mm for achieving a uniform depth of penetration.

Anaesthesia protocol. The induction in general anaesthesia was done with 15 mg/kg i.m. Zoletil. Fifteen minutes later, 5 mg/kg Xylazine was applied i.m. Anaesthesia was maintained with Isoflurane through a mask until the end of the surgery. All operative interventions were done under strict aseptic conditions.

Tibial and femoral grafts. Skin incisions' size was up to 3 cm. Experimental rabbits were fixed in lateral recumbency. After successive dissection of tissues, the cortical surface of the underlying bone was exposed. One bone defect was created in each of the two femurs and tibias per animal – a total of 4 bone defects in a rabbit, 40 for all 10 animals. The total number of experimental defects was 36, distributed into 6 groups and filled with Bio Oss, Emdogain or Bio Oss+Emdogain. The total number of control defects was 4 – distributed in 2 groups, healed with coagulum. The tissues over the operative defects were sutured in layers. During the first 3-5 post operative days, the rabbits were treated with Baytril at a dose of 1 ml/10 kg body weight.

Histology and histomorphometry. The animals were euthanised by intravenous injection of Euthanasin "N" until cessation of respiratory and cardiac activity. The respective regions of the limbs were dissected and surrounding soft tissues – removed. The specimens were stored in 10% formalin. Preparations for light microscopy were made.

Histomorphometric evaluation of bone defect healing treated with various xenograft(s) was conducted on permanent preparations for light microscopy. The ImageJ software, developed by the National Institute of Health, USA was used for this purpose. ImageJ is an open-source software that could be used on a computer with Java pre-installed for processing and morphometric analysis of images. All useless elements in the analysed field that are not relevant and could influence adversely the final result, are removed. A monochromatic mask of the analysed area is then created. This allows the measurement of the number of pixels in the studied field. The mask analysis function is used for determination of the area of studied objects in pixels. The results are entered into a table for calculation of the relative share of studied objects from the entire visible field.

Statistical analysis. Values are presented as mean ± standard deviation. The normal pattern of distribution within a group was tested with the Kolmogorov-Smirnov test. The differences between means were assessed using GraphPad InStat 3.0 statistical software.

Results

The central parts of the histological preparations corresponding to central parts of the bone defect were chosen for evaluation of new bone formation quality in order to decrease the influence of the natural bone around the defect [10]. All experimental and control groups exhibited changes in the amount of formed woven and lamellar bone between the 3rd and the 4th month ($p < 0.001$), **(Table 1)**.

Woven and lamellar bone volume by post treatment month 3

The time course of the two types of newly formed bone – woven and lamellar was the same during the first observation period. The smallest proportion of newly formed bone structures was established in defects healed with Emdogain only, followed by those healed with Bio Oss only, the combination Bio Oss+Emdogain and finally, in specimens healed naturally with coagulum.

At the end of the 3rd month, the differences between the relative shares of woven bone were statistically significantly different between defects treated with Bio Oss+Emdogain vs. Emdogain only ($p < 0.001$) and between the proportion of the control group versus the treatment groups with self-administration of Bio Oss and Emdogain ($p < 0.001$). There were no considerable difference between the woven bone volumes in Bio Oss+Emdogain and control groups ($p>0.05$), as well as between those with either

Table 1. Relative proportion of woven and lamellar bone in bone defects with respect to the applied treatment and post treatment period, and statistical significance of differences between the 3rd and the 4th month

Xenografts and coagulum→	**Bio Oss Bio Gide**		**Emdogain Bio Gide**		**Bio Oss Emdogain Bio Gide**		**Coagulum Bio Gide**	
Periods ► Structures ▼↓	**month 3**	**month 4**	**month 3**	**month 4**	**month 3**	**month 4**	**month 3**	**month 4**
Woven bone	16.58 ±1.00	23.75 ±1.14	13.66 ±1.07	18.50 ±1.45	28.58 ±1.17	32.75 ±1.22	36.50 ±1.24	42.17 ± 1.03
Month 3 vs. month 4	$p < 0.001$		$p < 0.001$		$p < 0.001$		$p < 0.001$	
Lamellar bone	10.58 ±1.17	28.08 ±1.17	8.83 ±0.83	16.58 ±1.17	19.67 ±1.23	33.25 ±1.49	28.67 ±1.67	52.83 ±1.19
Month 3 vs. month 4	$p < 0.001$		$p < 0.001$		$p < 0.0011$		$p < 0.0011$	

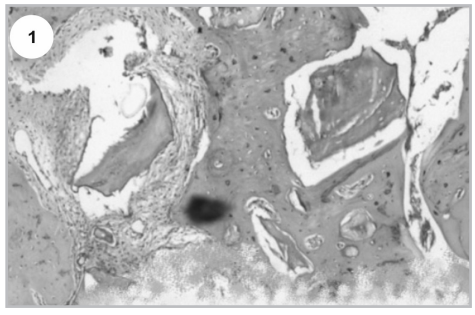

Fig. 1. Histology of a section of bone defect treated with GBR+Bio Oss+Emdogain 3 months after the start of the experiment

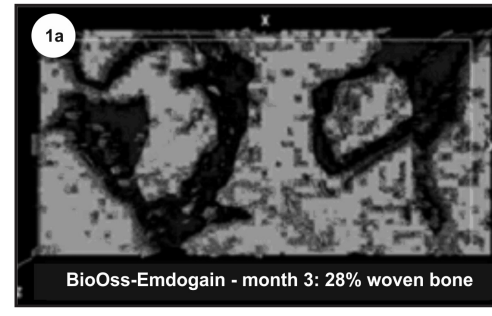

Fig. 1a. Histomorphometry of woven bone formed in the defect treated with GBR+Bio Oss+Emdogain 3 months after the start of the experiment

Bio Oss or Emdogain only ($p > 0.05$) and Bio Oss+Emdogain vs Bio Oss - ($p>0.05$), (**Figs. 1** and **1A**)

By the end of the 3rd month, the differences of relative amounts of lamellar bone were comparable to those observed for the woven bone (**Figs. 2 and 2A**).

Woven and lamellar bone volume by post treatment month 4

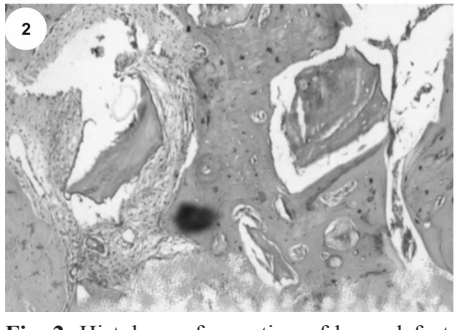

Fig. 2. Histology of a section of bone defect treated with GBR+Bio Oss+Emdogain 3 months after the start of the experiment

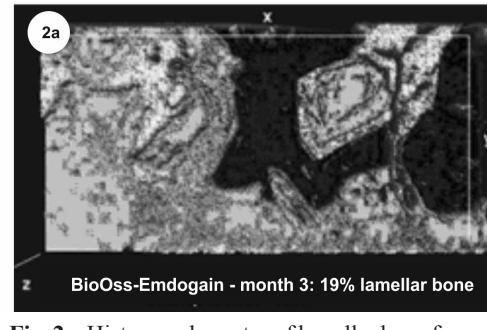

Fig. 2a. Histomorphometry of lamellar bone formed in the defect treated with GBR+Bio Oss+Emdogain 3 months after the start of the experiment

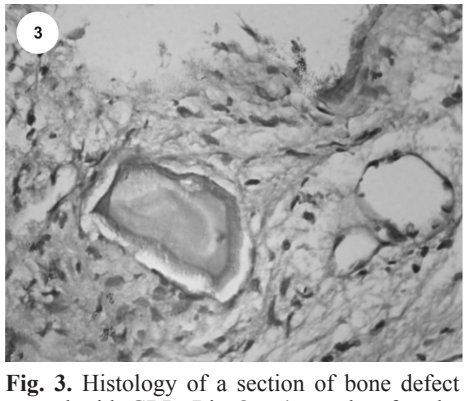

Fig. 3. Histology of a section of bone defect treated with GBR+Bio Oss 4 months after the start of the experiment

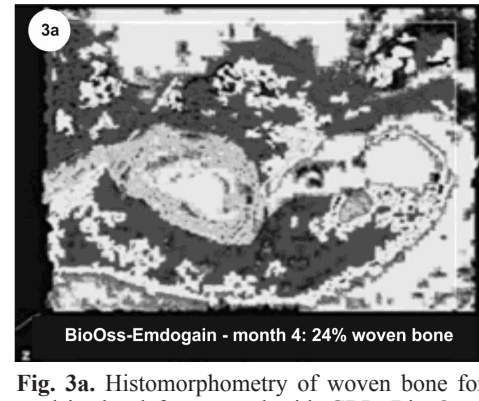

Fig. 3a. Histomorphometry of woven bone formed in the defect treated with GBR+Bio Oss 4 months after the start of the experiment

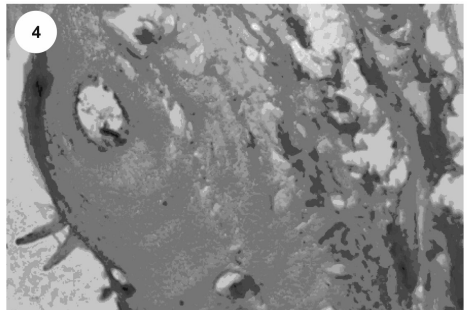

Fig. 4. Histology of a section of bone defect treated with GBR+Bio Oss 4 months after the start of the experiment

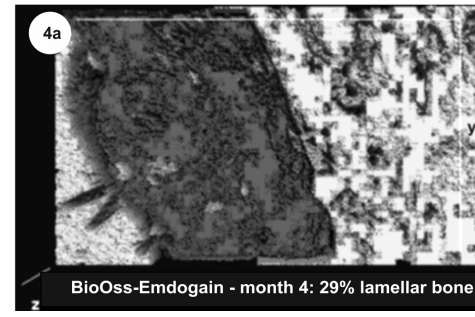

Fig. 4a. Histomorphometry of lamellar bone formed in the defect treated with GBR+Bio Oss 4 months after the start of the experiment

By the end of the 4th month, the relative proportions of woven and lamellar bone formation increased from the group treated with Emdogain, through the groups with Bio Oss and Bio Oss+Emdogain until the control group with naturally healed defects.

Four months from the beginning of the experiment, the differences between the relative amounts of woven bone differed very significantly among all experimental groups as well as between each of experimental groups vs controls ($p < 0.001$) (**Figs. 3** and **3A**).

At this time interval, the comparison of relative shares of lamellar bone in the different groups showed statistically significant differences between the groups of defects healed with Bio Oss+Emdogain and Emdogain only ($p < 0.001$), as well as between control defects and the groups with either Bio Oss or Emdogain only ($p < 0.001$). No significant differences were found out between the groups treated independently with Bio Oss and Emdogain ($p > 0.05$), and between Bio Oss+Emdogain vs Bio Oss only ($p > 0.05$) (**Figs. 4** and **4A**).

Discussion

In all studied groups (experimental and control), the differences between newly formed woven and lamellar bone by the end of the 3rd month were very different from those observed one month later at a very high level of statistically significance ($p < 0.001$ – **Table 1**) and reflect the effect of experiment's duration. Similar results are reported by numerous investigators [2].

In all groups, osteogenesis was expressed at a various extent. Initially, by the end of the 3rd month, all groups exhibited enhanced formation of woven bone as compared to lamellar bone (**Table 1**). Woven bone is formed relatively rapidly – at a daily rate of 30-50-60 μm. That is why it is irregularly organised. It also contains cells. These features speak about a immature bone structure. Its mechanical strength is low, partly compensated by its relatively good mineralisation. Although with a small mechanical strength, the biological significance of woven bone is substantial. It is gradually replaced by lamellar bone [4] (**Table 1**). By the 4th month, the opposite event was observed: the amount of lamellar bone increased as compared to the woven bone. Lamellar bone is the main component of mature cortical and trabecular, cancellous bone. Lamellae are formed slowly (at a daily rate of < 1.0 μm). Its collagen network is well arranged and mineralised. Lamellar bone is composed by numerous unidirectionally oriented layers, termed lamellae [4].

On the basis of our results (**Table 1**) the greatest proportion of newly formed woven and lamellar bone was observed in defects healed naturally with coagulum, which affirms the leading importance of the guided bone regeneration [11]. One of advantages of placing a barrier membrane over the coagulum was its stabilisation. Thus, a natural spatial scaffold, facilitating the osteogenesis, is created [3]. Despite the advancement of biotechnologies and bone tissue engineering, the developed and widely implemented grafts Bio Oss and Emdogain could not compete with natural healing within the framework of this experiment as the quality of newly formed bone was concerned.

The results obtained with the combination Bio Oss+Emdogain were attributed both to the synergic effect of the advantages of each of the two grafts [14, 15] – osteoconductive properties of Bio Oss and osteoinductive properties of Emdogain [3], as well as to the biological properties of the latter superimposed on Bio Oss. Additionally, at the time of the preliminary mixing of both materials, the staining of Bio Oss granules with blood from the wound that could impair the adhesion, proliferation and differentiation of osteoblasts on the graft's surface, is avoided [8]. The presence of molecules resembling bone morphogenetic proteins (BMP) in Emdogain contribute to attraction, proliferation and differentiation of osteogenic cells' precursors into osteogenic cells. The studies provide evidence for the presence of limited amount of organic proteins in Bio Oss, regardless of the deproteinisation of the material. According to their biological behaviour, they are determined as BMP-2 [12]. The osteoinductive effect of Bio Oss is not exhibited as it is small, but the addition of Emdogain with its osteoinductive properties rendered the array of biological properties of the combination more complete and diverse. The more obvious osteogenesis, established previously with the combination of both grafts, allowed assuming that Bio Oss was an appropriate carrier of Emdogain.

The greater although statistically insignificant amount of the formed woven and lamellar bone with Bio Oss compared to Emdogain could be attributed to the higher porosity of the graft resembling the structure of the natural cancellous bone, its osteoconductive properties and biological compatibility. The Bio Oss granules placed inside the defect separate the space into smaller compartments. Thus, vascularisation and osteogenesis are facilitated [11]. At the same time, the excessive compression of Bio Oss granules impairs these events [1], which is a probable explanation for the reduced bone formation rate when defects are filled with Bio Oss only compared to healing with the combination.

The smaller amount of newly formed woven and lamellar bone in the group treated with Emdogain could be the decreased intensity of the initial active formation of new bone after the 14th day observed by Shimizu-Ishiura et al. [13] as well as the probability for predominance of osteoconductive properties of grafts reported by Hockers et al. [5] which were not present in Emdogain.

Conclusion

The histomorphometric studies demonstrated repair of bone in all control bone defects and in defects healed with the combination Bio Oss+Emdogain. The relative proportion of mature bone structures, which are essential for the stability of implants, was significantly greater in control groups followed by Bio Oss+Emdogain combination compared to the independent use of either of grafts. The duration of healing was also of primary significance. The proportion of lamellar bone was statistically significantly higher by the 4th compared to the 3rd month. Regardless of the success of bone tissue engineering, the healing quality with xenografts Bio Oss and Emdogain was inferior to repair under GBR and coagulum.

References

1. **Bodde, E., J. Wolke, R. Kowalski, J. Jansen.** Bone regeneration of porous beta-tricalcium phosphate (Conduit TCP) and of biphasic calcium phosphate ceramic (Biosel) in trabecular defects in sheep. – *J. Biomed. Mater. Res*., **82**, 2007, 711-722.
2. **Chiapasco, M., M. Zaniboni.** Clinical outcomes of GBR procedures to correct peri-implant dehiscences and fenestrations: a systematic review. – *Clin. Oral Impl. Res*., **20**, 2009, 113-123.
3. **Donos, N., D. Bosshardt, N. Lang, F. Graziani, M. Tonetti, T. Karring, I. Kostopoulos.** Bone formation by enamel matrix proteins and xenografts: an experimental study in the rat ramus. – *Clin. Oral Impl. Res*., **16**, 2005, 140-146.
4. **Garg, A. K.** Bone Physiology for Dental Implantology. – In: Garg, A. K. *Bone. Biology, Harvesting, Grafting for Dental Implants. Rational and Clinical Applications. Quintessence*. Publ. Co, Inc, Hanover Park, 2004, 3-20.
5. **Hockers, T., D. Abensur, P. Valentini, R. Legrand, Chr. Hämmerle.** The combined use of bioresorbable membranes and xenografts or autografts in the treatment of bone defects around implants. A study in beagle dogs. – *Clin. Oral Impl. Res*., 10, 1999, 487-498.
6. **Martinez, H., M. Davarpanah, P. Missika, R. Celletti, R. Lazzara.** Optimal implant stabilization in low density bone. – *Clinical Oral Implants Res*., **12**, 2001, 423-432.
7. **Meredith, N.** Assessment of implant stability as a prognostic determinant. – *International Journal of Prostodontics*, **11**, 1998, 491-501.
8. **Miron, R., D. Bosshardt, E. Hedbom, Y. Zhang, B. Haenni, D. Buser, A. Sculean.** Adsorption of enamel matrix proteins to a bovine-derived bone grafting material and its regulation of cell adhesion, proliferation, and differentiation. – *J. Periodontol*., **83**, 2012, 936-947.
9. **Nkenke, E., M. Hahn, K. Weinzierl, M. Radespiel-Tröger, F. W. Neukam, K. Engelke.** Implant stability and histomorphometry: a correlation study in human cadavers using stepped cylinder implants. – *Clin. Oral Impl. Res*., **14**, 2003, 601-609.
10. **Rokn, A., M. Khodadoostan, A. Ghahroudi, P. Motahhary, K. M., Fard, H. De Bruyn, R. Afzalifar, E. Soolar, A. Soolari.** Bone Formation with Two Types of Grafting Materials: A Histologic and Histomorphometric Study. – *The Open Dentistry Journal*, **5**, 2011, 96-104.
11. **Schmid, J., C. H. F. Hämmerle, L. Flückiger, J. R. Winkler, A. Olah, S. Gogolewski, N. Lang.** Blood-filled spaces with and without filler materials in guided bone regeneration. A comparative experimental study in the rabbit using bioresorbable membranes. – *Clin. Oral Impl. Res.*, **8**, 1997, 75-81.
12. **Schwartz, Z., T. Weesner, S. Van Dijket, D. Cochran, J. Mellonig, C. Lohmann, D. Carnes, M. Goldstein, D. Dean, B. Boyan.** Ability of deproteinized cancellous bovine bone to induce new bone formation. – *J. Periodontol*., **71**, 2000, 1258-1269.
13. **Shimizu-Ishiura, M., S. Tanaka, W-S. Lee, K. Debari, T. Sasaki.** Effects of enamel matrix derivative to titanium implantation in rat femurs. – *J. Biomed. Mater. Res*., **60**, 2002, 269-276.
14. **Valentini, P., D. Abensur, B. Wenz, M. Peetz, R. Schenk.** Sinus grafting with porous bone mineral (Bio-Oss) for implant placement: a 5-year study on 15 patients. – *Int. J. Periodontics Restorative Dent*., **20**, 2000, 245-253.
15. **Инджова, Ж.** *Направлявана костна регенерация и мониторинг на стабилността на интраосални дентални имплантати с електронни устройства*. Дисертация. София, 2016.

Institute of Experimental Morphology, Pathology and Anthropology with Museum
Bulgarian Anatomical Society

Acta morphologica et anthropologica, 24 (1-2)
Sofia ● 2017

Morphological Studies on the Spermatogenesis and Graffi Myeloid Tumor Cell Dissemination (Methastases) in the Testes of Tumor-Bearing Hamsters

Iliana Ilieva[1*], *Reneta Toshkova*[1], *Elisaveta Zvetkova*[2], *Iskra Sainova*[1], *Ivelin Vladov*[1]

[1] *Institute of Experimental Morphology, Pathology and Anthropology with Museum, Bulgarian Academy of Sciences, Sofia, Bulgaria*
[2] *Bulgarian Society of Biorheology*

*Corresponding author: e-mail: iilieva@abv.bg

The *aim* of the present study was to evaluate the *in vivo*-effects of the transplantable *Graffi* myeloid tumor (GMT) on the testicular morphology and spermatogenesis in tumor-bearing hamsters. In the experimental hamsters from days 25th to 30th post transplantation (p.t.), destructive changes in germinal epithelium organization were found. Increased number of abnormal and atypical spermatogenic cells was established together with decreased number and/or even lack of differentiated spermatids/spermatozoa in the seminiferous tubules. In most of the tubules, strong injury and/or suppression of the spermatogenesis was observed. In the cases of day 30th p.t., proliferation of atypical cells was assessed, as well as their infiltration in both tubule lumen and testicular interstitial spaces, near to small blood vessels (neo-angiogenesis). Atypical cells (neo-blast cells) dissemination additionally injured seminiferous tubules and formed metastases.

Key words: myeloid leukemia, myeloid Graffi tumor, testicular metastases, spermatogenesis, germinal epithelium, seminiferous tubules

Introduction

Microscopic evidence of disseminated neoplastic disease – involving infiltration of the testis by myeloid leukemia cells, was detected in 64% of patients with acute myeloid leukemia (AML) and in 22% of cases with chronic myeloid leukemia (CML) [7]. The higher frequency of leukemic cell infiltration in the testis was obtained in patients with acute monocytic (monoblastic-, myelomonocytic) leukemia (AMoL), followed by patients with AML [13, 18]. Less commonly, other myeloproliferative and/or myelodysplastic disorders as chronic myeloid leukemia (CML), myeloid sarcoma (MS) and myelodysplastic syndrome (MDS), involving the testis, have been reported [22, 23].

In this aspect the well explored in our previous study [10] experimental model of transplantable *Graffi* myeloid tumor in hamsters which is very similar in nature and presents basic features of the acute monocytic (monoblastic-, myelomonocytic) leukemia in humans [24]. Thus, it is a main reason to continue our experimental work on the model of *Graffi* myeloid tumor in hamsters, as a myeloid malignant diseases affecting testicular structure and spermatogenic process.

The *aim* of the present study was to evaluate the *in vivo* effects of the transplantable *Graffi* myeloid tumor (GMT) on the testicular morphology and spermatogenesis in tumor-bearing hamsters.

The transplantable myeloid tumor used in this study originated as a *Graffi* murine leukemia virus-induced tumor in newborn hamsters, adapted and maintained to mature Golden Syrian hamsters [12, 20, 21].

Materials and Methods

Experimental hamster Graffi tumor model

Golden Syrian hamsters, 2 months old, were used in experiments. The experimental animals were kept under standard conditions with free access to food and water. The model of *Graffi* tumor was primary created by the Graffi-virus in new-born hamsters, and maintained monthly *in vivo* by subcutaneous transplantation of live tumor cells (2×10^6/ml PBS) in the interscapular area of hamsters, for keeping the tumor's survival [12, 20, 21]. The tumor is 100% cancerous, and the animals died usually up to the 30th day after transplantation.

Histopathological examination

Testes samples from control (n = 6) and tumor-bearing hamsters (TBH) were taken, fixed and embedded in paraffin using routine histological practice. Tissue sections (5-7 μm) were stained by hematoxylin-eosin and examined under light microscope Leica DM5000B. The morphological changes were evaluated in testes from experimental animals at the day 10th (n = 4), 25th (n = 6) and 30th (n = 3) post transplantation (p.t.) and compared with the control group.

All studies were performed in accordance to the Guide for Care and Use of Laboratory Animals, as proposed by the Committee on Care Laboratory Animal Resources, Commission on Life Sciences and National Research Council, and a work permit No 11130006.

Results

Our morphological investigation on the testes of the control (untreated) hamsters revealed normal testicular structure and function (spermatogenesis) in healthy animals (**Fig. 1A**). Comparative testicular studies have been estimated in the group of GMT-bearing hamsters (at the day 10th, 25th and 30th p.t.).

The seminiferous tubules and the interstitial tissue in the testes of GMT-bearing hamsters at the day 10th p.t., were not affected by myeloid tumor cell growth. At this early stage of GMT-proliferation and probable micro-dissemination in the experimental animals, no destructive changes were observed in the testes tissue of the tumor-bearing animals (**Fig. 1B**).

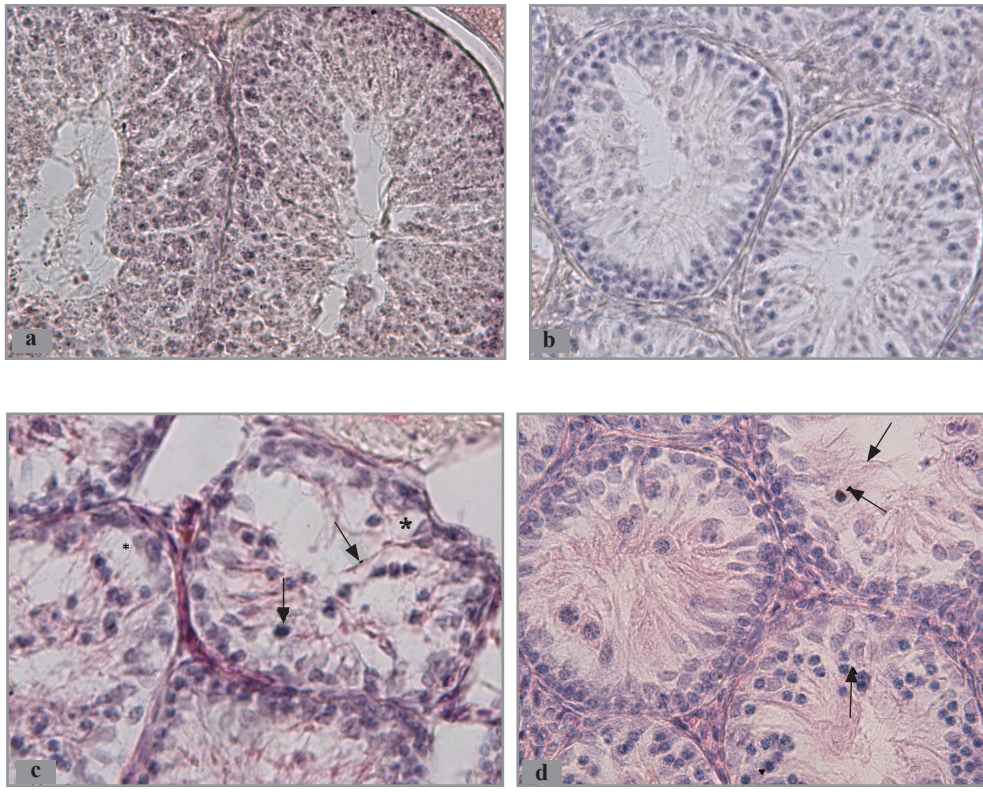

Fig. 1. Testicular cross-sections of control and tumor-bearing hamster (TBH): **A**) Control hamster – seminiferous epithelium appeared normal; **B**) Section of TBH from day 10th; **C-D**) Sections of TBH from day 25th. The germinal epithelium is disorganized, with many cavities (*) and showing depletion of germ cells. The degenerating primary spermatocytes with abnormal chromatin condensation and distribution were seen in tubules (arrowhead). Hematoxylin-eosine staining, × 200-400

The seminiferous tubules and the interstitial tissue in the testes of GMT-bearing hamsters at the day 25th p.t. showed severe changes in testicular morphology and progression of spermatogenesis (**Fig. 1C**) Intact spermatogonia were seen on the basal membranes of the seminiferous tubules together with some degenerating cells probably primary spermatocytes. Single differentiated germ cells can be found as spermatocytes and round spermatids in contrast to the controls (**Fig. 1C, D**).

At this stage of GMT development in hamsters no morphological changes in Sertoli and Leidig testicular cells were established.

In the testes of the experimental animals at the day 30th p.t., profound destruction was observed in the seminiferous tubules and the surrounding interstitial tissue (**Fig. 2**). The spermatogenesis looks incomplete and suppressed. In the most of the tubules, strongly suppressed spermatogenesis was found together with many degenerative germ cells. The seminiferous epithelium is disorganized, showing depletion of germ cells. As a result of injured spermatogenesis elongated spermatids and spermatozoa were not visible (**Fig. 2A-D).**

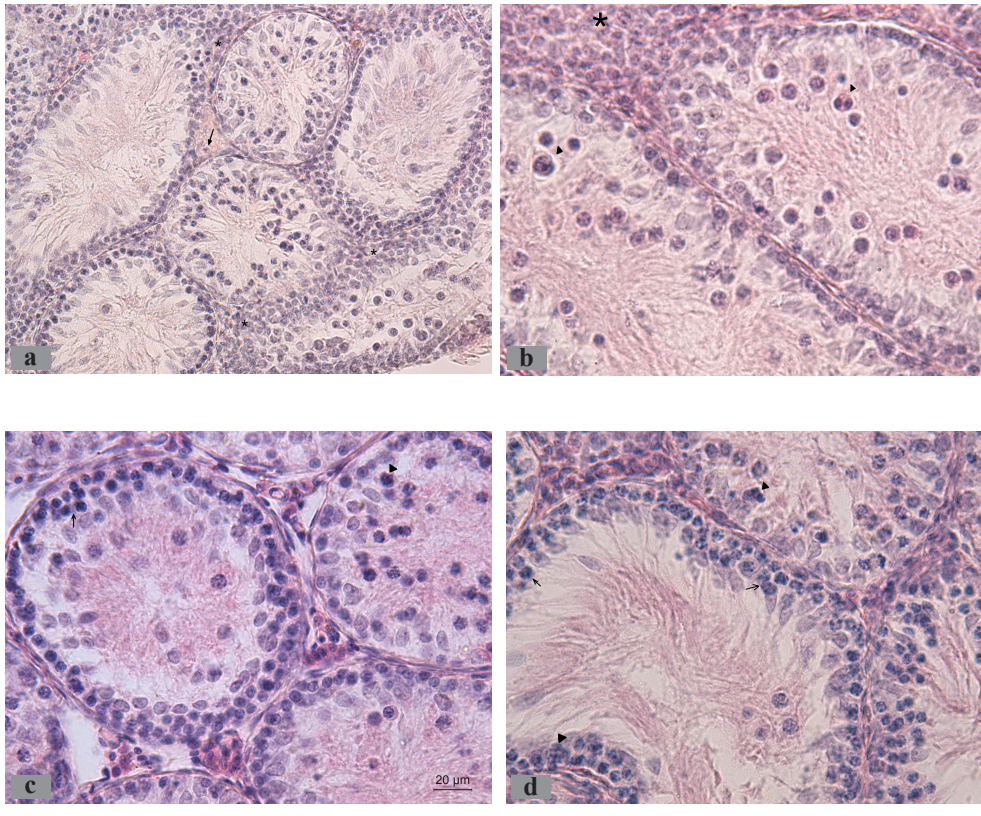

Fig. 2. Testicular cross-section of TBH at day 30th p.t.: The spermatogenesis looks incomplete and suppressed. The germinal epithelium in the tubules is disorganized, showing depletion of germ cells. **A**) The basal membranes of four testicular seminiferous tubules (in the right) are injured by invasion of atypical GMT-blast cells (infiltrating the testicular interstitial spaces as well as the tubular walls and lumina, and thus forming GMT micro-methastases); **B-D**) The similar patho-histological changes were obtained: GMT-blast cell-invasion in the testicular micro-vessels, in interstitium and in one of the seminiferous tubules - localized in the left part of the slide, could be well visualized. Many degenerating primary spermatocytes (St) with abnormal chromatin condensation and/or fragmentation were present. Atypical immature spermatids and giant multinuclear cells were also visualized. (small arrows) – microvessels, (*) – interstitium, (big arrows) – St, (arrowheads) – giant multinuclear and atypical/ GMT-blast cells. Hematoxylin-eosine staining, × 200-400.

From the morphological point of view, interesting findings are the cases of "detachment" of the germ cells from the basal membrane of the tubules, which probably lead to the degeneration of the germ cells and formation of clusters of degenerative spermatogenic cells in the lumen of seminiferous tubules (**Fig. 3A**). Seminiferous tubules with injured structure and integrity of the basal membranes were visualized very near or in direct contact to the new vessels (neo-vascularization), leading to the penetration of atypical GMT cells into the testicular interstitium and forming of metastases (**Fig. 3B**).

We could point summarize the main morphological features and characteristics of the seminiferous tubules with suppressed spermatogenesis in the both groups of experimental hamsters – examined at the day 25th and 30th p.t., as follow:

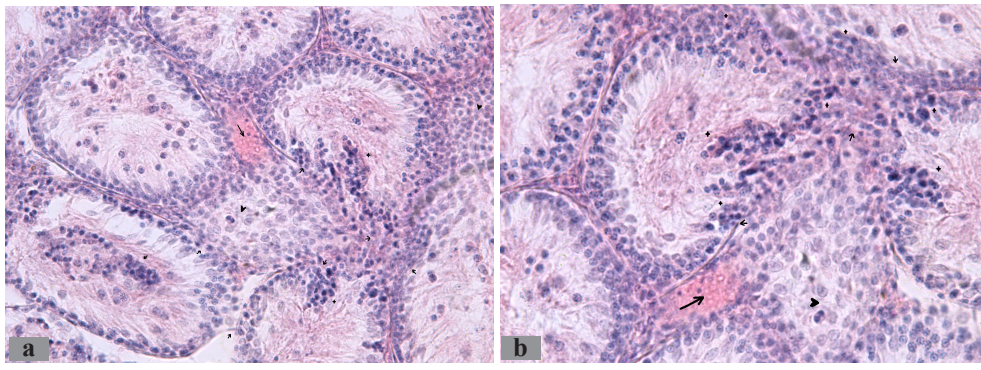

Fig. 3. Testicular cross-section of TBH at day 30th p.t.: **A-B**) Together with injured tubular basal membranes, clusters of tumor cells/methastases were seen spreading from the microvessels to the testicular interstitium, and infiltrating the walls and lumena of the adjacent seminiferous tubules. The highly invasive GMT-cells form the tubular and interstitial, micro-methastases were formed. The seminiferous tubule with "detachment" of abnormal germ cells and atypical cells from the basal membrane in the lumen of tubule were observed. (+) - tumor cells, (big arrow) - microvessels, (arrowhead) – interstitium, (small arrows) - basal membranes. Hematoxylin-eosine staining, × 200-250

– Depletion of differentiated spermatogenic cells (spermatocytes and spermatids) and formation of giant multinucleated cells in the tubular lumen;

– Increased number of degenerative germ cells manly in the tubular regions localized near to the basal membranes;

– Increased number of undifferentiated germ (blast-like) cells in the lumen of the seminiferous tubules **(Fig. 4).**

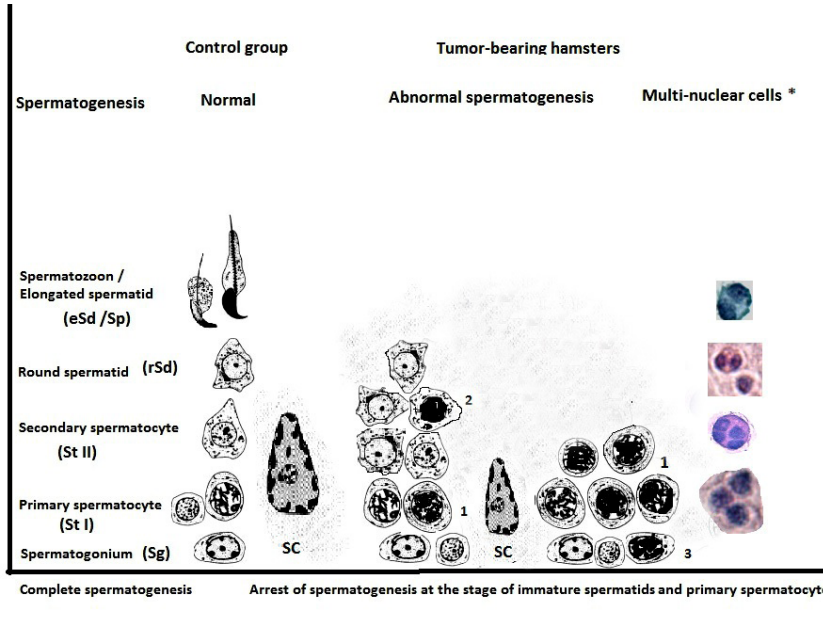

Fig. 4. Schematic presentation of influence of *in vivo* GMT on the spermatogenesis and morphology of germinal epithelium in the seminiferous tubules of tumor-bearing hamsters (at the day 25th and 30th p.t.) - versus control group. (SC) - Sertoli cells, (1) - atypical degenerative primary spermatocytes, (2) - degenerative round spermatids, (3) - degenerative spermatogonia, (*) - see also [11]

Discussion

Excluding leukemia and lymphoma, the metastatic tumors in the testis, are rare: the most common primary site is the prostate, followed by the lung, gastrointestinal tract, melanoma, seminal vesicles and kidney [9, 16, 17]. Some authors described cases with unilateral and bilateral testicular involvement, as well as testicular, combined with multiple metastases.

Microscopically, the testicular metastases are disseminated as nets of tumor cells in the intersticium. In other cases, a simultaneous invasion of metastatic carcinoma in the interstitium and seminiferous tubules of testis could be obtained [16].

Three types of tumor growth in the testes – interstitial, intracanalicular and mixed, have been reported [9, 17]. Five main mechanisms of metastatic spread – hematogenous (arterial–retrograde venous), retrograde lymphatic, trans-peritoneal, by means of vas deferens and epididymis, were described [9, 16]. Testicular blast cell infiltration is a known complication in myeloid leukemia and especially in cases of AML (preferably occurring in patients with myelomonocytic or monoblastic blast cell differentiation) [6, 15, 19]. This is the purpose for clinical and histological/cytological examination of testes in these patients – at the time of relapses or in the remission of myeloid malignancies.

Histological/cytological analysis showed infiltration of the testicular stroma by myeloid blast displaying the typical morphology (with preferably monoblastic – and/or myelo-monocytic-cell differentiation, according to sub-type of AML) [6]. The positive reaction of the blast cells to myeloperoxidase and a cytogenetic chromosomal karyotype analysis in patients completed diagnosis.

Pioneer microscopically investigations on the elevated testes in tumor-bearing rats (concerning Yoshida – and-MTK-sarcomas), have been undertaken by K. Kano in early 1952 [14]. The histological studies of the seminiferous tubules showed attenuated – suppressed- or absent spermatogenic activity as a result of germinal cell degeneration. Cytological features of nuclear chromatin and chromosomal abnormalities in all phases of cell cycle were described. The general consideration of K. Kano [14] was that abnormal spermatogenesis and the subsequent disintegration of germ cells in the tumor-bearing rats might be induced under the influence of body fluids containing produced and secreted by tumor cells injurious substances (humoral cell and tissue factors), to which pathological effects the testicular germinal cells are most sensitive and susceptible.

In all cases of testicular relapse in AML, leukemic infiltrates are located in the interstitial spaces reaching the testis through the enlarged, permeable and injured capillaries (as a result of neoplastic process and neo-angiogenesis related) [10, 19, 24]. In this sense, our previous studies [10] demonstrated precisely neo-vasculature (neo-capillaries, enlarged small blood vessels – venules including) adjacent to the interstitial spaces of the testes in *Graffi* myeloid tumor-bearing hamsters. In the current research we demonstrated the appearance of leukemic infiltrates of monoblastoid cells in the interstitial space – through the disruption of blood vessel walls and injuries in the blood-testicular barrier (BTB). Morphologically, BTB is identified as the tight junctions between adjacent Sertoli cells in the basal compartment of the seminiferous tubules [2]. From the physiological point of view, the BTB serves to protect spermatogenesis in the seminiferous tubules. In the current research we suggest possible disintegration of the BTB (disrupted by neoplastic process) in the cases of detachment (ablation) of the germinal cells from the basal membrane of seminiferous tubules. Our results are in agreement with data of other authors [19] which also identified leukemic infiltrates as located in the testicular interstitial tissue – with secondary atrophy of the seminiferous tubules. We also obtained light-microscopically the secondarily involved seminiferous tubules, due to the local spread of monocytoid-like blasts (blast of monocytoid appearance [19]), simultaneously with disruption of the BTB.

We described this process first in the scientific literature in a case of model of myeloid malignancy - the experimental model of transplantable *Graffi* myeloid tumor in hamsters.

Evidence in the literature also suggested that the dissemination of malignant myelogenous disease could affect a man's fertility by influencing spermatogenesis [1, 8]. Instead that causes of poor semen quality in cancer- and leukemia patients are not yet well understood, our contributions in this field tended to be concerned about cell- and tissue (humoral) factors involved in impaired spermatogenesis in the testes of leukemia and cancer patients.

The similar changes of spermatogenesis have been observed by other authors only in cases of primary testicular germ cell tumors (TGCTs) and some sarcomas [5, 14]. The authors suggested that spermatogenesis could be retained (suppressed) in the premalignant testis tissues adjacent to the more aggressive nonseminomas, sarcomas etc., but not those adjacent to less invasive seminomas. Moreover, DNA methylation level is higher in the preneoplastic testis tissue adjacent to the nonseminomas. It is interesting fact that essentially all TGCTs arrised because of failure to undergo normal spermatogenesis.

These findings from the literature are in good agreement with our data on the retained (suppressed) spermatogenesis in the experimental conditions of transplantable myeloid tumor of *Graffi*. The data could be discussed in different aspects and in relationship to the premalignant/malignant testicular tissue adjacent to the seminiferous tubules and influencing (suppressing) intratubular spermatogenesis in the conditions of the testicular tubular involvement by differently aggressive and invasive myeloid malignancies. Our and other similar findings on the appearance and development of less or more aggressive, primary or metastatic testicular tumors, deeply influencing (suppressing) spermatogenesis, could be used as new diagnostic tools and for successful therapeutic targeting of disseminated/relapsed myeloid malignancies with testicular involvement. The simultaneous expression of several cancer/testis antigens (CTA) in the course of both processes – spermatogenesis and carcinogenesis has been also investigated [3, 4].

Conclusion

The current study, in which is used experimental model of TBHs, clearly indicates the possibility *Graffi* myeloid tumor to cause destructive pathological changes in the testicular tissue, including formation of metastases, and these morphological changes could lead to significant suppression and/or injury of the spermatogenesis process. The simultaneous expression of several cancer/testis antigens (CTAs) in the course of both processes – spermatogenesis and carcinogenesis, could be also evaluated in future investigations on *Graffi* myeloid tumor model.

The morphological assessment of the degree of injury in the spermatogenesis, and of the cytological changes of the germ cells in the seminiferous tubules in experimental or pathological conditions (as GMT model), could be helpful for the development of new methods and directions about therapy and prevention of the male fertility in malignancy development and neoplastic metastases in the testes.

Acknowledgements: This research was financially supported by the Bulgarian National Science Fund (Grant BO2/5-2014). The authors wish to thank M. Pavlova, medical laboratory assistant, for tissue processing and preparation of microscope slides.

References

1. **Agarwal, A., Sh. S. R. Allamaneni**. Disruption of Spermatogenesis by the cancer disease process. – J. Natl. Cancer Inst. Monogr., **34**, 2005, 9-12.
2. **Bart, J., H. J. Groen, W. T. van der Graaf, H. Hollema, N. H. Hendrikse, W. Vaalburg et al.** An oncological view on the blood-testis barrier. – *Lancet Oncol*., **3**(6), 2002, 357-363.
3. **Caballero, O. L., Y. T. Chen**. Cancer/testis (CT) antigens: Potential targets for immunotherapy. – *Cancer Sci*., 100, 2009, 2014-21.
4. **Cheng, Y. H., E. W. P. Wong, C. Y. Cheng**. Cancer/testis (CT) antigens, carcinogenesis and spermatogenesis. – *Spermatogenesis*, **1**(3), 2011, 209-220.
5. **Gainetdinov, I. V., S. A. Kondratieva, Y. V. Skvortsova, M. V. Zinovyeva, E. A. Stukacheva, A. Klimov, A. A. Tryakin, T. L. Azhikina**. Distinguishing epigenetic features of preneoplastic testis tissues adjacent to seminomas and nonseminomas. – *Oncotarget*, **7**(16), 2016, 22439-47.
6. **Giagounidis, A. N., B. Hildebrandt, S. Braunstein, M. Aivado, U. Germing, M. Heinsch, C. Aul.** Testicular infiltration in acute myeloid leukemia with complex karyotype including t(8;21). – *Ann. Hematol.*, **81**, 2002, 115-118.
7. **Giver, R. L.** Testicular involvement in leukemia and lymphoma. – *Cancer*, **23**, 1969, 1290-1295.
8. **Hallak, J., A. Mahran, J. Chae, A. Agarwal**. Poor semen quality from patients with malignancies does not rule out sperm banking. – *Urol. Res*., **28**, 2000, 281-284.
9. **Hanash, K. A., J. A. Carney, P. P. Kelalis.** Metastatic tumors to testicles: routes of metastasis. – *J. Urol.*, **102**, 1969; 465-468.
10. **Ilieva. I., R. Toshkova, I. Sainova, I. Vladov, E. Zvetkova.** Histopathological changes in the testis of hamsters with experimentally induced myeloid tumor of Graffi. – *Acta Morphol. Anthropol*., **23**, 2016, 32-39.
11. **Ilieva, I. N., P. D. Tzvetkova, I. Sainova, P. S. Taushanova, M. I. Kacarov, E. B. Zvetkova**. Immature spermatogenic cells in semen fluids of infertile men. – *Compt. rend. Acad. bulg. Sci*., **69**(1), 2016, 85-94.
12. **Jakimov, M., Z. Mladenov, A. Konstantinov, I. Yanchev.** Transplantable myeloid tumor in hamsters (MTH) induced by Graffi virus. – *Gen. Compar. Pathol*., **6**, 1979, 24-35.
13. **Kamiyama, R., N. Funata.** A study of leukemic cell infiltration in the testis and ovary. – *Bull. Tokyo Med. Dent. Univ.*, **23**, 1976, 203-210.
14. **Kano, K**. Degeneration of Germ Cells in the Testes of Tumor-bearing Rats (Studies on Abnormal Nuclear Divisions. **–** *Cytologia*, **16**, 1952, 341-346.
15. **Kumar, P.V.** Testicular leukemia relapse. Fine needle aspiration findings. – *Acta Cytol*., **42**, 1998, 312-316.
16. **Lu, L. Y., J. Y. Kuo, T. L. A. Lin, Y. H. Chang, K. K. Chen, C. C. Pan, L. S. Chang**. Metastatic Tumors Involving the Testes. – *J. Urol. Roc*., **11**(1), 2000, 12-16.
17. **Nistal, M., P. Gonzalez-Peramato, R. Paniagua.** Secondary testicular tumors. – *Eur. Urol*., 16, 1989, 185-188.
18. **Peterson, L., L. P. Dehner, R. D. Brunning.** Extramedullary masses as presenting features of acute-monoblastic leukemia. – *Am. J. Clin. Pathol*., **75**, 1981, 140-148.
19. **Shaffer, D. W., H. A. Burris, T. J. O'Rourke.** Testicular relapse in adult acute myelogenous leukemia. – *Cancer*, **70**, 1992, 1541-1544.
20. **Toshkova, R.** *Attempts for immunomodulation in hamsters with transplanted myeloid tumor, previously induced by Graffi virus. PhD Thesis*, 1995, Sofia, Bulgaria, p. 168.
21. **Toshkova, R., N. Manolova, E. Gardeva, M. Ignatova, L. Yossifova, I. Rashkov, M. Alexandrov.** Antitumor activity of quaternized chitosan-based electrospun implants against Graffi myeloid tumor. – *J. Intern. Pharm*., **400** (1-2), 2010, 221-233.
22. **Valbuena, J. R., J. H. Admirant, P. Lin, L. J. Medeiros.** Myeloid sarcoma involving the testis. – *Am. J. Clin. Pathol*., **124**, 2005, 445-452.
23. **Yuceturk, C. N., B. C. Ozgur, H. Sarici, P. Borcek, O. Telli.** Testicular Involvement of Chronic Myeloid Leukemia 10 Years after the Complete Response. – *J. Clin. Diagn. Res*., **8**(4), 2014.
24. **Zvetkova, E., R. Toshkova.** Photos of monoblast from the peripheral blood of *Graffi* myeloid tumor-bearing hamster. – In: *BloodMed – Slide Athlas*, Oxford – UK, 2006. **(**http://www.bloodmed.com/home/slide.asp?id=741)

Institute of Experimental Morphology, Pathology and Anthropology with Museum
Bulgarian Anatomical Society

Acta morphologica et anthropologica, 24 (1-2)
Sofia ● 2017

Erosive Pustular Dermatosis of the Scalp

Valentina Broshtilova[1], *Mary Gantcheva*[2]

[1] *Department of Dermatology and Venereology, Faculty of Medicine, Sofia Medical University, Sofia, Bulgaria*
[2] *Institute of Experimental Morphology, Pathology and Anthropology with Museum, Bulgarian Academy of Sciences, Sofia, Bulgaria*

*Corresponding author. e-mail: mary_gant@yahoo.com

Erosive pustular dermatosis of the scalp is a rare clinical entity with unclear etiology and pathogenesis. A very few cases have been described worldwide. We present a case of a 62-year-old woman with burning pustular lesions, erosions and crusts on scalp, following a seborrheic keratosis cryotherapy, dated 6 years ago. The persisting subjective symptoms and the conventional therapeutic refractivity classified the patient as having a psychosomatic disorder. Histology examination together with a thorough work-up resumed the diagnosis. Disulone was successfully introduced. The patient improved dramatically at the end of the first month and was advised to continue the therapeutic modality for 6 months.

Key words: erosive pustular dermatosis

Introduction

Erosive pustular dermatosis, also known as erosive pustulosis and erosive pustular dermatitis of the scalp is a chronic skin condition usually affecting the scalp, presented by pustules and eroded plaques, covered with crusts [8]. Most patients are elderly men and women that have suffered previous injury, skin cancer surgery or herpes zoster. A case of epidermal growth-factor receptor inhibitor – gefitinib – induced erosive pustular dermatosis is also anecdotally described [10]. The etiology of the disease remains obscure. Possibly, it is triggered by a minor injury, followed by impaired wound healing process [4]. Although inevitable by-stander, infection is not the primary cause, since the erosive lesions persist despite antibiotic therapy. Erosive pustular dermatosis usually starts with tiny pustules on the scalp, evolving into lakes of pus, erosions and erythematous patches, covered with yellowish crusts. Extensive disease often complicates with scarring and extensive balding [2].

Case report

A 62-year-old Caucasian female reported a 6-year history of pustular lesions on the scalp that have been extended to a different level, but persist chronically together with erosions (**Fig. 1**), pus lakes and areas of scarring alopecia. The lesions evolved abruptly upon cryotherapy of seborrheic keratosis of the right temporal zone. Various therapeutic modalities have been tried during the years including topical and systemic antibiotics, topical corticosteroids and calcineurin inhibitors. The patient claimed to have burning and tingling sensation, due to which she had been referred to as having artificial dermatitis (pathomimia). Histologic examination of a skin biopsy specimen revealed a thick parakeratotic crust on top, next to superficial acantholysis at the level of spinous keratinocytic layer, atrophic epidermis and a chronic inflammatory dermal infiltrate composed of many neutrophils, lymphocytes and a few tissue macrophages in the papillary dermis (**Fig. 2**). Fibrous and thickened reticular dermis was presented with a reduced number of hair follicles. Microbiological swabs and direct immunofluorescence microscopy were negative. Her routine blood examination results were witnin normal ranges. No evidence of monoclonal gammopathy, nutrition and vitamin deficits was detected. Superficial pyoderma gangrenosum was excluded due to the absence of an underlying systemic disease. The diagnosis of erosive pustular dermatosis of the scalp was made. Systemic therapy with disulone 25 mg daily was introduced in attempt to cease neutrophilic haemotaxis at the site of inflammation. At the follow-up visit one month later the pustular lesions were replaced by atrophic scars and minor zones of cicatricial alopecia. The subjective symptoms were resolved and the patient felt in good shape. Six month-continuation of therapy was recommended.

Fig. 1. Erythema-based erosion in the front part of the capillitium

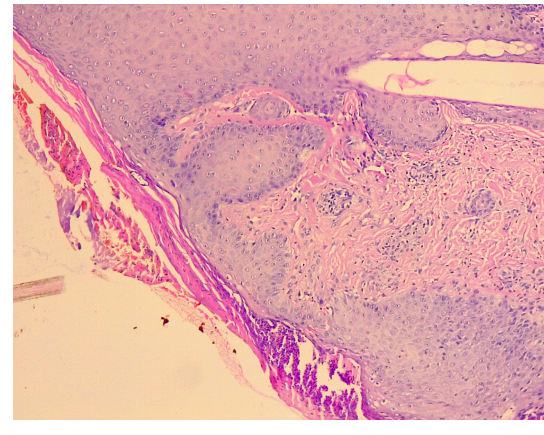

Fig. 2. Parakeratotic squamous crust, subcorneal acantolysis, neutrophil exocytosis with pronounced spongiosis of the epidermis, mixed inflammatory infiltrate with abundant polymorphonuclear cells in the papillar derma, interstitial and perivascular. Hematoxylin-eosin staining, × 400

Discussion

Erosive pustular dermatosis of the sclap (EPDS) is a rare clinical entity. Probably, it is underestimated, since there are no more than 50 cases reported worldwide. The disease usually presents with sterile pustules, erosions and crusts, developing on sun-exposed areas of scalp after a minor injury. Most cases are reported to occur after the treatment of actinic keratoses or squamous cell carcinoma by X-ray radiation therapy, skin grafting, fluorouracil cream, or topical tretinoin [3, 6, 7, 9, 11]. To our knowledge, the first case of EPDS occurring after cryotherapy of seborrhoic keratosis of the scalp is herein reported.

The etiology and pathogenesis of the disease is unclear. In all cases, histology shows profound superficial or deep dermal neutrophilic infiltrate with a spectrum of epidermal changes from atrophy, erosions and ulcerations to hyperkeratosis and irregular acanthosis. In long-standing cases hair follicles are being reduced in number and replaced by fibrous tracts. Some authors speculated that EPDS might affect the legs of patients with chronic venous insufficiency thus raising the hypothesis that ineffective wound healing process provokes the inflammatory reaction [1]. We rather consider EPDS as an entity in the spectrum of auto-inflammatory disorders.

EPDS is a diagnosis of exclusion. The clinical presentation is more superficial than the one of folliculitis decalvans, more extended than the cicatricial pemphigoid and less severe than the pyoderma gangrenous [2, 4]. However, all those entities have to be ruled out via sophisticated broad-spectrum examinations, together with a thorough work-up for an underlying systemic disease. Negative microbiological skin cultures are always expected, however, not persistently presented due to secondary super-infections.

The most provocative EPDS issue is the therapeutic implications. It is a real treatment challenge since many different modalities are being tested but none of them showed to be beneficial enough. Response of EPDS has been variable with oral isotretinoin, zinc sulfate or aspartate, dapsone and topical calcineurin inhibitors [2, 5, 6, 7]. Although topical potent corticosteroids have been reported to be the most effective, the risk of atrophy on a prolonged use is crucial [3, 5]. Our patient proved to be refractory to topical corticosteroids and tacrolimus, therefore, our treatment choice was sulfones. Disappearance of the pustular and erosive lesions was observed within 1 month. A long follow-up is needed, however, to fully judge the therapeutic effectiveness.

EPDS is a rare and rather unknown clinical entity. Patients are often classified as having psychosomatic or obsessive-compulsive disorders. The proper recognition, verification and beneficial therapeutic approach are essential for restoring the physical and emotional integrity as well as the quality of life of the affected persons.

References

1. **Bull, R., P. Mortimer.** Erosive pustular dermatosis of the leg. – *Br. J. Dermatol*., **132**, 1995, 279-282.
2. **Burton, J., R. Peachey, R. Pye.** Erosive pustular dermatosis of the scalp - a definition. – *Br. J. Dermatol*., 1988, 119-411.
3. **Ena, P., M. Lissia, G. Doneddu, G. V. Campus.** Erosive pustular dermatosis of the scalp in skin grafts: report of three cases. – *Dermatology*, **19**, 1997, 480-484.
4. **Grattan, C., R. Peachey, A. Boon.** Evidence for a role of local trauma in the pathogenesis of erosive pustular dermatosis of the scalp. – *Clin. Exp. Dermatol*., 1988, 137-140.
5. **Laffitte, E., G. Kaya, V. Piguet, J. H. Saurat.** Erosive pustular dermatosis of the scalp – treatment with topical tacrolimus. – *Arch. Dermatol*., **139**, 2003, 712-714.

6. **Layton, A., W. Cunliffe.** Erosive pustular dermatosis of the scalp following surgery. – *Br. J. Dermatol*., **132**, 1995, 472-473.
7. **Lovell, C., R. Harman, J. Bradfield.** Cutaneous carcinoma arising in erosive pustular dermatosis of the scalp. – *Br. J. Dermatol*., **103**, 1980, 325-328.
8. **Pye, R., R. Peachey, J. L. Burton.** Erosive pustular dermatosis of the scalp. – *Br. J. Dermatol.*, **100**, 1979, 559-566.
9. **Rongioletti, F., S. Delmonte, M. Rossi, G.F. Strani, A. Rebora.** Erosive pustular dermatosis of the scalp following cryotherapy and topical tretinoin for actinic keratoses. – *Clin. Exp. Dermatol*., **24**, 1999, 499-500.
10. **Toda, N., N. Fujimoto, T. Kato, N. Fujii, G. Nakanishi, T. Nagao, T. Tanaka.** Erosive pustular dermatosis of the scalp-like eruption due to gefitinib: case report and review of the literature of alopecia associated with EGFR inhibitors. – *Dermatology*, **225**, 2012, 18-21.
11. **Trueb, R, M. Krasovec.** Erosive pustular dermatosis of the scalp following radiation therapy for solar keratoses. – *Br. J. Dermatol*., **141**, 1999, 763-765.

Institute of Experimental Morphology, Pathology and Anthropology with Museum
Bulgarian Anatomical Society

Acta morphologica et anthropologica, 24 (1-2)
Sofia ● 2017

Anthropology and Anatomy

Cranial Base Angulation in Metopic and Non-metopic Cranial Series

Silviya Nikolova[1*], *Diana Toneva*[1], *Ivan Georgiev*[2,3]

[1] *Department of Anthropology and Anatomy, Institute of Experimental Morphology, Pathology and Anthropology with Museum, Bulgarian Academy of Sciences, Sofia, Bulgaria*
[2]*Department of Scientific Computations, Institute of Information and Communication Technologies, Bulgarian Academy of Sciences, Sofia, Bulgaria*
[3] *Department of Mathematical Modeling and Numerical Analysis, Institute of Mathematics and Informatics, Bulgarian Academy of Sciences, Sofia, Bulgaria*

*Corresponding author: e-mail: sil_nikolova@abv.bg

Metopic skulls possess specific distinctive characteristics in the configuration of the neurocranium. Due to the close developmental interrelation between neuro- and basicranium we assumed that the angulation of the cranial base could differ as well. This study aimed to compare the cranial base angle (CBA) in metopic and non-metopic series. The CBA was investigated in a sample of 246 skulls of contemporary adult males – 93 metopic and 156 non-metopic. Lateral projections were captured using digital radiography, performed on an industrial CT system. CBA was constructed between definite craniometric points and measured digitally. CBA was assessed as basilar kyphosis, normal and platybasia. Distribution by categories did not show significant differences between the series. Thus, despite the close interrelation between the neuro- and basicranium, the preservation of the MS connected with a specific construction of the neurocranium was not found to be related to an alteration of the basicranium expressed by CBA.

Key words: metopism, cranial base angle (CBA), platybasia, basilar kyphosis, digital radiography

Introduction

The metopic suture (MS) lies between the halves of the fetal frontal bone and is the first suture to close physiologically during the first or second year, but its fusion can last until the 8th year as well [11]. Sometimes, however, the halves of the frontal bone failed to fuse and the MS persists in adults, a condition known as *metopism* [4]. It has been established that metopic skulls usually possess a greater inter-frontal and inter-orbital

breadth [2, 3], as well as greater frontal curvature [13] compared to the the non-metopic ones. It was also ascertained that the cranial capacity in metopic skulls was slightly smaller [2, 3], as the length and height were reduced, but the breadth remains stationary. Thus, the metopic skulls attain a given capacity by a greater expansion in the forward and a smaller development in the hinder part of the vault. Therefore, the *metopism* could not be explained merely by a supposed expansion of the frontal regions of the hemispheres, but rather as an adjustment of the brain-case as a whole to its contents [3].

The brain is a major factor controlling cranial size, but is less involved as controlling force producing cranial form. Growth of the bones of the skull base has been shown to be an important factor in determining the shape of the skull [10]. According to Lieberman et al. [6], the role of the cranial base in influencing overall cranial shape is essential. It has also been determined that basicranial development is affected by changes in vault shape and vice versa [1]. The cranial base angle (CBA) expresses the orientation of the anterior versus posterior parts of the cranial base in the midsagittal plane and could vary from extreme flexion (kyphosis) to abnormal flattening (platybasia). According to the spatial packing model, since the brain grows on top of the cranial base, a more flexed (or less extended) cranial base helps to accommodate a larger volume of brain without having to change the width and length of the cranial base [8].

Because of the close interrelation between the neuro- and basicranium, and bearing in mind the general distinctions in the configuration of neurocranium in the metopic and non-metopic skulls, we assumed that the angulation of the cranial base could differ as well. However, in the relevant literature we could not find information if the preservation of the MS interacted with the cranial base angulation. Thus, the goal of this study was to compare the CBA in metopic and non-metopic cranial series.

Materials and Methods

Materials

The CBA was investigated in a sample of 246 dry skulls of contemporary adult males from Bulgaria. The skulls belonged to soldiers who died in the wars at the beginning of the 20th century. Their bone remains were preserved in the Military Mausoleum with Ossuary at the National Museum of Military History of Bulgaria. The individuals were fit for service without severe disorders and malformations. The selected sample was distributed into two series: a metopic series consisting of 93 skulls with an entirely preserved MS and a control one including 153 skulls without traces of a MS.

Methods

A digital radiography was performed on an industrial computed tomography system Nikon XT H 225, developed by Nikon Metrology. The software Inspect-X was used to adjust the parameters and manage the capture of the projections. The settings ranged dependent on the density of the specimens: voltage 85-126 kV, 80-140 μA tube current and exposure time of 500-708 ms.

All of the skulls were oriented in lateral view. The projections were captured and saved in TIFF format. To avoid the error in placement of the points on the radiographs, *nasion* and *basion* were marked in advance on the skulls with radio-dense copper markers glued at the points. Due to its internal location, *sella* was subsequently determined and marked directly on the radiographs (**Fig. 1**).

Cranial points (see **Fig. 1**):

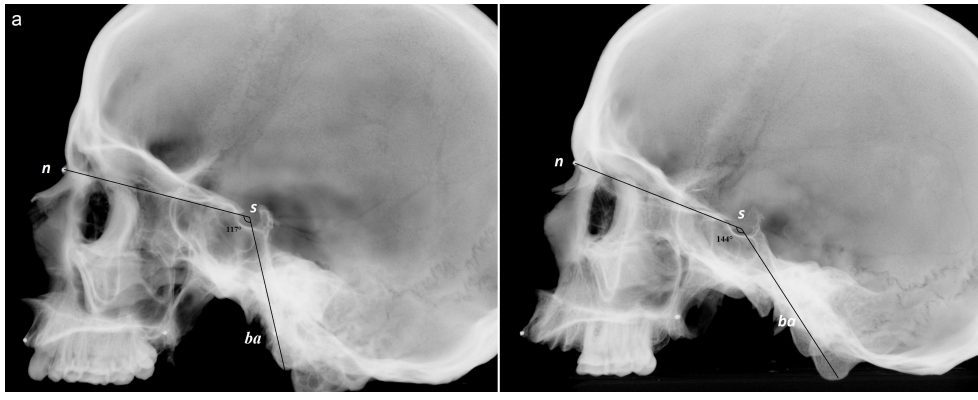

Fig. 1. Cranial base angle: a) basilar kyphosis; b) platybasia

***basion* (*ba*)**: the midsagittal point on anterior margin of foramen magnum;

***nasion* (*n*)**: the point of intersection between the frontonasal suture and the midsagittal plane;

***sella* (*s*):** the center of sella turcica, independent of contours of clinoid processes.

The CBA was constructed between the line joining nasion (*n*) with the centre of the pituitary fossa (*s*) and the line joining anterior border of the foramen magnum (*ba*) with the centre of the pituitary fossa.

The borderline values of CBA delimiting a normal from flexed and extended base angle were used after Koenigsberg et al. [5]:

1. Basilar kyphosis, an extensive flexion of the skull base, CBA < 125°
2. Normal angulation, CBA between 125-143°
3. Platybasia, an abnormal flattening of the skull base, CBA > 143°

After the CBA was constructed, the angle was digitally measured on the radiographs using ImageJ, a public domain, Java-based image processing program.

Intra- and interobserver reliability was assessed using intraclass correlation coefficient (ICC). The angle was measured twice by two observers as the replicated measurements were performed on a sample of randomly selected 30 projections. The significance of the differences in the distribution of the CBA categories was assessed using chi-square test (χ^2). The comparison between CBA in both series was performed using Independent Samples t-test.

Results

Almost perfect intra- and interobserver reliability (ICC > 0.994) was found for the CBA measurements. Basilar kyphosis was observed with almost equal frequency in both series: 7.53% (7 out of 93 skulls) in the MS series and 7.19% (11 out of 153 skulls) in the control one. A single case of platybasia (1.08%) was observed among the metopic skulls (Fig. 1b). The distribution by categories did not show significant differences between both series ($\chi^2 = 1.69$, k = 2). The CBA did not differ between the series ($p > 0.05$), even the mean values were equal (MS: min 117, max 144, mean 131.67 ± 5.43; Control: min 119, max 144, mean 131.68 ± 5.00).

Discussion

According to our preliminary unpublished data, the configuration of the neurocranium in the metopic and non-metopic series differed significantly, especially in the frontal region. The frontal bone in the metopic skulls tended to be wider, more curved with *bregma* located lower. The sutures allow the skull to change shape and grow during development. They function as signaling centers for bone growth and remain patent postnatally to accommodate cranium expansion [12]. In this point of view, the greater breadth of the frontal bone in the metopic skulls [2, 3] was explicable with the MS preservation which allows growing of the frontal bone in width.

The basicranium differs from the neurocranium and splanchnocranium as it grows mostly from endochondral ossification processes in which the chondrocranium develop *in utero* and is gradually replaced by bone postnatally. The basicranium is also the first region of the skull to reach adult size, and is the structural foundation of many aspects of the craniofacial architecture [6]. The basicranium comprises the central axis of the skull with the brain and neurocranium growing above, and the face growing below, and it provides all the necessary foramina through which the brain connects to the face and the body [8].

Angulation (flexion or extension) of the cranial base affects the relative positions of the three endocranial fossae, and thereby influences a wide range of spatial relationships among the cranial base, brain, face, and pharynx [7]. In phylogenetic aspect, in most mammals the CBA is relatively flat or obtuse, whereas in humans, it is highly flexed. In the non-human primates, the CBA varies considerably, with the ape configuration approximately intermediate between humans and other mammals in terms of the degree of basicranial flexion [8]. Ontogenetically, in gestation the basicranium initially flexes rapidly during the period of rapid hindbrain growth in the first trimester, remains fairly stable during the second trimester, and then extends during the third trimester in conjunction with facial extension, even while the brain is rapidly increasing in size relative to the rest of the cranium. The human cranial base flexes rapidly after birth, almost entirely prior to 2 years of age, before the brain has ceased to expand appreciably [7]. In the same period, the MS usually obliterates. Obviously, despite the interrelation between the developing cranial parts, failed closure of the MS, which give rise to specific configuration on the neurocranium, was not related to a different angulation of the basicranium expressed by CBA. Additional evidence for some degree of independence between the brain and cranial base during development was provided by microcephaly and hydrocephaly, in which cranial base angles tended to be close to the individuals with normal encephalization [7].

It has been established that artificial cranial deformation of an anteroposterior and a circumferential types causes slight but significant increases in the cranial base angulation with respect to the undeformed sample, as the degree of platybasia was greatest in the circumferential type [1]. Platybasia can occur in a variety of congenital disorders like craniofacial anomalies, osteogenesis imperfecta, craniocleidodysostosis and Arnold-Chiari malformation or in acquired diseases like Paget disease, osteomalacia, rickets and trauma [5]. Isolated and mild platybasia is asymptomatic and insignificantly affects the posterior fossa volume. Moderate to severe platybasia is often associated with basilar invagination, a condition in which the caudal part of the occipital bone is displaced inward and upward and the vertebral column and the skull base abnormally approximate each other [9]. Basilar invagination could be primary or congenital and secondary referred to as basilar impression, which is associated with a softening of the skull base as the result of an acquired disease [5]. In our series, a mild platybasia was found in a single case from the MS series and most probably was asymptomatic.

Conclusion

Notwithstanding the considerable distinctions in the configuration of the neurocranium in metopic and non-metopic skulls, there were no significant differences in the basicranial angulation. Thus, despite the close developmental interrelation between the neuro- and basicranium, the preservation of the MS connected with a specific construction of the neurocranium was not found to be related to an alteration in the basicranium expressed by CBA.

Acknowledgements: This study was supported by the "Program for Support for Young Scientists in Bulgarian Academy of Sciences", research grant DFNP – 73/27.04.2016. The authors would like to acknowledge the kind assistance given by the staff of the National Museum of Military History (Bulgaria).

References

1. **Anton, S. C.** Intentional cranial vault deformation and induced changes of the cranial base and face. – *Am. J. Phys. Anthropol*., **79**(2), 1989, 253-267.
2. **Ashley-Montagu, M. F.** The Medio-Frontal Suture and the Problem of Metopism in the Primates. – *The Journal of the Royal Anthropological Institute of Great Britain and Ireland*, **67**, 1938, 157-201.
3. **Bryce, T. H.** Observations on Metopism. – *J. Anat*., **51**(2), 1917, 153-166.
4. **Hauser, G., G. F. De Stefano.** *Epigenetic Variants of the Human Skull*. Stuttgart: E. Schweizerbart'sche Verlagsbuchhandlung, 1989.
5. **Koenigsberg, R. A., N. Vakil, T. A. Hong, T. Htaik, E. Faerber, T. Maiorano, M. Dua, S. Faro, C. Gonzales.** Evaluation of platybasia with MR imaging. – *AJNR Am. J. Neuroradiol*., **26**(1), 2005, 89-92.
6. **Lieberman, D. E., O. M. Pearson, K. M. Mowbray.** Basicranial influence on overall cranial shape. – *J. Hum. Evol*., **38**(2), 2000, 291-315.
7. **Lieberman, D. E., C. F. Ross, M. J. Ravosa.** The primate cranial base: ontogeny, function, and integration. – *Yearbook of Physical Anthropology*, **43**, 2000, 117-169.
8. **Lieberman, D. E., B. Hallgrímsson, W. Liu, T. E. Parsons, H. A. Jamniczky.** Spatial packing, cranial base angulation, and craniofacial shape variation in the mammalian skull: testing a new model using mice. – *J. Anat*., **212**(6), 2008, 720-735.
9. **Mohammadali, S. M. et al.** Embryology of the Craniocervical Junction and Posterior Cranial Fossa. – In: *The Chiari Malformations*. Tubbs, R. Shane, Oakes, Jerry W. (Eds.), 2013, 13-54.
10. **Pickering, S. P.** Correlation of brain and head measurements, and relation of brain shape and size to shape and size of the head. – *Am. J. Phys. Anthropol*., **15**(1), 1930, 1-52.
11. **Scheuer, L., S. Black.** *Developmental Juvenile Osteology*. London, Academic Press, 2000.
12. **Tubbs, R. S., A. N. Bosmia, A. A. Cohen-Gadol.** The human calvaria: a review of embryology, anatomy, pathology, and molecular development. – *Childs. Nerv. Syst*., **28**(1), 2012, 23-31.
13. **Woo, J.-K.** Racial and sexual differences in the frontal curvature and its relation to metopism. – *Am. J. Phys. Anthropol*., **7**(2), 1949, 215-226.

Institute of Experimental Morphology, Pathology and Anthropology with Museum
Bulgarian Anatomical Society

Acta morphologica et anthropologica, 24 (1-2)
Sofia ● 2017

Application of Digital Radiography for Examination of the Calvarial Diploic Venous Channels in Intact Dry Skulls

Silviya Nikolova[1*], *Diana Toneva*[1], *Ivan Georgiev*[2,3]

[1] *Department of Anthropology and Anatomy, Institute of Experimental Morphology, Pathology and Anthropology with Museum, Bulgarian Academy of Sciences, Sofia, Bulgaria*
[2] *Department of Scientific Computations, Institute of Information and Communication Technologies, Bulgarian Academy of Sciences, Sofia, Bulgaria*
[3] *Department of Mathematical Modeling and Numerical Analysis, Institute of Mathematics and Informatics, Bulgarian Academy of Sciences, Sofia, Bulgaria*

* Corresponding author: e-mail: sil_nikolova@abv.bg

The diploic venous channels (DVCs) are tunnels in the *diploë*, between the outer and inner tables of the cranial bones. Because of its enclosed location, the diploic venous system is challenging to study. It has been claimed that the radiological examination provides a non-destructive, simple and accurate method to inspect DVCs. In this study, we tested the application of the digital radiography for investigation of the DVCs in intact dry skulls. A series of 345 intact skulls of contemporary adult males were radiographed using an industrial computed tomography. The digital radiography was applicable for visualization of the main DVCs in intact dry skulls, but showed some limitations due to the overlaying and difficult differentiation from the grooves for the middle meningeal vessels. The main shortcoming resulted from the superimposition of structures beyond the plain of interest and the impossibility to trace the complete pattern of DVCs throughout the cranial bones.

Key words: diploic veins, diploic venous channels, digital radiography, visualization

Introduction

The diploic venous channels (DVCs) are tunnels in the *diploë*, between the outer and inner tables of the flat cranial bones, which house the diploic veins (DVs). The protected location preserves the channels from taphonomic processes and gives an opportunity for an indirect examination of this portion of the vascular tree on dry specimens. Due to their variable anatomy, the diploic venous imprints have been compared to fingerprints by their individuality and been considered "skull glyphics" [2]. Furthermore, the topographic localization of the DVs is important to prevent implications during routine neurosurgical procedures such as placement of pins, bur holes, bone drilling and craniotomies [1].

The diploic venous system (DVS) is challenging to study because of its enclosed location between two layers of hard compact bone. By this reason, studies on the DVS are scarce and the DVs are still poorly understood from anatomical, physiological, and surgical perspectives. A dissection-based direct examination of the DVs is difficult and requires an external lamina removal [1]. According to Hershkovitz et al. [2], the radiological examination provides a non-destructive, simple and accurate method to study these vascular channels. In this study, we tested the application of the digital radiography for visualization of the DVCs in intact dry skulls for examination of their distribution and branching pattern through the calvarial bones.

Materials and Methods

A series of 345 intact dry skulls of contemporary adult males from Bulgaria were investigated. The skulls belonged to soldiers who died in the wars at the beginning of the 20th century and were kept in the Military Mausoleum with Ossuary at the National Museum of Military History of Bulgaria. The skulls were digitally radiographed using an industrial computed tomography system Nikon XT H 225, developed by Nikon Metrology. The Inspect-X software was used to adjust the parameters and manage the capture of the projections. The settings ranged dependent on the density of the specimens: voltage 85-126 kV, 80-140 μA tube current and exposure time of 500-708 ms.

The skulls were oriented in lateral and posteroanterior (PA) views (**Fig. 1a, b**). Most of the PA radiographs were captured within the range considered a "Caldwell view", i.e. the skulls were angled in the interval of 15-20° towards the Frankfurt plane (FH). Using the tilt function of the manipulator, selected skulls in the PA view (n=10) were inclined from Frankfurt plane (FH) up to +45° (Waters' view) at an interval of 5 degrees (**Fig. 2**). Trying to avoid the superimposition, selected skulls were also inclined under various degrees in different positions, and the oblique projections were captured. Moreover, we injected a radiographic contrast agent (urografin) into DVCs of a sec-

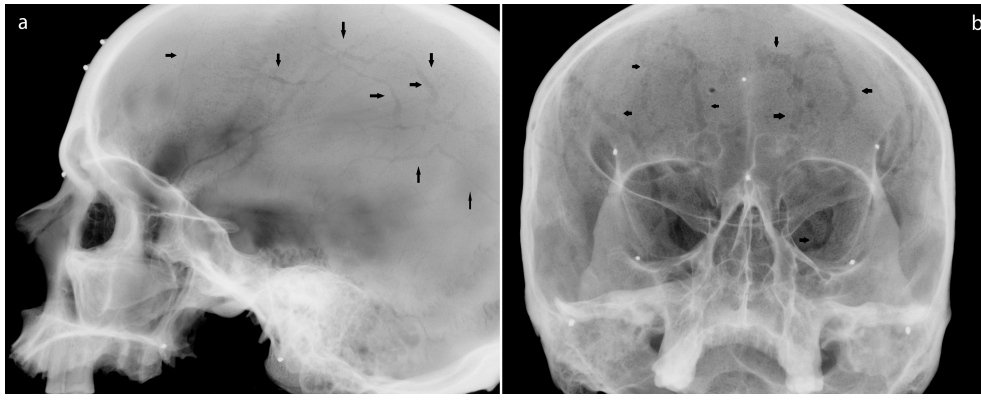

Fig. 1. Skull projections: a) lateral view; b) posteroanterior view. The diploic venous channels were indicated with arrows

Fig. 2. Posteroanterior views: a) at the Frankfurt plane (0˚); b) inclined to +10˚; c) inclined to +25˚; d) inclined to +40˚. The diploic venous channels were indicated with asterisk

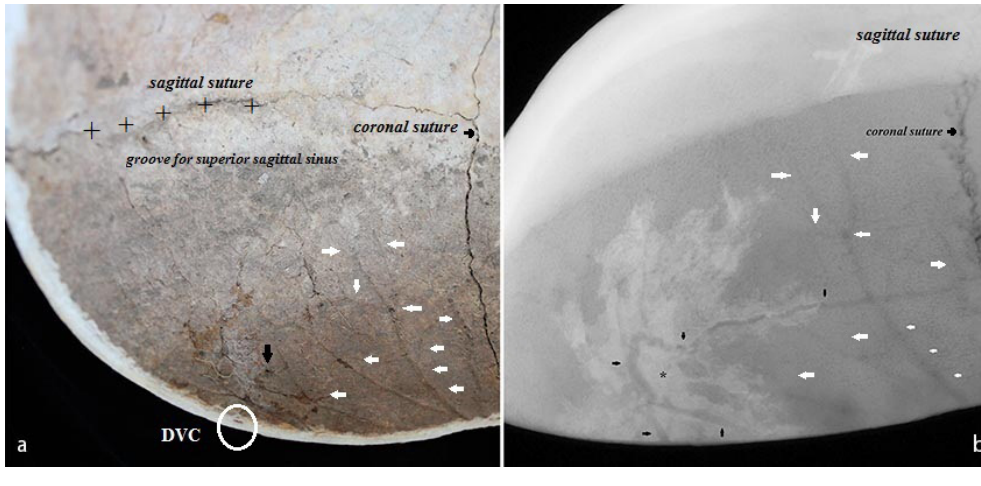

Fig. 3. A sectioned calvaria: a) an image of the internal aspect; b) a radiograph after injection with a radiocontrast agent. Indications: diploic venous channels (DVCs, black arrows); grooves for middle meningeal vessels (white arrows); radiocontrast agent (asterisk); groove for superior sagittal sinus (plus signs)

tioned calvaria which was subsequently radiographed (**Fig. 3a, b**). The sectioning level lied at the parietal bones above *lambda* and both temporal squamas and trough the frontal eminences. All of the generated projections were saved in TIFF format.

Results and Discussion

The digital radiography has many advantages compared to the conventional one like rapidity, effectiveness, inexpensiveness, short expositions, immediate inspection, transfer, processing and storage of the generated images. The digital radiography also allows rapid and accurate radiographic documentation of large samples.

Generally, the 2D radiography of an intact dry skull causes a superimposition of the shadows beyond the plain of interest on the obtained image. The plain radiography could be of benefit in cases of sectioned skulls in the sagittal or transversal plain, as in such manner the superimposition would be avoided (Jefferson and Stewart, 1928; Hershkovitz et al., 1999).

In a lateral projection of an intact skull, the main DVCs were visible and distinguishable from the grooves for the middle meningeal vessels (**Fig. 1a**). The finer ones, however, could be easily confused with the grooves even following the recommendations of Jefferson and Stewart [3] for their demarcation. Furthermore, the right and left DVCs superimposed and their delimitation was difficult as well (**Fig. 1a**). In a PA projection, the frontal DVCs were visible, but the superimposition impeded visualization of the occipital ones (**Fig. 1b**). Furthermore, the inclination of the skull at an interval of 5° showed that the optimal visualization of the DVCs was between FH (0°) and +25° (**Fig. 2**). The oblique projections were useful for distinguishing of the DVCs. However, the overall distribution, places of anastomoses and branching pattern of the DVCs in the cranial bones could not be clearly traced and determined.

For better visualization of the DVCs, we injected a radiocontrast agent into a sectioned skull as it was suggested by Hershkovitz et al. [2]. A subsequent radiography revealed that the substance soaked up into the surrounding diploic space instead to accumulate in the channel itself. In this way, the contrast outlines the DVCs, but does not differentiate them from the grooves for middle meningeal vessels on the inner table (**Fig. 3b**). Our observations showed that this approach was not easily applicable to a sectioned skull part and entirely impracticable for an intact skull.

Illumination of the skull from within has also been used for DVCs inspection [5]. A superior non-destructive method for visualization of the DVS is the volumetric imaging obtained by patients undergoing magnetic resonance (MR) and computed tomography (CT) scanning with radiocontrast agents [1, 4]. Besides the advantages of the 3D imaging, the low resolution appears to be the main shortcoming. However, scanning of dry skulls using micro-computed tomography (μCT) could generate high resolution 3D images. Segmentation of the DVS from such models is a challenge and an objective of further examinations.

Based on our experience, we could conclude that the digital radiography was applicable for visualization of the main DVCs in intact dry skulls, but showed some limitations due to the overlaying and difficult differentiation from the grooves for middle meningeal vessels. The main shortcoming to examine the DVCs resulted from the superimposition of structures beyond the plain of interest and the impossibility to trace the complete pattern of distribution throughout the cranial bones.

Acknowledgements: This study was supported by the "Program for Support for Young Scientists in Bulgarian Academy of Sciences", research grant DFNP – 73/27.04.2016. The authors would like to acknowledge the kind assistance given by the staff of the National Museum of Military History (Bulgaria).

References

1. **García-González, U., D. D. Cavalcanti, A. Agrawal, et al.** The diploic venous system: surgical anatomy and neurosurgical implications. – *Neurosurg. Focus*, **27**, 2009, E2.
2. **Hershkovitz, I., C. Greenwald, B. M. Rothschild, B. Latimer, O. Dutour, L. M. Jellema, et al.** The elusive diploic veins: anthropological and anatomical perspective. – *Am. J. Phys. Anthropol*., **108**, 1999, 345-358.
3. **Jefferson, G., D. Stewart.** On the veins of the diploë. – *The British Journal of Surgery*, **16**(61), 1928, 70-88.
4. **Jivraj, K., R. Bhargava, K. Aronyk, A. Quateen, A. Walji.** Diploic venous anatomy studied in-vivo by MRI. – *Clin. Anat*., **22**, 2009, 296-301.
5. **Lang, J.** *Clinical Anatomy of the Head*. Springer, 1983.

Institute of Experimental Morphology, Pathology and Anthropology with Museum
Bulgarian Anatomical Society

Acta morphologica et anthropologica, 24 (1-2)
Sofia ● 2017

Accuracy of Linear Measurements on Polygonal Models of Dry Mandibles Generated from Industrial CT Data

Diana Toneva[1], *Silviya Nikolova*[1], *Ivan Georgiev*[2,3]

[1] *Institute of Experimental Morphology, Pathology and Anthropology with Museum, Bulgarian Academy of Sciences, Sofia, Bulgaria*
[2] *Institute of Information and Communication Technologies, Bulgarian Academy of Sciences, Sofia, Bulgaria*
[3] *Institute of Mathematics and Informatics, Bulgarian Academy of Sciences*, *Sofia, Bulgaria*

*Corresponding author: e-mail: ditoneva@abv.bg

The aim of the study was to assess the accuracy of linear measurements taken on surface models of dry mandibles generated from industrial CT data compared to the corresponding measurements taken directly on the mandibles. Ten mandibles were scanned through computed tomography. The CT scanning was performed on a Nikon XTH 225 system. The polygonal models were generated using VGStudio-Max 2.2. Ten linear measurements were taken on both dry mandibles and 3D models. The conventional measurements were taken with a digital caliper. The digital measurements were obtained using Geomagic Verify Viewer. All parameters were measured twice by two observers. Almost perfect intra- and interobserver reliability was obtained for all digitally and directly taken measurements. The repeated measures ANOVA did not establish statistically significant differences between both measuring methods for any of the metric parameters. The overall absolute error was 0.37 mm and the overall relative error was 1.00%.

Key words: mandible, CT, polygonal model, measurements, accuracy

Introduction

Industrial computed tomography (CT) is an appropriate method for data acquisition of complex objects. It gives accurate representation of shape at high resolution, but the accessibility to this kind of CT scanners is limited. The very large file size of the 3D volume-rendered images is another shortcoming. The surface models generated from CT data enable a reduction of the size of the file maintaining an acceptable level of details. However, one of the most critical factors influencing the CT process for metrology applications and causing loss of accuracy during CT measurements is the edge detection also called surface extraction or image segmentation, which is the process of surface formation from the CT volume data [17]. Thus, the precise surface determination is es-

sential for nearly all kinds of CT analyses [21], since size and shape differences could appear in the process of segmentation.

The accuracy of linear measurements of the mandible and maxillofacial region has been assessed using different imaging technologies, because of their significance in the maxillofacial surgery and orthodontic practice. Nowadays, cone-beam CT (CBCT) is widely used in dental practice, because of its advantages over conventional CT, including higher resolution, short scanning time and reduced radiation exposure. Thus, it has been increasingly reported recently. The accuracy of CBCT measurements of the mandible has been assessed on 2D tomographic slices and 2D virtual cephalographic images [7, 8, 9, 10, 11, 13, 24], 3D volume-rendered CBCT images [1, 7, 10, 16, 18, 23], and 3D surface-rendered CBCT images generated through segmentation and thresholding method [3, 4, 5, 8, 20, 22]. Some of the authors showed a tendency for the CBCT measurements to underestimate the direct ones [1, 3, 4, 23]. Glover and Pelc [6] have explained the underestimation and overestimation in the CBCT measurements with so-called partial volume effect, which occurs when a voxel is occupied by two structures with different densities, and the voxel reflects an average density value. However, Ye et al. [26] have suggested that the choice of the threshold value during the segmentation procedure was a more acceptable reason for underestimation of the measurements. Engelbrecht et al. [5] have also noticed that when threshold-based methods were used, the 3D surface models produced by CBCT were accurate but slightly inferior to reality. Although there have been a lot of studies about the accuracy of mandibular measurements, it was not tested on virtual models generated through industrial CT.

The aim of this study was to assess the accuracy of linear measurements taken on polygonal models of dry mandibles generated from industrial CT data in comparison to the directly taken mandibular measurements.

Materials and Methods

The study was conducted on a sample of 10 dry mandibles from the Military Mausoleum with Ossuary, National Museum of Military History, Bulgaria. The mandibles were scanned through computed tomography. The scanning was performed on an industrial CT system Nikon Metrology XT H 225 with reflection head and a voltage of 85 kV and 95 μA tube current. To generate a 3D CT volume, a series of sequential 2D X-ray images (projections) were captured as the object was rotated through 360°. For each scan 3000 projections were registered, as each projection was taken with an exposure time of 500 ms. The polygonal models in STL format were generated from voxel data by automatic surface determination and surface extraction using VG Studio Max 2.2 software. Automatic surface determination is suitable for volumes containing object with only one material. Usually in such cases the histogram consists of two peaks - the background peak and the material peak. The isosurface value is calculated as an average of the two gray values corresponding to two peaks.

Ten linear measurements between definite landmarks described according to Martin and Saller [14] were taken on both dry mandibles and polygonal models (**Table 1**).

The conventional measurements of the mandibles were obtained using a digital caliper (Würth, Germany) with accuracy to 0.03 mm. The digital measurements were accomplished on the 3D models using the free software Geomagic Verify Viewer (3D Systems, Inc). All parameters were measured twice by two observers. The 1st and 2nd measurements of all samples were taken on separate days.

The intra- and interobserver reliability was estimated using intraclass correlation coefficient (ICC), two-way mixed model. The absolute and relative errors were calcu-

Table 1. Mandibular measurements

Measurements		Definition
M1	kdl (R) – kdl (L)	The direct distance between the left and right kondilion laterale (kdl)
M2	kdm (R) –kdm (L)	The direct distance between the left and right kondilion mediale (kdm)
M3	kr (R) – kr (L)	The direct distance between the left and right koronion (kr)
M4	go (R) – go (L)	The direct distance between the left and right gonion (go)
M5	ml (R) – ml (L)	The direct distance between both landmarks mentale (ml)
M6	id-gn	The direct distance from infradentale (id) to gnation (gn)
M7	kdl (L) -kdm (L)	The direct distance between left kondilion laterale and left kondilion mediale
M8	id-kr (L)	The direct distance from infradentale to the left koronion
M9	id-kdl (L)	The direct distance from infradentale to the left kondilion laterale
M10	id-kdm (L)	The direct distance from infradentale to the left kondilion mediale

(R) – right; (L) – left

lated. The absolute error represented the difference between digital and direct measurements. The relative error was calculated as an index of the absolute error related to the direct measurements multiplied by 100. The comparison between both digital and conventional measurements was performed using with repeated measures ANOVA. Values of $p < 0.05$ were considered significant.

Results

Reliability

Almost perfect intra- and interobserver reliability (> 0.8) was found for all digitally and directly taken measurements. The intraobserver ICCs for the digital measurements ranged from 0.932 to 0.999 for the first observer and from 0.961 to 0.999 for the second one. The intraobserver ICCs for the direct measurements ranged from 0.974 for the first observer and from 0.966 for the second one up to 0.999. Interobserver ICC values were within 0.917-0.999 for the digital measurements and 0.969-0.999 for the direct ones. The most reliable measurement was M1 and the measurement with lower ICC values was M10.

Accuracy

The means and SD of the digital and direct measurements are presented in **Table 2**. Because of the high agreement in the measurements within and between the observers, the assessment of the differences between digital and direct measurements was based on the combined repeated measurements of both observers for each measuring method.

The overall absolute error was 0.37 ± 0.96 mm, as 7 of the 10 distances had lower values on polygonal models. The smallest error was observed for the M9 and the grea-

Table 2. Means and SD of the digital and direct measurements. Comparison of the measurements using repeated measures ANOVA

Measurements	Digital measurements		Direct measurements		*F*-value*	*p*-value
	Mean	SD	Mean	SD		
M1	116.16	7.12	116.96	7.09	0.060	0.810
M2	80.33	5.80	79.70	5.87	0.054	0.819
M3	93.09	3.79	92.45	4.35	0.115	0.738
M4	99.38	4.58	100.48	4.63	0.266	0.613
M5	44.72	2.67	44.88	2.54	0.018	0.894
M6	30.95	2.14	32.65	1.82	3.487	0.078
M7	18.79	2.22	19.53	2.34	0.499	0.489
M8	82.51	3.57	82.67	3.98	0.008	0.929
M9	107.56	2.54	107.49	2.89	0.004	0.953
M10	103.18	2.12	103.51	2.31	0.112	0.742

*Degrees of freedom (df) for each *F*-ratio are (1.18).

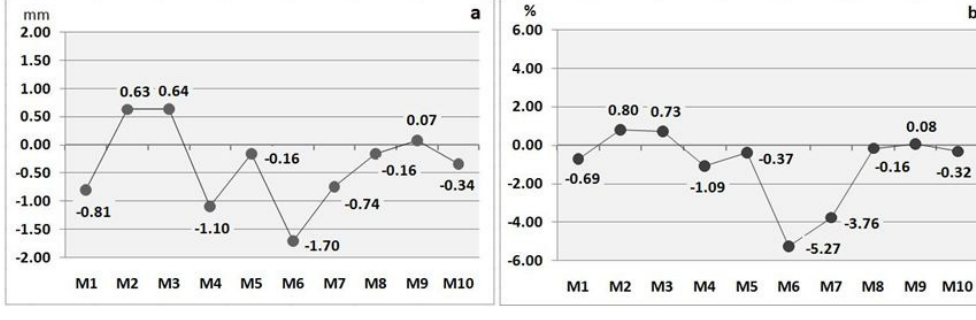

Fig. 1. Measurement errors: a) Absolute measurement errors; b) Relative measurement errors

test one for the M6 (**Fig. 1a**). The overall relative error was 1.00 ± 1.97%. The biggest relative errors (> 3%) were obtained for the measurements M6 and M7 (**Fig. 1b**).

The factorial repeated measures ANOVA did not show statistically significant size differences between polygonal models and dry mandibles (**Table 2**).

Discussion

The comparison between linear measurements taken on polygonal models derived from industrial CT data and dry mandibles did not show statistically significant differences. Statistically non-significant differences have been also established between the 3D CBCT and direct measurements by Baumgaertel et al. [1], Gribel et al. [7], Kamburoglu et al. [10], Tarazona-Álvarez et al. [23]. However, Periago et al. [18] and Brown et al. [3] have found that most of the 3D measurements differed significantly from those

on dry skulls. Rieth-Hoerst et al. [21] have established that the conversion from voxel data into STL resulted in a measurement deviation ≥ 1/10 of a voxel for 20% of the measurements and some deviations added a measurement uncertainty of more than 5% compared to the voxel data. In our study, a relative measurement error > 5% in relation to the direct measurements was established only for the mandibular height (M6), which was the most differing variable between both measuring methods. Pinsky et al. [19] have also found the largest error in height measurements on the mandible. However, because of the lack of other vertical measurements in our study, it could not be assessed if this difference was due to the concrete measurement or was a result affecting the mandibular heights as a whole.

The 3D measurements on surface models are susceptible to errors connected with the landmark location on the virtual models as well as with the choice of the operator or software on the threshold in the process of segmentation. Some studies are conducted on objects marked with different kind of fiducial markers [2, 7, 12, 20]. Gribel et al. [7] have noticed that the use of fiducial markers leads to higher accuracy, but their size, material, and shape in combination with the scan resolution can influence the results. Brown et al. [3] have suggested that the landmark identification on the 3D rendering without the aid of radiopaque fiducial markers is a more representative simulation of the clinical situation and provides a combined assessment of 3D landmark identification error and error due to imaging procedure. In the present study, similar to these of Baumgaertel et al. [1], Hilgers et al. [9] and Periago et al. [18], such markers were not used, so the differences could be referred to the landmark location and segmentation error. The agreement in the measurements of both observers indicated that measurements were reliable with almost perfect intra- and interobserver reliability. In other studies with and without use of fiducial markers, the intra- and interobserver reliability was also found to be almost perfect [1, 7, 10, 16, 18]. In our previous study [25], the technical error of measurement was reported on the same sample and results showed that the largest total relative technical error was observed for the measurements demonstrating the largest relative measurement errors (M6 and M7) in the present study. Actually, landmarks of reference such as gnathion located on a prominence or curvature have been previously reported as difficult for identification [15]. However, it should be noticed that the measurement imprecision in our study was in the acceptable limits, so the landmark location could have led to greater inaccuracy but to a certain degree.

Concerning the segmentation process, Periago et al. [18] have summarized that it could be influenced by the software algorithm, the contrast resolution of the scan, the thickness and degree of calcification of the bony structure, and the technical skills of the operator. It should be taken into account that results obtained in our study were derived from scanning of dry mandibles with an industrial CT scanner and the bone surface was extracted from high-resolution 3D CT data (**Fig. 2**), unlike the segmentation performed on patients CT scans. The image quality could severely affect the segmentation results. Periago et al. [18] have noticed that the image quality from medical CT scanners decreases because of soft tissue attenuation, patient motions, number of basis projection images, voxel size, etc. Although Periago et al. [18] have assessed the accuracy on 3D surface-rendered images of dry skulls, 50% of the measurements had a mean difference between 1 mm and 2 mm and 10% differed with more than 2 mm. Measurement errors up to 1 mm have been reported as clinically acceptable for diagnosis and planning [4]. In our study, four of the 10 measurements differed with less than 0.5 mm, four of them had measurement errors between 0.5 mm and 1 mm and the measurement errors for the other two measurements (M4 and M6) were between 1 mm and 2 mm.

According to Poleti et al. [20], the 3D surface models segmented from CBCT data have been reported as accurate models of the real objects with reliable and accurate

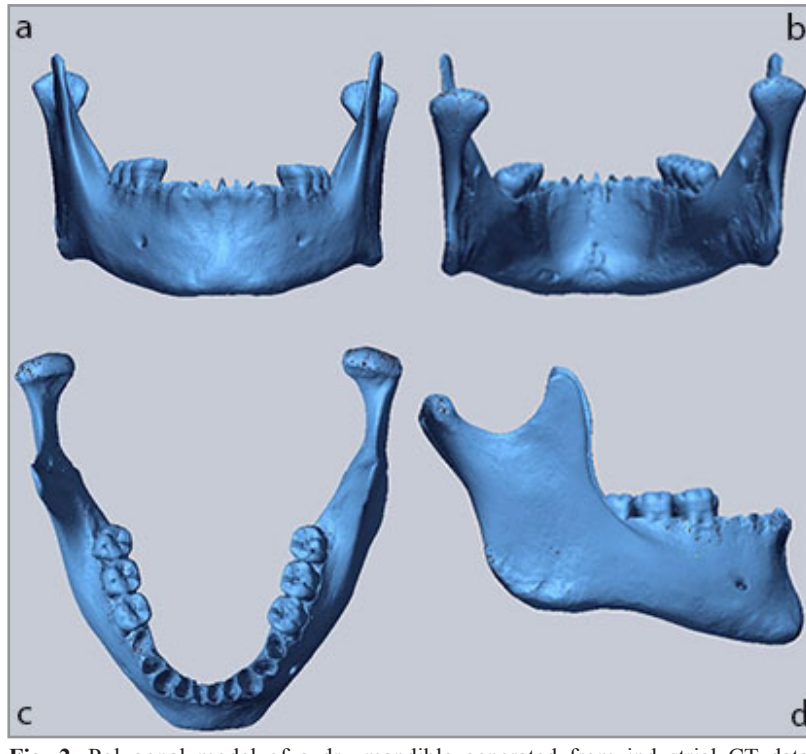

Fig. 2. Polygonal model of a dry mandible generated from industrial CT data: a) Anterior view; b) Posterior view; c) Superior view; d) Lateral view

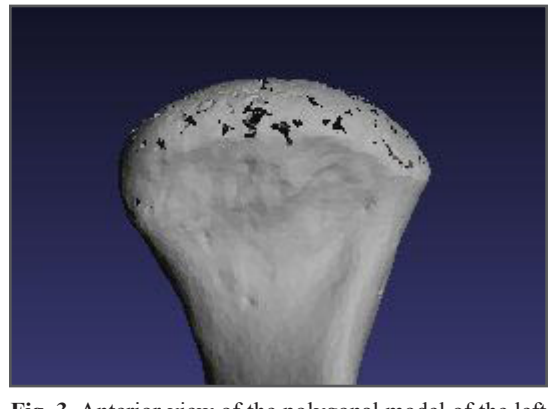

Fig. 3. Anterior view of the polygonal model of the left mandibular condyle after surface extraction from industrial CT data

linear measurements compared to the physical ones. However, Engelbrecht et al. [5] have suggested the need of a more advanced segmentation technique especially at the condylar region and the lingual side of the mandible. According to our observations, the condyle was also affected by the surface extraction process, but it did not lead to statistically significant differences from the direct measurements (**Fig. 3**).

Conclusion

As a whole, the polygonal models generated from industrial CT data were established to represent accurate copies of the scanned objects. The linear measurements obtained from the polygonal models were reliable and accurate compared to the directly taken ones.

Acknowledgement: This study was supported by the "Program for Support for Young Scientists in Bulgarian Academy of Sciences", research grant DFNP – 75/27.04.2016. The authors would like to acknowledge the kind assistance given by the staff of the National Museum of Military History, Bulgaria.

References

1. **Baumgaertel, S., J. Martin, L. Palomo, M. G. Hans.** Reliability and accuracy of cone-beam computed tomography dental measurements. – *Am. J. Orthod. Dentofacial. Orthop*., **136**, 2009, 19-28.
2. **Berco, M., P. H. Rigali Jr, R. M. Miner, S. DeLuca, N. K. Anderson, L. A. Will**. Accuracy and reliability of linear cephalometric measurements from cone-beam computed tomography scans of a dry human skull. – *Am. J. Orthod. Dentofacial. Orthop*., **136**, 2009, 11-19.
3. **Brown, A. A., W. C. Scarfe, J. P. Scheetz, A. M. Silveira, A. G. Farman.** Linear accuracy of cone beam CT 3D images. – *Angle Orthod*., **79**, 2009, 150-157.
4. **Damstra, J., Z. Fourie, J. J. Huddleston Slater, Y. Ren.** Accuracy of linear measurements from cone-beam computed tomography-derived surface models of different voxel sizes. – *Am. J. Orthod. Dentofacial. Orthop*., **137**, 2010, 1-7.
5. **Engelbrecht, W. P., Z. Fourie, J. Damstra, P. O. Gerrits, Y. Ren.** The influence of the segmentation process on 3D measurements from cone beam computed tomography-derived surface models. – *Clin. Oral Investig*., **17**, 2013, 1919–1927.
6. **Glover GH, Pelc NJ.** Nonlinear partial volume artefacts in X-ray computed tomography. – *Med Phys*., **7**, 1980, 238-248.
7. **Gribel, B. F., M. N. Gribel, D. C. Frazäo, J. A. McNamara Jr, F. R. Manzi.** Accuracy and reliability of craniometric measurements on lateral cephalometry and 3D measurements on CBCT scans. – *Angle Orthod*., **81**, 2011, 2635.
8. **Hassan, B., P. van der Stelt, G. Sanderink.** Accuracy of three dimensional measurements obtained from cone beam computed tomography surface-rendered images for cephalometric analysis: influence of patient scanning position. – *Eur. J. Orthod*., **31**, 2009, 129–134.
9. **Hilgers, M. L., W. C. Scarfe, J. P. Scheetz, A. G. Farman.** Accuracy of linear TMJ measurements with cone beam computed tomography and digital cephalometric radiography. – *Am. J. Orthod. Dentofacial. Orthop*., **1278**, 2005, 803-811.
10. **Kamburoğlu, K., E. Kolsuz, H. Kurt, C. Kiliç, T.** Özen**, C. S. Paksoy.** Accuracy of CBCT measurements of a human skull. – *J. Digit. Imaging*, **24**, 2011, 787-793.
11. **Kumar, V., J. B. Ludlow, A. Mol, L. Cevidanes.** Comparison of conventional and cone beam CT synthesized cephalograms. – *Dentomaxillofacial Radiology*, **36**, 2007, 263-269.
12. **Lagravere, M. O., J. Carey, R. W. Toogood, P. W. Major.** Threedimensional accuracy of measurements made with software on cone-beam computed tomography images. – *Am. J. Orthod. Dentofacial. Orthop*., **134**, 2008, 112-116.
13. **Ludlow, J. B., W. S. Laster, M. See, L. J. Bailey, H. G. Hershey.** Accuracy of measurements of mandibular anatomy in cone beam computed tomography images. – *Oral Surg. Oral Med. Oral Pathol. Oral Radiol. Endod*., **103**, 2007, 534-542.
14. **Martin, R., K. Saller.** Kraniometrische Technik. – In: *Lehrbuch der Anthropologie* (Eds R. Martin, K. Saller), Band I, Stuttgart, Gustav Fischer, 1957.
15. **Medelnik, J., K. Hertrich, S. Steinhäuser-Andresen, U. Hirschfelder, E. Hofmann.** Accuracy of anatomical landmark identification using different CBCT- and MSCT-based 3D images. An in vitro study. – *J. Orofac. Orthop*., **72**, 2011, 261-278.

16. **Moreira, C. R., M. A. Sales, P. M. Lopes, M. G. Cavalcanti.** Assessment of linear and angular measurements on three-dimensional cone-beam computed tomographic images. – *Oral Surg. Oral Med. Oral Pathol. Oral Radiol. Endod*., **108**, 2009, 430-436.
17. **Ontiveros-Zepeda, S., J. A. Yagüe-Fabra, R. Jiménez Pacheco, F. J. Brosed-Dueso**. A Comparative of 3D Surface Extraction Methods for Potential Metrology Applications. – *Key Engineering Materials*, **615**, 2014, 15-21.
18. **Periago, D. R., W. C. Scarfe, M. Moshiri, J. P. Scheetz, A. M. Silveira, A. G. Farman.** Linear accuracy and reliability of cone beam CT derived 3-dimensional images constructed using an orthodontic volumetric rendering program. – *Angle Orthod*., **78**, 2008, 387-395.
19. **Pinsky, H. M., S. Dyda, R. W. Pinsky, K. A. Misch, D. P. Sarment.** Accuracy of three-dimensional measurements using cone-beam CT. – *Dentomaxillofac. Radiol*., **35**, 2006, 410-416.
20. **Poleti, M. L., T. M. Fernandes, O. Pagin, M. R. Moretti, I. R. Rubira-Bullen.** Analysis of linear measurements on 3D surface models using CBCT data segmentation obtained by automatic standard pre-set thresholds in two segmentation software programs: an in vitro study. – *Clin. Oral Invest*., **20**(1), 2016, 179-185.
21. **Rieth-Hoerst, S., C. Reinhart, T. Günther, T. Dierig, J. Fieres.** Methods to ensure accuracy and reliability of analyses and measurements done on CT data-sets. – *Proceedings of 11th European Conference on Non-Destructive Testing*, Prague, Czech Republic, 2014.
22. **Stratemann, S. A., J. C. Huang, K. Maki, A. J. Miller, D. C. Hatcher.** Comparison of cone beam computed tomography imaging with physical measures. – *Dentomaxillofac. Radiol.*, **37**, 2008, 80-93.
23. **Tarazona-Álvarez, P., J. Romero-Millán, D. Peñarrocha-Oltra, M. Á. Fuster-Torres, B. Tarazona, M. Peñarrocha-Diago.** Comparative study of mandibular linear measurements obtained by cone beam computed tomography and digital calipers. – *J. Clin. Exp. Dent*., **6**(3), 2014, e271-e274.
24. **Tomasi C., E. Bressan, B. Corazza, S. Mazzoleni, E. Stellini, A. Lith.** Reliability and reproducibility of linear mandible measurements with the use of a cone-beam computed tomography and two object inclinations. – *Dentomaxillofac. Radiol*., **40**, 2011, 244-250.
25. **Toneva D., S. Nikolova, I. Georgiev, A. Tchorbadjieff.** Intra- and interobserver measurement error of linear measurements on three-dimensional computed tomography models of dry mandibles. – *Acta Morphologica et Anthropologica*, **23**, 2016, 102-110.
26. **Ye, N., F. Jian, W. Lai.** Effect of voxel size and partial volume effect on accuracy of tooth volumetric measurements with cone beam CT. – *Dentomaxillofac. Radiol*., **42**, 2013, 20130070.

Institute of Experimental Morphology, Pathology and Anthropology with Museum
Bulgarian Anatomical Society

Acta morphologica et anthropologica, 24 (1-2)
Sofia ● 2017

Hand Grip Strength in Prepubescent Tennis Players

(Preliminary study)

*Albena Dimitrova**

Institute of Experimental Morphology, Pathology and Anthropology with Museum, Bulgarian Academy of Sciences, Sofia, Bulgaria

*Corresponding author: e-mail: albena_84 @abv.bg

The aim of the present study is to investigate a grip strength in young male tennis players aged 9-11 years. A total of 39 children (15 tennis players and 24 pupils) took part in the study. All participants were assessed for height, weight and BMI. The grip strength was measured by hand dynamometer in kilograms-force at both (dominant and non-dominant) upper limbs. Statistical analysis was made by SPSS 16.00 for Windows. The measuring showed that sportsmen have higher values on right upper limb hand grip strength than the control group (11.8 kg and 8.00 kg). There are similar results on the left upper limb: 7.79 kg (athletes) and 6.92 kg (non-athletes). A considerably higher difference of hand grip strength between the right and left hand was discovered in athletes (3.67kg.), compared to the control group (0.87 kg). The correlation is significantly higher between the left hand grip strength and body mass index ($p < 0.01$), weight and hand grip strength on the left hand ($p < 0.05$), and height and right hand grip strength ($p < 0.05$) in athlete group. Only in non-athlete group there is a high level of correlation between right and left hand grip strength ($p < 0.01$).

Key words: tennis players, prepubescent children, grip strength, BMI

Introduction

Hand grip strength (HGS) is often used as an indicator of physical strength and of individual hand and forearm muscle performance [4, 6]. It is important for any sport in which the hands are used for catching, throwing or lifting. Tennis is a sport that required mainly the use of hand, because excellent upper extremity power and hand grip strength are necessary to be successful. Without adequate grip and forearm strength, tennis players may run the risk of developing lateral epicondylitis [8].

The handgrip strength meassurement is also widely used to assess the assymetry between the dominant and non-dominant hand in the tennis players [5]. Hand grip strength is affected by a different factors including age, gender and body size. Some investigations report that there is a strong correlation between the hand grip strength and basic anthropological features like height, weight and etc. [3, 4].

The aim of the present study is to investigate the hand grip strength in young male tennis players aged 9-11 years.

Materials and Methods

A total of 39 children (15 tennis players and 24 pupils) aged 9-11 years took part in the study. All children were in good health in the day of assessment and declared that they were not presented any injury in the upper limbs for at least two months.The parents of the participants were informed about aim and methodology of the study and they were signed a consent (regarding Helsinki declaration). Individuals completed questionnaire regarding hours of training per week and training years. Basic anthropometric features: height (HT, cm), weight (WT, kg) were measured by Martin-Saller's classical methods. A hand grip test (European Test of Physical Fitness - EUROFIT) was performed to defined static arm strength [2]. The right hand grip strength (RHGS, kg) and left hand grip strength (LHGS, kg) were measured using a standard calibrated handgrip dynamometer at standing position with the shoulder adducted and neutrally rotated and elbow in full extension. The subjects were asked to put maximum force on the dynamometer thrice from both sides of the hands. The best scores were recorded in kilograms. Body Mass Index (BMI, kg/m^2) was calculated by the formula: Body Mass Index = Weight/Height^2, for each child.

Statistical analysis was made by software package SPSS 16.00 for Windows. Statistically significant differences were evaluated by T-test of Student at $P \leq 0.05$. Correlation analysis was used for the assessment of relationship between anthropometric variables.

Results

The mean age for tennis players is 10.20 ± 0.86 and 9.88± 0.85 for control group. A training experience (TE) for athletes are distributed in three categories: TE (years); TE (days/weekly); TE (hours/daily) (**Table 1**). The handedness of the individuals is defined by questionnaire regarding, and showed that 80% of investigated tennis players are right handed and 20 % are left-handed. Result is similar in the control group: 87% are right handed and 13 % - left-handed.

The anthropometric characteristics (height, weight and BMI) in tennis players and control group are presented in **Table 2**. There are significant differences in height ($p < 0.01$) between both investigated groups, but there are no significance in values of weight and BMI.

Table 1. Age and training experiences of participants

Variables	Tennis players (n = 15)		Control group (n = 24)	
	mean	SD	mean	SD
Age (years)	10.20	0.86	9.88	0.85
TE (years)	3.88	1.46	–	–
TE (days/weekly)	4.08	1.44	–	–
TE (hours/daily)	1.66	0.44	–	–

TE – Training experience

Table 2. Anthropometric characteristic of tennis players and control group

Variables	Tennis players (n = 15)		Control group (n = 24)		Differences
	mean	SD	mean	SD	T-test
HT	146.80	6.78	127.00	6.22	9.12*
WT	38.78	7.66	38.88	8.74	0.001
BMI	17.93	2.40	18.52	3.21	-1.43

* Statistically significant differences at $p \leq 0.01$;
HT – height; WT – weight; BMI – body mass index.

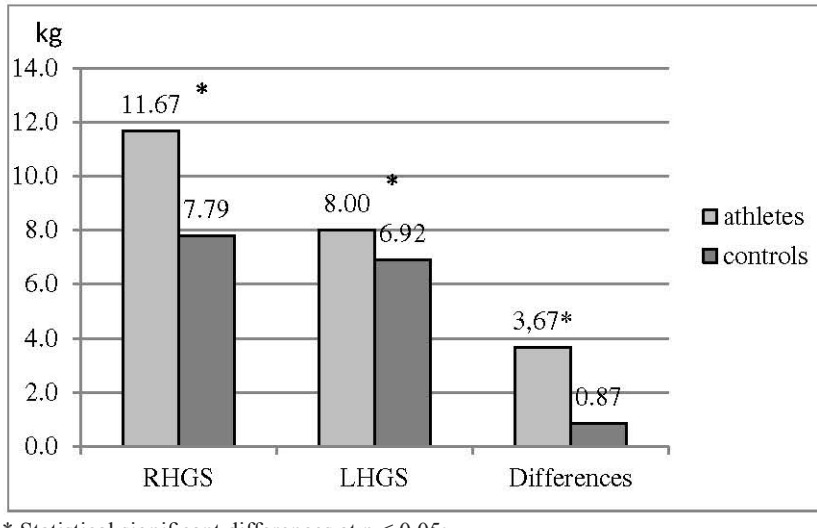

* Statistical significant differences at $p \leq 0.05$;
PHGS – right hand grip strength; LHGS – left hand grip strength;
Differences – between RHGS and LHGS in both groups

Fig. 1. Comparison between right and left hand grip strength in tennis players and control group

Our results indicate that tennis players have significantly greater values of hand grip strength of both hands compared to control group. The measuring show that sportsmen have higher values hand grip strength than the control group (11.8 kg and 8.00 kg) on the right upper limb. We get similar results for the left upper limb: 7.79 kg (athletes) and 6.92 kg (non- athletes). A considerably higher difference of hand grip strength between the right and left hand was discovered in athletes (3.67 kg), compared to the control group where the difference is only 0.87 kg (**Fig. 1**)

The correlation coefficients between hand grip strength on the left and right upper limb and some anthropometric features (height; weight; BMI) are presented in **Table 3** and **Table 4**. The correlations are significantly higher between the LHGS and BMI ($p < 0.01$); LHGS and WT ($p < 0.05$), and between RHGS and HT ($p < 0.05$) in athlete group. In non-athlete group there is a high level of correlation only between RHGS and LHGS ($p < 0.01$).

Table 3. Correlation of hand grip strength and some selected anthropometric variables in tennis players

Variables	HT	WT	BMI	RHGS	LHGS
HT	1	0.752**	0.360	0.560*	0.152
WT		1	0.881**	0.462	0.593*
BMI			1	0.241	0.734**
RHGS				1	0.399
LHGS					1

* Significant at 0.05 level; ** Significant at 0.01 level; HT = Height; WT = Weight; BMI = Body mass index; RHGS = Right hand grip strength; LHGS = Left hand grip strength

Table 4. Correlation of hand grip strength and some selected anthropometric variables in control group

Variables	HT	WT	BMI	RHGS	LHGS
HT	1	0.705**	0.413*	0.325	0.369
WT		1	0.934**	0.365	0.269
BMI			1	0.313	0.159
RHGS				1	0.653**
LHGS					1

* Significant at 0.05 level; ** Significant at 0.01 level;
HT = Height; WT = Weight; BMI = Body mass index; RHGS = Right hand grip strength; LHGS = Left hand grip strength

Discussion

The comparative evaluation of hand grip strength and basic anthropometric features in tennis players and non-athletic prepubescent individuals is presented.

The analysis of basic anthropometric features (HT, WT, BMI) in Bulgarian prepubescent tennis players showed that mean value for body height; body weight; and BMI are: 146.8 cm; 38.78 kg and 17.93 kg/m^2, respectively. The mean values of body height and body weight in Spanish tennis players on the same age was similar: HT - 147.7 cm; WT - 40.36 kg. according to Berdejo-del-Fresno1 et al. [1] and HT - 146.7 cm; WT - 37.4 according to Sanchis-Moysi et al. [7]. The authors concluded that tennis at prepubertal age is associated with marked hypertrophy of the dominant arm, leading to a marked level of asymmetry (+13%), much greater than observed in non-active controls (+3%) [7].

Gigova [10] studied a physical performance and an anthropometric profile of Bulgarian tennis players (9-13 years old) and reported an average body mass of 41.44 kg and height of 152.44 cm, showing superior values compared to the present study.

Strength must be required in muscles and joints for good performance and also like a protection (ligaments, tendons, joints and etc.) of injuries. An optimal stroke execution is needed from solid contact between the racket and the ball, and it depends by grip strength [8].

Our results indicate that tennis players have significantly greater values of hand grip strength of both hand compared to control group. A statistically significant difference was reported between RHGS and LHGS in tennis players` group: 3.67 kg. In non-athletes' group it was only 0.87 kg. The results obtained from Lucki and Nikolay [5] also suggested that tennis players had significant asymmetry in grip strength. The au-

thors establish that tennis players increased muscle mass and strength of the dominant limb. In similar study [9] an isometric strength of the flexors of the upper limbs with sportsmen (tennis and javelin throwing) and general population were tested. The results showed that in the case of the dominant upper limb sportsmen on average reached higher values of isometric handgrip strength than men belonging to general population. These deviation in the hand grip strength between the dominant and non-dominant upper limb could have negative influence of the athletes` health.

Conclusion

The differences in height between the groups reach statistically significant difference.

Prepubescent tennis players have significantly greater values of hand grip strength of both hands compared to control groups.

In the athletes` group LHGS correlated positively with BMI and weight and there is also significant correlation between height and RHGS. In non-athletes' group the correlation is significant only between grip strength of both hands.

The findings of the present study might be useful in future investigation on player selection, talent identification in tennis and training program development.

References

1. **Berdejo-del-Fresno, D., G. Vicente-Rodriguez, J. M. González-Ravé, L. A. Moreno, J. P. Rey-López.** Body composition and fitness in elite Spanish children tennis players. – *J. Hum. Sport Exerc*., Vol. **V**, No II, 2010, 250-264.
2. **Council of Europe Committee for the Development of Sport.** *Eurofit: Handbook for the EUROFIT Test of Physical Fitness*. Rome, 1988.
3. **Koley, S., J. Singh, S. J. Sandhu.** Anthropometric and physiological characteristics on Indian inter-university volleyball players. – *Journal of Human Sport and Exercise*, Vol. **5**, Iss. 3, 2010, 389-399.
4. **Koley, S., M. Yadav, J. Sandhu.** Estimation of Hand Grip Strength and its Association with some Anthropometric traits in Cricketers of Armitsar, Punjab, India. – *The Internet Journal of Biological Anthropology*, **3**(1), 2008.
5. **Lucki, N. C., C. W. Nicolay.** Phenotypic plasticity and functional asymmetry in response to grip forces exerted by intercollegiate tennis players. – *The American Journal of Human Biology*, **19**, 2007, 566-577.
6. **Nwuga,V.** Grip strength and grip endurance in physical therapy students. – *Arch. Phys. Med. Rehab.*, 56, 1975, 296-299.
7. **Sanchis-Moysi, J., F. Idoate, J. A. Serrano-Sanchez, C Dorado, J. A. L. Calbet.** Muscle Hypertrophy in Prepubescent Tennis Players:A Segmentation MRI Study. – *PLoS ONE*, Vol. **7**(3), 2012, 33622.
8. **Vergauwen, L., A. J. Spaepen, J. Lefevre, P. Hespel.** Evaluation of stroke performance in tennis. – *Med. Sci. Sports Exerc*., **30**(8), 1998, 1281-1288.
9. **Vilím, M., M. Juránková, P. Janíčková.** Comparison of isometric strength men´s upper limbs from the Czech Republic with a group of athletes from different sectors. – *J. Hum. Sport Exerc.*, **9**(1), 2015, 308-313.
10. **Гигова, И.** *Взаимовръзка между двигателните способности, техническите умения и психичните качества при подрастващи тенисисти.* Автореферат на дис. труд. София, 2016.

Institute of Experimental Morphology, Pathology and Anthropology with Museum
Bulgarian Anatomical Society

Acta morphologica et anthropologica, 24 (1-2)
Sofia ● 2017

The Abductor Pollicis Longus Tendon as Grafting Material for Reconstructive Surgery of the Hand

Alexandar Iliev[1*], *Georgi P. Georgiev*[2], *Georgi Kotov*[1], *Boycho Landzhov*[1]

[1]*Department of Anatomy, Histology and Embryology, Medical University of Sofia, Bulgaria*
[2]*Department of Orthopaedics and Traumatology, University Hospital Queen Giovanna-ISUL, Medical University of Sofia, Bulgaria*

[*]Corresponding author: e-mail: dralexiliev@abv.bg

The abductor pollicis longus muscle (APL) is one of the most variable muscles in the hand and often presents with numerous distal tendons, known as accessory or supernumerary tendons. They are an often used source of grafting material for reconstructive hand surgery. The aim of the present study was to examine and describe different variations in the number and morphology of the tendons of the APL and to discuss their possible use as grafting material for reconstructive hand surgery. A total of 30 upper limbs from cadavers were used for the study. We found accessory tendons in 26 of the hands, of which 18 had only one accessory tendon, 6 hands had two, and 2 hands had three accessory tendons. Knowledge of variations in the number of APL tendons is important for successful hand reconstructive surgery, as well as in the context of pathologies, such as De Quervain's syndrome.

Key words: abductor pollicis longus, accessory tendons, grafting material, hand surgery

Introduction

The abductor pollicis longus (APL), an often variable structure in the human hand [8, 25], is responsible for abduction of the thumb and together with the extensor carpi ulnaris muscle acts as a dynamic collateral ligament of the wrist [20, 26]. It originates from the posterior surface of the interosseous membrane, the radius and the ulna, passes through the first extensor compartment of the wrist together with the extensor pollicis brevis muscle (EPB) and attaches to the base of the first metacarpal bone [26, 29]. Variations of the distal attachment of the APL have been well documented. They include insertion into the opponens pollicis muscle [17, 32] and the abductor pollicis brevis [4, 29, 30], attachment to the scaphoid [6] and trapezium bone [26], the carpometacarpal joint capsule [32], the flexor pollicis brevis muscle [33], etc. Moreover, data exist on the presence of supernumerary or accessory tendons of the APL [19, 24]. They may contribute to the development of De Quervain's syndrome, or stenosing tenosynovitis

of the first extensor compartment of the wrist, which is characterised by pain resulting from resisted gliding of the tendons of the APL and EPB within the fibro-osseous canal [3, 18, 22].

The use of grafting material is often needed in reconstructive hand surgery in cases of osteoarthritis or damage to tendons or ligaments [5, 8]. Most often, grafting material is used from the palmaris longus muscle or plantaris muscle [13, 14, 15, 28]. However, the palmaris longus in particular is a very variable muscle and may not always be present or suitable for grafting [11]. An alternative surgical technique is to use accessory tendons of the APL if such are present [28]. A key principle when using tendons as grafting material is to avoid donor site morbidity [5]. The APL is considered an excellent choice of grafting material for reconstructive surgery of tendons of the hand because of its multiple bellies, suitable size, relatively easy extraction and limited donor site morbidity [28].

The aim of the present study was to examine and describe different variations in the number and morphology of the tendons of the APL and to discuss their possible use as grafting material for reconstructive hand surgery.

Materials and Methods

We used a total of 30 upper limbs from Caucasian cadavers, fixed with 10% formalin, from the autopsy material available at the Department of Anatomy, Histology and Embryology at the Medical University of Sofia, Bulgaria. All examinations were approved by the Medico-Legal Office and the Local Ethic Committee. They were dissected and thoroughly examined for the presence of accessory tendons of the APL. The dissections were performed through a dorsal approach on the forearm. Skin and subcutaneous fat tissue were dissected layer-by-layer and the underlying fascia of the forearm was exposed. We then cut through the fascia and demonstrated the extensor retinaculum and the extensor muscles of the forearm. We carefully identified the first extensor compartment of the wrist and opened it to expose the APL and the EPB muscles. We then proceeded to identify the presence of accessory tendons of the APL and the point of their distal attachment. We used a calibrated caliper to measure the length, width and thickness of the accessory tendons and then calculated the mean values for all three parameters. Photographs of the discovered anomalies were taken.

Results

The presence of the tendon of the APL was observed in all of the examined upper limbs and attached in the usual way at the base of the first metacarpal bone (**Fig. 1a**). Accessory tendons were detected in 26 hands (86.7%), of which one accessory tendon was identified in 18 cases (69.2%) (**Fig. 1b**), 6 hands had two accessory tendons (23.1%) (**Fig. 1c**) and 2 hands had three accessory tendons (7.7%) (**Fig. 1d**). The presence of accessory tendons showed no side-to-side differences. None of the observed accessory tendons had a separate compartment. We also noted variations in the distal attachment of the supernumerary tendons of the APL. The insertion site of the accessory tendons was the trapezium in 10 cases (38%), the thenar muscles in 7 cases (27%) (**Fig. 1b**), the abductor pollicis brevis in 4 cases (15%), the base of the first metacarpal bone in 3 cases (12%) (**Fig. 1c**), double insertion to the first metacarpal bone and the thenar muscles in 1 case (4%) (**Fig. 1d**) and the opponens pollicis brevis in 1 case (4%). Mean length, width and thickness of the accessory tendons were 63.2, 4.9 and 1.9 mm, respectively.

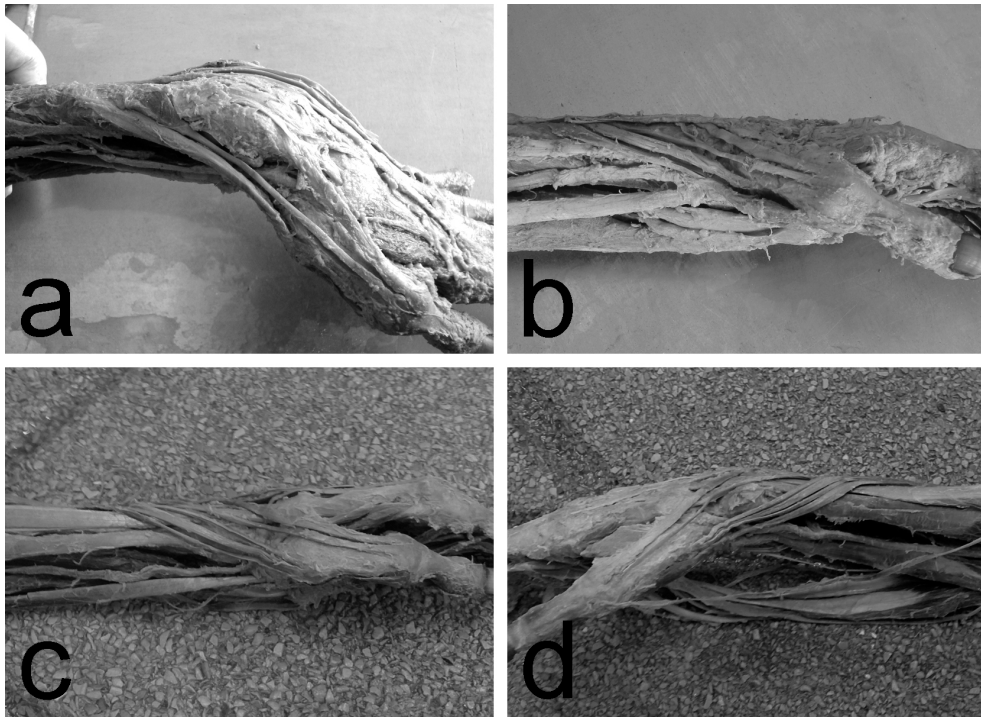

Fig. 1.a) Usual APL insertion to the first metacarpal bone; **b**) APL accessory tendon attached to the thenar muscles; **c**) Two APL accessory tendons attached to the first metacarpal bone; **d**) APL with three accessory tendons - the first two inserted to the first metacarpal bone and the third attached to the thenar muscles

In 4 of the examined upper limbs we did not discover the presence of supernumerary tendons of the APL. We also performed a thorough revision for the presence of any other variations in the anatomical structure of the examined upper limbs but such were not reported.

Discussion

In the present study we examined the presence of accessory tendons of the APL and noted the variations in their attachment sites. Accessory tendons were discovered in 26 out of 30 upper limbs (86.7%). This high percentage correlates with data from the study of Gonzalez et al. (57 out of 66 upper limbs or 86.4%) [17]. This study found one accessory tendon in 9 cases (13.6%), two tendons in 46 cases (69.7%), three tendons in 9 cases (13.6%) and four tendons in 2 cases (3%) [17]. These data differ from the results obtained in the present study, in which we discovered the presence of one accessory tendon to be predominant, followed by presence of two and three tendons, respectively. We did not report presence of four accessory tendons in the examined upper limbs. According to Zancolli and Cozzi, APL tendon duplicity has been described in 56% to 98.5% of hands [34], which has been supported by the data obtained by Bravo et al. (85%) [5] and Loomis (92%) [23]. Our results with regard to attachment sites of the aberrant tendons

confirmed the data obtained in previous studies. Attachment to the trapezium was found in 41% of cases by Bravo et al. [5] and in 61% of upper limbs studied by Brandsma et al. [4]. Khoury et al. reported that when two tendons were present, they most often attached to the base of the first metacarpal bone, while in the case of three tendons, two of them attached to the base of the first metacarpal bone, while the remaining tendon attached to the thenar muscles [21]. These findings were illustrated and confirmed by the present study.

Although the APL muscle plays a key role in the abduction of the thumb, it cannot abduct the thumb by itself, which has been shown in cases of thenar muscles paralysis [9]. Another study has underlined the important function of the tendon of the APL in terms of preventing overextension of the metacarpo-phalangeal joint while performing a pincer grasp between the thumb and the index finger [26, 27]. Therefore, variations in the APL may have an important clinical and functional significance. The presence of supernumerary tendons, which appears to be the rule rather than an exception [10], can present with clinical symptoms such as De Quervain's syndrome, or stenosing tenosynovitis of the first extensor compartment [29]. They can also compromise the accuracy of steroid injection or make it difficult to achieve, thereby leading to a failure to treat De Quervain's syndrome properly [31].

The use of accessory tendons of the APL as grafting material has been well documented [5, 28, 29, 31]. Jackson et al. report that the first extensor compartment of the wrist almost always contains a tendon that can be used for grafting procedures [19]. The dimensions of the accessory tendons of the APL make them appropriate as grafts for reconstructive hand surgery [5]. Trapezial excision with APL tendon interposition arthroplasty in cases of arthrosis or osteoarthritis of the trapeziometacarpal joint (TMC) has been widely performed and good outcomes have been achieved [1]. In addition to tendon interposition, APL arthroplasty includes stabilization of the first metacarpal bone through suspension of its base between the tendons of the APL and the flexor carpi radialis muscle and introduction of an APL strip [1]. One reason for the decreased morbidity when using an accessory tendon of the APL is that TMC stability is still maintained [5]. The recommended length of the tendon in TMC arthroplasty is 5 cm [2]. The mean length of the accessory tendons measured in the present study was a little over 6.3 cm, which makes them an adequate grafting material. Chitnis and Evans report the use of the APL tendon in tendon transfer due to rupture or division of the extensor pollicis longus muscle, in order to restore extension of the thumb [7]. Furthermore, rerouting an accessory tendon of the APL in order to use it as insertion for tendon transfer is a possible mechanism for restoration of thumb abduction [19]. APL tendons, as well as the tendons of the radial wrist extensors may be used for restoration of impaired flexion of the fingers in case of flexor muscle loss, for correction of claw hand deformities and tendon transfer in rheumatoid hands [12, 16].

Conclusion

The presence of accessory tendons of the APL is an often encountered phenomenon and is generally considered to be beneficial, since injury to one of the tendons can be partially compensated by the function of the remaining tendons. However, they can also contribute to the development of certain pathologies, such as De Quervain's syndrome. The wide use of the supernumerary tendons of the APL as grafting material for hand reconstructive surgery clearly shows that knowledge of the different variations of this muscle is important for a successful postoperative result.

References

1. **Atroshi, I., G. Axelsson, E. L. Nilsson**. Osteotomy versus tendon arthroplasty in trapeziometacarpal arthrosis: 17 patients followed for 1 year. – *Acta Orthop. Scand*., **69**(3), 1998, 287-290.
2. **Atroshi, I., G. Axelsson.** Extensor carpi radialis longus tendon arthroplasty in the treatment of primary trapeziometacarpal arthrosis. – *J. Hand Surg. Am*., **22**, 1997, 419-427.
3. **Bahm, J., Z. Szabo, G. Foucher.** The anatomy of de Quervain's disease. A study of operative findings. – *Int. Orthop*., **19**(4), 1995, 209-211.
4. **Brandsma, J. W., E. Van Oudenaarde, R. Oostendorp.** The abductores pollicis muscles. Clinical considerations based on electromyographical and anatomical studies. – *J. Hand Ther*., **9**(3), 1996, 218-222.
5. **Bravo, E., R. Barco, A. Bullón.** Anatomic study of the abductor pollicis longus: a source for grafting materialof the hand. – *Clin. Orthop. Relat. Res*., **468**, 2010, 1305-1309.
6. **Celik, H. H., E. Sendemir, C. Simşek.** Anomalous insertion of abductor pollicus longus: case report. – *J. Anat*., **184**, 1994, 643-645.
7. **Chitnis, S. L., D. M. Evans.** Tendon transfer to restore extension of the thumb using abductor pollicis longus. – *J. Hand Surg. Br*., **18**, 1993, 234-238.
8. **El-Beshbishy, R. A., G. A. Abdel-Hamid.** Variations of the abductor pollicis longus tendon: An anatomic study. – *Folia Morphol. (Warsz)*, **72**, 2013, 161-166.
9. **Elliott, B. G.** Abductor pollicis longus: A case of mistaken identity. – *J. Hand Surg. Br*., **17**, 1992, 476-478.
10. **Fabrizio, P. A., F.R. Clemente.** A variation in the organization of abductor pollicis longus. – *Clin. Anat*., **9**(6), 1996, 371-375.
11. **Georgiev, G. P., A. A. Iliev, I. N. Dimitrova, G. N. Kotov, L. G. Malinova, B. V. Landzhov.** Palmaris longus muscle variations in the Bulgarian population: significance for hand surgery and proposal of new classifications. – *Fol. Med. (Plovdiv)*, **59**(3), 2017, DOI: 10.1515/folmed-2017-0035, (in press).
12. **Georgiev, G. P., L. Jelev, L. Surchev.** Presence of a palmaris longus related variations in three members of a family. – *J. Hand Surg.* (European Vol.), **34**, 2009, 277-278.
13. **Georgiev, G. P., L. Jelev, L. Surchev.** Reversed palmaris longus muscle simulating soft-tissue mass as a possible cause of median nerve compression. – *Bulg. J. Orthop. Trauma*., **45**, 2008, 92-94.
14. **Georgiev, G. P., L. Jelev, W. A. Ovtscharoff.** Unusual combination of muscular and arterial variations in the upper extremity: a case report of a variant palmaris longus and an additional tendinous portion of the flexor carpi ulnaris together with a persistent median artery. – *Anat.*, **3**, 2009, 58-61.
15. **Georgiev, G. P., L. Jelev.** Unusual coexistence of a variant abductor digiti minimi and reversed palmaris longus and their possible relation to median and ulnar nerves entrapment at the wrist. – *Rom. J. Morphol. Embryol*., **50**(4), 2009, 725-727.
16. **Georgiev, G. P., L. Surchev, L. Jelev.** Transposition of parts between the extensor carpi radialis muscles and their significance for hand surgery. – *Bulg. J. Orthop. Traum*., **43**, 2006, 130-134.
17. **Gonzalez, M. H., R. Sohlberg, A. Brown, N. Weinzweig.** The first dorsal extensor compartment: an anatomic study. – *J. Hand Surg.* (Am), **20**(4), 1995, 657-660.
18. **Ilyas, A. M., M. Ast, A. A. Schaffer, J. Thoder.** De quervain tenosynovitis of the wrist. – *J. Am. Acad. Orthop. Surg*., **15**(12), 2007, 757-764.
19. **Jackson, W. T., S. F. Viegas, T. M. Coon, K. D. Stimpson, A. D. Frogameni, J. M. Simpson.** Anatomical variations in the first extensor compartment of the wrist. A clinical and anatomical study. – *J. Bone Joint Surg. Am*., **68**(6), 1986, 923-926.
20. **Kauer, J. M.** Functional anatomy of the carpometacarpal joint of the thumb. – *Clin. Orthop*., **7**, 1987, 13.
21. **Khoury, Z., J. Bertelli, A. Gilbert.** The subtendons of the abductor pollicis longus muscle. – *Surg. Radiol. Anat*., **13**(3), 1991, 245–246.
22. **Landzhov, B., G. Georgiev, A. Iliev, B. Matev, I. Dimitrova, L. Malinova.** Anatomical variations of the abductor pollicis longus muscle tendon – relation to de Quervain's disease. – *Scr. Sci. Med*., **48** (suppl. 2), 2016, 60.
23. **Loomis, K. L.** Variations of stenosing tenosynovitis of the radial styloid process. – *J. Bone Joint Surg. Am*., **33**, 1951, 340-346.

24. **Melling, M., R. Reihsner, M. Steindl, D. Karimianteherani, M. Schnallinger, M. Behnam.** Biomechanical stability of abductor pollicis longus muscles with variable numbers of tendinous insertions. – *Anat. Rec*., **250**(4), 1998, 475-479.
25. **Nayak, S. R., A. Krishnamurthy, M. M. Pai, L. V. Prabhu, L. A. Ramanathan, C. Ganesh Kumar, et al.** Multiple variations of the extensor tendons of the forearm. – *Rom. J. Morphol. Embryol.*, **49**(1), 2008, 97-100.
26. **Paul, S., S. Das.** Multiple tendons of abductor pollicis longus muscle: A cadaveric study with clinical implications. – *Kathmandu Univ. Med. J*., **4**, 2006, 501-502.
27. **Paul, S., S. Das.** Variant abductor pollicis longus muscle: a case report. – *Acta Med.* (Hradec Kralove), **50**(3), 2007, 213-215.
28. **Rosas, S., C. Mesa, F. Mesa.** The Abductor Pollicis Longus Tendon as an Alternative Graft in Hand Surgery. – *J. Hand Surg. Am*., **42**(3), 2017, e205-e208.
29. **Sarikcioglu, L., F. B. Yildirim.** Bilateral abductor pollicis longus muscle variation. Case report and review of the literature. – *Morphol*., **88**(282), 2004. 160-163.
30. **Sehirli, U. S., S. Cavdar, M. Yüksel.** Bilateral variations of the abductor pollicis longus. – *Ann. Plast. Surg*., **47**(5), 2001, 582-583.
31. **Tewari, J., P. R. Mishra, S. K. Tripathy.** Anatomical variation of abductor pollicis longus in Indian population: A cadaveric study. – *Indian J. Orthop*., **49**(5), 2015, 549-553.
32. **Van Oudenaarde, E.** Structure and function of the abductor pollicis longus muscle. – *J. Anat.*, **174**, 1991, 221-227.
33. **Yüksel, M., S. Onderoglu, Z. Arik.** Case of an abductor pollicis longus muscle: variation or differentiation? – *Okajimas Folia Anat. Jpn*., **69**(4), 1992, 169-171.
34. **Zancolli, E. A., E. P. Cozzi.** Thumb muscles. – In: *Atlas de anatomia quirurgica de la mano* (Ed. Medica Panamericana), Madrid, 1993, 296-297.

Institute of Experimental Morphology, Pathology and Anthropology with Museum
Bulgarian Anatomical Society

Acta morphologica et anthropologica, 24 (1-2)
Sofia ● 2017

A Rare Case of Bilateral Occipitoscapular Muscle

Stancho Stanchev[*]*, Alexandar Iliev, Lina Malinova, Boycho Landzhov*

Department of Anatomy, Histology and Embryology, Medical University of Sofia, Bulgaria

* Corresponding author: e-mail: stanchev_1989@abv.bg

In the present study, we described a variation of the neck muscles of a 73-year-old male cadaver during a routine anatomical dissection. The finding was represented by bilateral occipitoscapular muscle – a muscle that is normally not present in human. On the right side, the muscle was composed of inferior oblique, middle straight and superior oblique parts. The left muscle was represented by inferior and superior oblique parts. The muscles originated from the superior angle of the scapula and the tendons inserted on the lateral half of superior nuchal line of occipital bone. We observed and described the relations of these supernumerary muscles with the adjacent structures and their blood supply. In addition, we discussed the presence of this variation in the context of the embryonic development of neck muscles and phylogenetic development of mammals, as well as its clinical significance.

Key words: neck muscle, bilateral variation, occipitoscapular muscle

Introduction

The posterior cervical region is characterized by the presence of various muscles which can be classified into two main groups – muscles of neck and back. According to the origin, length and direction of muscle bundles, as well as the place of attachment, some of them may have action in more than one joint. Functionally, this musculature is associated with maintenance of posture of head and movements in the cervical and thoracic segments of the vertebral column. In addition, the levator scapulae and rhomboid muscles that are attached to the scapula may permit movements in the shoulder girdle. There is evidence for numerous variations of the muscles in the neck region: different tendinous insertions, especially for scalene and longisimus capitis muscle [27]; accessory caudal attachments of levator scapulae muscle to the serratus anterior, serratus posterior or first and second rib [1]; the cleido-occipitalis cervicalis bundle of the trapezius muscle [16]. Furthermore, the rhomboid muscles are characterized by varieties in their size and shape [14] and the presence of the third of the rhomboids has been described [11]. Occipitoscapularis muscle, known as rhomboid capitis or rhomboid occipitalis was first described by Wood in 1867 as arising from the occipital bone at the level on

the superior nuchal line and attached to the medial border of the scapula at the level of the scapular spine [26]. Rhomboideus occipitalis or capitis muscle was observed by Patten in 1935. It inserted between the attachments of levator scapulae and rhomboideus minor muscles [18]. Rogavski claimed to have described the third case of rhomboideus capitis in his study [21].

The aim of the current study was to present a multiple variation of bilateral occipitoscapular muscles in the cervical region and to describe their relations with adjacent structures. We also discussed the possible clinical significance of the observed finding.

Materials and Methods

The finding was made during a routine anatomical dissection of a 73-year-old male cadaver of Caucasian origin from the autopsy material available at the Department of Anatomy, Histology and Embryology, Medical University of Sofia, Bulgaria. The dissection was approved by the Medical Legal Office and the Local Ethics Committee. The body was preserved by an injection of a 10% formalin-based preservative and stored at – 40 °C.

Results

The present study describes two bilateral additional muscles, which were discovered in the posterior neck region during a routine anatomical dissection of a 73-year-old male cadaver. The right muscle was band-shaped. It originated from the superior angle of the scapula between the levator scapulae and rhomboideus minor muscles with a short tendon – 10 mm. Muscular fascicles ran parallel to each other in superomedial direction. The muscle was composed of three parts – initial inferior oblique – 52 mm, middle straight – 35 mm, and superior oblique – 59 mm. The distal tendon was 8 mm long and inserted on the lateral half of the superior nuchal line of the occipital bone. The muscle was situated over the splenius capitis and cervicis muscles just below the trapezoid muscle.

On the left side the muscle presented with two parts: inferior oblique – 72 mm, and superior oblique – 68 mm. It originated from the superior angle of the scapula with a short tendon – 11 mm and inserted on the lateral part of the superior nuchal line of the occipital bone. The distal tendon was 7 mm long. The muscle had the same relations to adjacent structures as described on the right side. The dissection revealed that these muscles were innervated by the dorsal scapular nerve (**Fig. 1**).

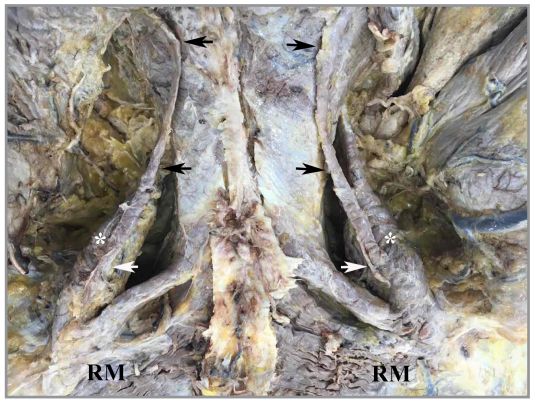

Fig. 1. Photograph of the posterior neck region:
Arrows – occipitoscapular muscle;
Asterisks – levator scapulae muscle;
RM – rhomboideus major muscle

Discussion

Numerous studies have discussed various accessory muscle bundles in the cervical region [3, 22]. The reason for the observed accessory muscles may be associated with the embryonic development of neck musculature. It is known that in vertebrates, the body musculature originates from the somites, while the head muscles originate from the cranial mesoderm. The transitional location of neck muscles and the evidence of occipital lateral plate mesoderm as a novel source for vertebrate neck musculature [25] show the structural complexity of the neck region. Similar variation has been discussed in earlier descriptions in which the aberrant muscle was named as the occipito-scapularis, the rhomboideus-occipitalis or the rhomboideus capitis. Rogawski described the muscle as rhomboideus capitis, which originated from the occipital bone and was related to the splenius capitis muscle distally attached to the scapula [21]. Zagyapan et al. reported the muscle as occipito-scapular, but it was not related to the splenius capitis muscle caudally [27]. In contrast to these descriptions, in our study, we observed a bilateral variation represented by two occipito-scapular muscles. The rhomboideus occipitalis muscle is not normally present in human but it can be observed in genetic disorders such as Edward's syndrome [2]. Furthermore, the presence of these aberrant muscles can be explained by the phylogenetic development of mammals, because rhomboideus capitis exists in other species. In dogs, the rhomboideus capitis muscle originates from the dorso-cranial border of the scapula and inserts on the nuchal crest [23]. In the present case, the accessory occipitoscapular muscles were attached between the rhomboideus minor and levator scapulae muscles. In cats, this muscle stretches between the cranial nuchal line and superior angle of scapula and is associated with adaptation of standing postures [19]. In Rhesus monkey, the rhomboid muscle consists of rhomboideus capitis head and two conjoined parts – rhomboideus cervicis and rhomboideus dorsi [20].

Knowledge of anatomical variations in the neck region is clinically important. The presence of these supernumerary muscles may be misdiagnosed as tumor-mimicking lesions [15]. Some cases of palpable neck mass, which were treated by unilateral radical neck dissection, revealed hypertrophy of the ipsilateral levator muscle. In addition, Shpizner and Holliday investigated that the normal morphology of the muscle may be referred to as a tumor mass, because of muscular atrophy on the contralateral side [24]. On the other hand, the levator scapulae syndrome is characterized by pain radiated to the shoulder girdle and neck. Variability in the insertion of the levator and the origin of the serratus anterior muscles has been discussed in the etiology of this pathological condition [17]. Different muscular and fibro-muscular variations may occur and provoke compression of the brachial plexus and subclavian vessels in the thoracic outlet region, between the neck and the axilla [4-9, 12, 13]. In surgery, the levator scapulae flap is used in head and neck reconstruction [10]. In some cases, the occipitoscapular muscle may also be used as a flap during surgical intervations.

Conclusion

The presence of bilateral occipitoscapular muscle described in the present study represents a rare multiple variation in human and knowledge of it is important for both morphological and clinical disciplines such as surgery, radiology and musculoskeletal-medicine.

References

1. **Au, J., A. L. Webb, G. Buirski, P. N. Smith, M. R. Pickering, D. M. Perriman.** Anatomic variations of levator scapulae in a normal cohort: an MRI study. – *Surg. Radiol. Anat*., **39**(3), 2017, 337-343.
2. **Aziz, M. A.** Muscular and other abnormalities in a case of Edwards' syndrome (18-trisomy). – *Teratology*, **20,** 1979, 303-312.
3. **Coskun, N., F. B. Yildirim, O. Ozkan.** Multiple muscular variations in the neck region-case study. – *Folia Morphol*. (Warsz), **61**, 2002**,** 317-319.
4. **Georgiev, G. P., L. Jelev, L. Surchev.** Axillary arch in Bulgarian population: clinical significance of the arches. – *Clin. A*nat., **20**, 2007, 286-291.
5. **Georgiev, G. P., L. Jelev.** Bilateral fibrous replacement of subclavius muscle in relation to nerve and artery compression of the upper limb. – *Int. J. Anat. Var*., **2**, 2009, 57-59.
6. **Georgiev, G. P., L. Surchev, L. Jelev.** Variant fibrous structures in costoclavicular interval – possible cause for thoracic outlet syndrome. – *Compt. rend. Acad. bulg. Sci*., **60**, 2007, 813-816.
7. **Georgiev, G. P., L. Jelev.** A rare case of unilateral chondroepitrochlearis muscle. – *Compt. rend. Acad. rulg. Sci*., **61**, 2008, 1481-1484.
8. **Georgiev, G., L. Jelev, L. Surchev.** Two cases of Langer's axillary arch. – *Symposium of Imaging Anatomy*, 2005, Abstracts, 90.
9. **Georgiev, G. P., L. Surchev, L. Jelev.** Bilateral fibrous structure in relation to thoracic outlet syndrome. **–** *Scr. Sci. Med*., **38** (Suppl. 2), 2006, 54.
10. **Goodman, A. L., P. J. Donald.** Use of the levator scapulae muscle flap in head and neck reconstruction. **–** *Arch. Otolaryngol. Head Neck Surg*., **116** (12), 1990, 1440-1444.
11. **Jelev, L., B. Landzhov.** A rare muscular variation: the third of rhomboideus. **–** *Int. J. Ex. Clin. Anat.***, 6-7**, 2012-2013, 63-64.
12. **Jelev, L., G. P. Georgiev, L. Surchev.** Axillary arch in human: common morphology and variety. Definition of "clinical" axillary arch and its classification. **–** *Ann. Anat*., **189**, 2007, 473-481.
13. **Jelev, L., G. P. Georgiev, W. Ovtscharoff.** Anatomical variations in relation to thoracic outlet syndrome. **–** *Scr. Sci. Med*., **43** (Suppl. 1), 2011, 129.
14. **Kamibayashi, L. K., F. J. Richmond.** Morphometry of human neck muscles. **–** *Spine*, **23**, 1998, 1314-1323.
15. **Kim, S. Y., J. S. Park, K. M. Ryu, W. Jin, S. Y. Park.** Various Tumor-Mimicking Lesions in the Musculoskeletal System: Causes and Diagnostic Approach. **–** *Korean J. Radiol*., **12**(2), 2011, 220-231.
16. **Kwak, H. H., H. J. Kim, K. H. Youn, H. D. Park, I. H. Chung.** An anatomic variation of the trapezius muscle in a Korean: the cleido-occipitalis cervicalis. – *Yonsei Med. J.,* **44**(6), 2003, 1098-1100.
17. **Menachem, A., O. Kaplan, S. Dekel.** Levator scapulae syndrome: an anatomic-clinical study. – *Bull. Hosp. Jt. Dis*., **53**(1), 1993, 21-24.
18. **Patten, C. J.** Proceedings of the Anatomical Society of Great Britain and Ireland. – *J. Anat*., **LXIX**, 1935, 147.
19. **Richmond, F. J., B. D. Corneil, K. Singh.** Animal models of motor systems: cautionary tales from studies of head movement. – *Prog. Brain Res*., **123**, 1999, 411-416.
20. **Richmond, F. J., K. Singh, B. D. Corneil.** Neck muscles in the rhesus monkey. I. Musclemorphometry and histochemistry. – *J. Neurophysiol*., **86**(4), 2001**,** 171728.
21. **Rogawski, K. M.** The rhomboideus capitis in man-correctly named rare muscular variation. – *Okajimas Folia Anat. Jpn*, **67**, 1990, 161-163.
22. **Rudisuli, T.** Demonstration of a musculus levator claviculae. – *Surg. Radiol. Anat*., **17**, 1995, 85-87.
23. **Sharir, A., J. Milgram, R. Shahar.** Structural and functional anatomy of the neck musculature of the dog (Canis famil-iaris). – *J. Anat*., **208**, 2006, 331-351.
24. **Shpizner, B. A., R. A. Holliday.** Levator scapulae muscle asymmetry presenting as a palpable neck mass: CT evaluation. – *AJNR Am. J. Neuroradiol*., **14**, 1993, 461-464.
25. **Theis, S., K. Patel, P. Valasek, A. Otto, Q. Pu, I. Harel et al.** The occipital lateral plate mesoderm is a novel source for vertebrate neck musculature. – *Development*, **137**(17), 2010, 2961-2971.
26. **Wood, J.** Variations in human myology observed during the winter session of 1866-67 at King's College, London. – *Proceedings of the Royal Society of London*, **XV**, 1867, 518-552.
27. **Zagyapan, R., C. Pelin, N. Mas.** A rare muscular variation: The occipito-scapularis muscle: case report. – *Turkiye Klinikleri J. Med. Sci*., **28**, 2008, 87-90.

Institute of Experimental Morphology, Pathology and Anthropology with Museum
Bulgarian Anatomical Society

Acta morphologica et anthropologica, 24 (1-2)
Sofia ● 2017

Review Articles

Kariosphere, the Enigmatic "Surrounded Nucleolus" of Maturing Oocytes: Review

Venera Nikolova[1*], *Maya Markova, Ralitsa Zhivkova, Irina Chakarova, Valentina Hadzhinesheva, Stefka Delimitreva*

Department of Biology, Medical Faculty, Medical University of Sofia, Bulgaria

[*]Corresponding author: e-mail: venera.nikolova@abv.bg

In mammals and other animals, the late prophase I oocyte undergoes large-scale chromatin remodeling. Condensing chromosomes associate with the inactive nucleolus and surround it with a rim of heterochromatin called karyosphere. This rim has been shown to contain centromeric and pericentromeric regions of chromosomes. Karyosphere formation coincides in time with global transcriptional silencing of oocyte genes, but this seems to reflect regulation by common upstream factors rather than causal relationship between the two processes. The function of karyosphere is not yet known, but is likely related to the positioning of bivalents in metaphase I by clustering chromosomes together in a limited volume before the nuclear envelope breakdown. Studies show that karyosphere formation, ("non-surrounded to surrounded nucleolus transition") indicates acquisition of meiotic and developmental competence by the oocyte. Methodological approaches are discussed to use this important morphological marker to select oocytes with better potential for assisted reproduction.

Key words: oocytes, meiosis, chromatin rearrangement, heterochromatin

The karyosphere as a temporary structure of germinal vesicle stage oocytes

In mammals, as in most other vertebrates and a number of invertebrate phyla, the mature oocyte at the time of fertilization is arrested in meiotic metaphase II and, hence, has no nucleus. In the immature oocyte, however, the nucleus plays a key role during the long prophase I arrest and the early stages of meiotic maturation. This nucleus, also known as germinal vesicle (GV), is unusual and remarkable in many respects. Its chro-

matin undergoes major rearrangements called by some authors "large-scale" changes or remodeling [11]. These changes transform the initially typical nucleolus of the oocyte into a transcriptionally inactive "nucleolus-like body" [10, 17]. In the final stage of meiotic prophase I, heterochromatin accumulates in a dense circular perinucleolar rim, forming a structure called surrounded nucleolus, rimmed nucleolus or karyosphere [5]. To be distinguished from it, the nucleolus of the early primary oocyte, which has a typical structure and function, is called non-surrounded nucleolus. The karyosphere is a result of all oocyte chromosomes joining in a limited nuclear volume with final formation of a single complex chromatin structure. It has been described in members of distantly related animal groups such as mammals, birds, amphibians, insects and annelids, suggesting a phylogenetically conserved process in metazoan oogenesis [7]. The scope of the present review is limited to mammals as a group relevant for the understanding of human oogenesis.

After a period of proliferation by mitosis, mammalian female germ cells in the fetal ovary undergo a transformation from oogonia to primary oocytes and start meiosis. They complete the first stages of prophase I, including the meiotic recombination (crossing over), and upon reaching diplotene are arrested for weeks, months or years, depending on the species. During this prolonged arrested diplotene, often referred to as dictyate stage, the prophase chromosomes are decondensed to a loose chromatin mass [16]. The reproductive period of the female, beginning at puberty, is characterized by secretion of hormonal signals that stimulate follicle growth and bring oocytes out of their quiescent state. With each menstrual/estrus cycle, a cohort of oocytes resumes meiosis. One or more of them will complete the 1st meiotic division, extrude the 1st polar body, start the 2nd meiotic division and reach its metaphase, where meiosis is arrested again until fertilization. These stages from late prophase I to metaphase II are collectively called "oocyte meiotic maturation" [12]. We shall discuss only its initial step, the "germinal vesicle" stage when the primary oocyte still possesses an intact nucleus until its envelope is disassembled at the "GV breakdown" stage, marking the transition to metaphase I.

Morphological classification of oocyte nucleoli

Oocytes isolated from growing preantral and antral follicles can be classified into discrete patterns according to the morphological organization of the chromatin in their nuclei. Initially, oocyte chromatin is mostly decondensed and dispersed throughout the nuclear volume. Then, the degree of condensation increases, and condensed chromatin foci start to associate with the nucleolar periphery. This continues until the nucleolus is encircled by a complete rim of heterochromatin, forming the karyosphere or "surrounded nucleolus" (**Fig. 1**). The described structural remodeling coincides with decrease and cessation of transcriptional activity, both in the nucleolus and outside it. These changes have been described in the human [16], mouse [14] and a number of other mammalian species. The morphological configuration in which the perinucleolar chromatin rim is absent is named "non-surrounded nucleolus" (NSN), while the configuration with present perinucleolar chromatin rim (karyosphere) is termed "surrounded nucleolus" (SN). Some authors also describe the intermediate configurations as "partly NSN" and "partly SN". The process shows some species specificity, as shown by horse and bovine oocytes. In them, chromatin condenses into a single compact clump instead of forming a clear rim around the nucleolus. For that reason, cattle prophase oocytes are classified into four stages designated, respectively, as GV0 (diffuse pattern of chromatin), GV1 (few foci of condensation), GV2 (distinct clumps of condensed chromatin)

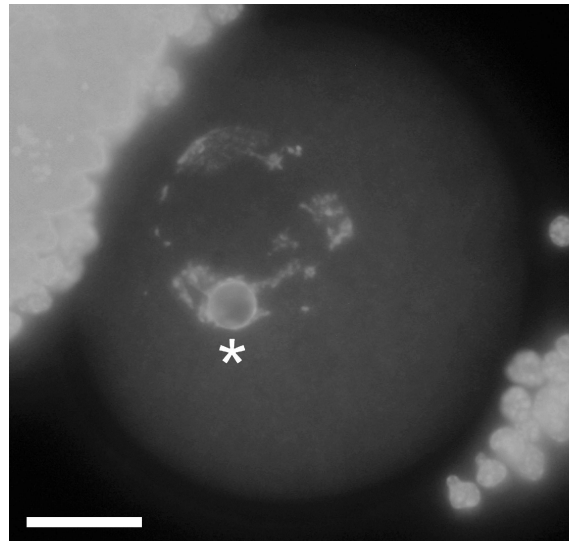

Fig. 1. Mouse oocyte in late GV stage, surrounded by follicle cells, stained with the chromatin dye Hoechst 33258. The karyosphere, indicated by an asterisk, is visible as a circular structure inside the nucleus. Several condensing bivalents are seen attached to it. Bar = 20 μm. Reprinted from [12]

and GV3 (chromatin organized into a single clump). Nevertheless, detailed microscopic studies have revealed that chromatin in GV3 oocytes is located near the inactive nucleolus, resembling the SN configuration of mouse and human [9]. This is in accordance with the theory that karyosphere formation is a phylogenetically conserved process across the mammalian class and even beyond it.

Composition of the karyosphere and the inactive nucleolus inside it

With regard to the reported presence of a karyosphere in the late GV-stage oocytes of many animal species, the question arises about the composition of the enclosed inactive nucleolus (or "nucleolus-like body") and the associated chromatin regions forming the karyosphere. Cytochemical and immunocytochemical studies reveal that the interior of the "surrounded nucleolus" is rich at proteins, including typical nucleolar proteins involved in rRNA processing and ribosome biogenesis. It is positive also for RNA, but nature of this RNA is still a mystery, because *in situ* hybridization experiments with specific probes show low rRNA content [17]. The composition and rearrangement of condensed chromatin regions forming the karyosphere has been studied by fluorescent *in situ* hybridization. In early GV-stage oocytes before karyosphere formation (NSN configuration), probes for centromeric and pericentromeric DNA sequences label masses of chromatin (chromocenters) in different regions of the nucleus. These chromocenters often have more than two centromeric spots, indicating clustering of two or more chromosomes. In late GV oocytes with karyosphere, centromeric and pericentromeric sequences are located in its rim. Curiously, while the general level of chromatin condensation increases, pericentromeric heterochromatin seems to undergo partial de-

condensation from the NSN chromocenters to the SN perinucleolar rim, allowing it to spread around the nucleolus and encircle it completely. Meanwhile, nucleolar organizer region become condensed during the NSN to SN transition and move out of the nucleolus proper to join the karyosphere heterochromatin, a rearrangement which reflects their transcriptional silencing [4]. It seems that the layer of heterochromatin forming the karyosphere effectively isolates its interior: according to our observations, in late GV oocytes, nuclear envelope is no longer a barrier for cytoplasmic proteins and they can be detected inside the nucleus, but not inside the karyosphere [13].

Relationship between karyosphere formation and transcriptional silencing

The temporal correlation between karyosphere formation and cessation of transcription in the oocyte nucleus has been mentioned early by microscopic observations of oocytes allowed to incorporate labeled nucleotides [16]. In the mouse, NSN oocytes are transcriptionally active and synthesize all classes of RNA, while SN oocytes are characterized by global repression of transcription [10]. This raises the question whether the condensation of chromatin leading to karyosphere formation is a mechanism of transcriptional repression. However, detailed studies have shown that large-scale chromatin changes and global transcriptional silencing can be experimentally dissociated. For instance, in oocytes from nucleoplasmin-2 knockout mice, transcription is stopped even though karyosphere fails to form [6]. On the other hand, in oocytes from histone 3-lysine 4 methyltransferase (MLL2) conditional knockouts, transcription is not silenced even though karyosphere formation is successful [1]. These data suggest that there is unlikely to be a direct causal relationship between large-scale chromatin remodeling and transcriptional silencing; rather, these two processes might normally be controlled by common upstream factors, which are unfortunately still unknown.

Epigenetic events correlating with karyosphere formation

Attempts have been made to link the transcriptional silencing of late GV oocytes to epigenetic markers. In bovine oocytes, the down-regulation of transcription that accompanies even the early steps of chromatin condensation correlates with a substantial increase in global DNA methylation [10]. On the other hand, acetylated histones known to keep the chromatin in a transcriptionally permissive state do not disappear during the NSN to SN transition but are found associated with the condensing chromatin, including the karyosphere [19]. A study including immunolocalization of several modified histones associated with either activated or repressed state has found these epigenetic markers to follow chromatin movements during the NSN to SN transition and to aggregate in the karyosphere without distinction between active and repressive signals. The authors conclude that the germinal vesicle may have a specific histone modification landscape and the common rules of the histone epigenetic code known from somatic cells are not valid for the oocyte [4].

If karyosphere formation is not causally related to transcriptional silencing and shows no straightforward correlation with the epigenetic reprogramming of the oocyte genome, its function could be related to the next step of oocyte maturation. The germinal vesicle, even in the small eutherian oocytes, is so large that the subsequent assembly of all bivalents in a metaphase plate becomes problematic. It has been hypothesized that microfilaments, which in metaphase I organize around the meiotic spindle into a spin-

dle-like structure, keep the bivalents together in a limited volume [2]. However, while this process could play an auxiliary role, it is not indispensable for the alignment of bivalents in a metaphase plate, because disruption of microfilaments by cytochalasin does not prevent the formation of a normal metaphase I spindle [8]. Karyosphere formation, which includes condensation and clustering of oocyte chromosomes in a limited nuclear volume, is expected to facilitate their subsequent positioning in a metaphase plate and to reduce the chance of isolated bivalents remaining outside the meiotic spindle. Data in accordance with this view are provided by time-lapse imaging of chromatin-stained mouse oocytes, which shows a 12% reduction in the germinal vesicle area immediately before its breakdown [3].

Correlation of oocyte meiotic and developmental competence with karyosphere formation

Perhaps the most significant finding about the karyosphere of GV-stage mammalian oocytes is the correlation between its presence and the ability of the oocyte to resume meiosis, to reach metaphase II and, if fertilized, to develop beyond the first mitotic division of the zygote. In 2002, a study on oocytes isolated from mouse antral follicles showed that most cells without karyosphere (the NSN configulation) failed to resume meiosis. Only 15% of oocytes with this chromatin configuration reached metaphase II and, upon fertilization, none of the obtained zygotes progressed beyond the 2-cell stage. By contrast, 75% of oocytes with karyosphere (the SN configuration) matured to metaphase II and, when fertilized, 47% of them developed to 4-cell stage and 18% to blastocyst [20]. Later studies, using mouse oocytes as well as oocytes from other mammals, confirmed that meiotic competence (i.e. the ability of the oocyte to resume meiosis and to reach metaphase II) is acquired at the time when chromatin condensation starts, while developmental competence (i.e. the ability of the oocyte, if successfully matured and fertilized, to develop beyond the 2-cell stage) is acquired slightly before the chromatin reaches its highest level of condensation [9]. This striking difference in oocyte potential is most likely due to accumulation of important regulatory proteins and mRNAs for them during the NSN-to-SN transition, notably the transcription factor OCT4, which is a marker of pluripotency [19].

The reliability of the karyosphere as an indicator of the oocyte developmental potential has prompted some researchers to seek a method to select oocytes with karyosphere for use in assisted reproduction. There are already reports of such protocols in which oocytes are sorted according to their chromatin configuration, revealed by supravital staining with Hoechst 33342 [15]. Unfortunately, intercalating dyes greatly increase the incidence of frameshift mutations, which makes this approach unsuitable for use in assisted reproduction of valuable animals and especially of humans. Selection of oocytes with high developmental potential based on the presence of karyosphere may become possible with the eventual introduction of other, less invasive methods to assess the chromatin configuration.

Conclusions

Although the precise functions of the karyosphere and the molecular mechanisms of its formation remain to be elucidated, it should be regarded as one of the most important cell type-specific structures of the maturing oocyte. This is evident from the correlation between its presence and the acquisition of meiotic and developmental competence, as

well as its phylogenetic conservation in the animal kingdom. In assisted reproduction, where the quality of oocytes is of crucial importance, the use of the karyosphere as a marker of meiotic and developmental competence to select cells with better potential could improve the outcome. However, this requires development of new methodological approaches for non-invasive assessment of the oocyte chromatin configuration.

References

1. **Andreu-Vieyra, C. V., R. Chen, J. E. Agno, S. Glaser, K. Anastassiadis, A. F. Stewart, M. M. Matzuk.** MLL2 is required in oocytes for bulk histone 3 lysine 4 trimethylation and transcriptional silencing. – *PLoS Biol*., **8**, 2010, pii: e1000453.
2. **Azoury, J., K. W. Lee, V. Georget, P. Rassinier, B. Leader, M. H. Verlhac.** Spindle positioning in mouse oocytes relies on a dynamic meshwork of actin filaments. – *Curr. Biol*., **18**, 2008, 1514-1519.
3. **Belli, M., G. Vigone, V. Merico, C. A. Redi, S. Garagna, M. Zuccotti.** Time-lapse dynamics of the mouse oocyte chromatin organisation during meiotic resumption. – *Biomed. Res. Int*., 2014, 207357.
4. **Bonnet-Garnier, A., P. Feuerstein, M. Chebrout, R. Fleurot, H. U. Jan, P. Debey, N. Beaujean.** Genome organization and epigenetic marks in mouse germinal vesicle oocytes. – *Int. J. Dev. Biol*., **56**, 2012, 877-887.
5. **De La Fuente, R.** Chromatin modifications in the germinal vesicle (GV) of mammalian oocytes. – *Dev. Biol*., **292**, 2006, 1-12.
6. **De La Fuente, R., M. M. Viveiros, K. H. Burns, E. Y. Adashi, M. M. Matzuk, J. J. Eppig.** Major chromatin remodeling in the germinal vesicle (GV) of mammalian oocytes is dispensable for global transcriptional silencing but required for centromeric heterochromatin function. – *Dev. Biol*., **275**, 2004, 447-458.
7. **Gruzova, M. N., V. N. Parfenov.** Karyosphere in oogenesis and intranuclear morphogenesis. – *Int. Rev. Cytol*., **144**, 1993, 1-52.
8. **Liu, S., Y. Li, H. L. Feng, J. H. Yan, M. Li, S. Y. Ma, Z. J. Chen.** Dynamic modulation of cytoskeleton during in vitro maturation in human oocytes. – *Am. J. Obstet. Gynecol.*, **203**, 2010, 151.e1-7.
9. **Lodde, V., S. Modina, C. Galbusera, F. Franciosi, A. M. Luciano.** Large-scale chromatin remodeling in germinal vesicle bovine oocytes: Interplay with gap junction functionality and developmental competence. – *Mol. Reprod. Dev*., **74**, 2007, 740-749.
10. **Lodde, V., S. C. Modina, A. M. Luciano.** On the chromatin of the immature oocyte: from morphology to function and regulatory mechanisms mediated by follicular cells. – In: *The genome and its expression through the microscope: the legacy of Maria Gabriella Manfredi Romanini* (Eds. C. Pellicciari, F. De Bernardi, L. De Carli), vol. 80. Milan: Istituto Lombardo – *Accademia di Scienze e Lettere*, 2015, 47-65.
11. **Luciano, A. M., F. Franciosi, C. Dieci, V. Lodde.** Changes in large-scale chromatin structure and function during oogenesis: a journey in company with follicular cells. – *Anim. Reprod. Sci*., **149**, 2014, 3-10.
12. **Markova, M., V. Hadzhinesheva, R. Zhivkova, V. Nikolova, I. Chakarova, S. Delimitreva.** Rearrangements of oocyte cytoskeleton during mammalian oogenesis. – *Acta Morphol. Anthropol*., **23**, 2016, 145-148.
13. **Markova, M. D., V. P. Nikolova, I. V. Chakarova, R. S. Zhivkova, R. K. Dimitrov, S. M. Delimitreva.** Intermediate filament distribution patterns in maturing mouse oocytes and cumulus cells. – *BioCell*, **39**, 2015, 1-7.
14. **Mattson, B. A., D. F. Albertini.** Oogenesis: chromatin and microtubule dynamics during meiotic prophase. – *Mol. Reprod. Dev*., **25**, 1990, 374-383.
15. **Monti, M., C. A. Redi.** Isolation and Characterization of Mouse Antral Oocytes Based on Nucleolar Chromatin Organization. – *J. Vis. Exp*., 107, 2016, doi: 10.3791/53616.
16. **Parfenov, V., G. Potchukalina, L. Dudina, D. Kostyuchek, M. Gruzova.** Human antral follicles: oocyte nucleus and the karyosphere formation (electron microscopic and autoradiographic data). – *Gamete Res*., **22**, 1989, 219-231.

17. **Shishova, K. V., E. A. Lavrentyeva, J. W. Dobrucki, O. V. Zatsepina.** Nucleolus-like bodies of fully-grown mouse oocytes contain key nucleolar proteins but are impoverished for rRNA. – *Dev. Biol*., **397**, 2015, 267-281.
18. **Zuccotti, M., M. Bellone, F. Longo, C. A. Redi, S. Garagna.** Fully-mature antral mouse oocytes are transcriptionally silent but their heterochromatin maintains a transcriptional permissive histone acetylation profile. – *J. Assist. Reprod. Genet*., **28**, 2011, 1193-1196.
19. **Zuccotti, M., V. Merico, M. Bellone, F. Mulas, L. Sacchi, P. Rebuzzini, A. Prigione, C. A. Redi, R. Bellazzi, J. Adjaye, S. Garagna.** Gatekeeper of pluripotency: a common Oct4 transcriptional network operates in mouse eggs and embryonic stem cells. – *BMC Genomics*, **12**, 2011, 1-13.
20. **Zuccotti, M., R. H. Ponce, M. Boiani, S. Guizzardi, P. Govoni, R. Scandroglio, S. Garagna, C. A. Redi.** The analysis of chromatin organisation allows selection of mouse antral oocytes competent for development to blastocyst. – *Zygote*, **10**, 2002, 73-78.

Institute of Experimental Morphology, Pathology and Anthropology with Museum
Bulgarian Anatomical Society

Acta morphologica et anthropologica, 24 (1-2)
Sofia ● 2017

Anatomical Features of Maxillary Bone Related to Removable Prosthetics: Review

Dobromira Shopova[1*], *Tanya Bozhkova*[1],
Diyan Slavchev[1], *Spas Muletarov*[2]

[1] *Department of Prosthetic Dentistry, Faculty of Dental Medicine, Medical University-Plovdiv, Bulgaria*
[2] *Department of Anatomy, Histology and Embryology', Medical University-Plovdiv, Bulgaria*

[*]Corresponding author: e-mail: dent.shopova@gmail.com

The maxillary bone is placed centrally, within the facial cranium. As well as the aesthetic appearance, it is related to normal vital functions – eating, breathing and speaking. There are physiological changes in the jaws of the growing organism, which are influenced by the presence or absence of the teeth, parafunctions, and transference of the masticatory pressure. Anatomical features of the upper jaw are directly related to the prosthetic method of choice.

Key words: anatomy, maxilla, prosthetics

The upper jaw (maxilla) is connected rigidly to the hard palate (os palatinum) and they often are considered together because of their morphological and functional properties. The main characteristics of this complex include apertures, protuberances, bone junctions and the shape of the dental arch. The apertures include: foramen incisivum and foramina palatina minora. The presence and the degree of growth of torus palatinus can be classified by four forms: strongly convex, flat, convex in an anterior part and convex in a distal part [26]. Bone junctions are: sutura incisiva, sutura intraincisiva and sutura palatina transversa. The configuration of sutura palatina transversa is formed by three classical types: straight directed, forward directed and backwards directed [18]. The shape of the upper dental arch can be described like an ellipse, U-shaped, semicircular and also parabolic [27].

Bone structures in the mouth are covered with soft tissues. The mucosa on a prosthetic field can be defined in three main types: immovable, which covers the alveolar crests and hard palate; movable, which is placed on the cheeks and lips; and transitional – which is placed between them. This transitional mucosa is called sulcus gingivobuccalis. The physiological range of the prosthetic field is determined by the following anatomical structures: spina nasalis anterior, crista zygomaticoalveolaris, m. buccinators, m. orbicularis oris, m. incisivus labii superioris. In the distal area this range is placed

behind Tuber maxillae to the facies infratemporalis maxillae [29]. Tuber maxillae can be either strongly or weakly developed, retentive or non-retentive [28].

The composition of the fully healed edentulous ridge of the posterior maxilla was recently examined and was found to contain approximately 50% mineralized bone and 16% bone marrow.The marginal portion of the jaws almost consistently contained a cortical cap that was significantly thinner in the maxilla.The bone marrow occupied was close to 40% of the anterior maxilla, while the posterior maxilla comprised between 13-18%. The maxillary anterior region was discovered to be poor in lamellar bone but rich in bone marrow [16].

There are similar studies for quantitative evaluationmodule of elasticity, density and hardness in different anatomical regions.The aim of these investigations was to determine whether elastic properties and apparent density of bone differ in different anatomical regions of the maxilla and mandible. Additional analysis assessed how elastic properties and apparent density were related. Elastic modulus and hardness were measured using the nano-indentation technique. Elastic modulus and hardness were higher in the posterior maxilla than in the anterior regions; the reverse was true for apparent density. Posterior maxillary density was significantly the lowest [17].

Bone densitometry of the jaws was performed with a densitometer, and bone mineral density was calculated at three regions of the maxilla. Significant differences were found between the mean bone mineral density of each site when compared with the three other locations. The mean bone mineral density of the anterior maxilla was measured (mean = 0.55 g/cm^{-2}). The bone mineral density of the posterior maxilla was significantly the lowest (mean = 0.31 g/cm^{-2}; and the hard palate, mean = 0.45 g/cm^{-2}) [6].

Bone density can be measured byHounsfield units (HU). The Hounsfield unit scale is a linear transformation of the original linear attenuation coefficient measurement into one in which the radiodensity of distilled water, at standard pressure and temperature, is defined as zero Hounsfield units (HU), while the radiodensity of air at standard pressure and temperature is defined as 1000 HU [11].Cortical and cancellous bone density was measured at the interradicular areas at the alveolar and basal bone levels of the maxilla and mandible, and the data was subjected to statistical analysis for comparisons. The highest cortical bone density was observed between the second premolar and first molar at the alveolar bone level and between the first and second molars at the basal bone level in the maxilla. Maxillary tuberosity showed the least bone density [3].

Parka's investigation showed very similar results. The highest bone density in the maxilla was observed in the canine and premolar areas, and maxillary tuberosity showed the lowest bone density [21].

Sogo's study examined the bone densities of edentulous posterior maxillae by computed tomography (CT). The density was calculated in the range from 150 to 2,000 Hounsfield units (HU) and it was categorized according to Misch's classification.Misch (1988) described four bone densities found in the edentulous regions of the maxilla and the mandible based on macroscopic cortical and trabecular bone characteristics: D1 bone is primarily dense cortical bone; D2 bone has dense to thick porous cortical bone on the crest and coarse trabecular bone underneath; D3 bone has thinner porous cortical crest and fine trabecular bone within and D4 has almost no crestal cortical bone and fine trabecular bone composes almost all of the total volume of bone [12]. More than 80% of the edentulous posterior maxillae consisted of porous cortical crest or no cortical bone according to CT, although the bone densities varied amongst individuals [24].

Bone density, in Fanuscu's study, values based on the Hounsfield scale ranged from 186 to 389 HU, in the maxilla, anterior site being higher. 3-D morphometric analysis in microCT produced a range of values within anterior specimens being favorable: bone volume density (0.12-0.291), trabecular thickness (0.12-0.16 mm), trabecular

separation (0.46-0.82 mm), trabecular number (1.08-2.071/mm) and structural model index (0.29-1.27) [7].

Cortical thickness, density, elastic properties, and the direction of greatest stiffness were obtained in Peterson's study. Results showed that cortical bone in the alveolar region tended to be thicker, less dense, and less stiff. Cortical bone from the body of the maxilla was thinner, denser, and stiffer. Palatal cortical bone was intermediate in some features but overall was more similar to cortical bone from the alveolar region. The principal axes of stiffness varied regionally. The regions with the greatest consistency was the alveolar area and the frontomaxillary pillar, where the grain of the cortical bone was aligned vertically from the incisors to the medial external aspect of the orbit. Elastic properties in the human maxilla, especially the orientation of the principal axes of stiffness, were more variable than in the mandible [22].

Maxilla's resorption is centripetal and it decreases in its volume. Edentulous jaws are classified according their shape, type and degree of atrophy [29]. According to the shape of alveolar crests there are three basic and many transitional forms. The basic are ovoid-shape, pointed-shape and square-shape. The type of atrophy can be symmetrical and non-symmetrical, regular and irregular. The type of atrophy is heavily influenced by sequence of tooth loss, and by premature extraction [30]. The inclination of alveolar crests is important for retention of the dentures. According to inclination alveolar crest can be retentive, vertical and non-retentive [29].

Boyanov classified the degree of atrophy in three basic and one additional form. First grade complies to normal non-functional atrophy, alveolar crests are round and good developed. Second grade is due to senile or pathological atrophy, alveolar crests are smaller and are covered with immovable mucosa. Third grade is due to senile or pathological atrophy in advanced form, alveolar crests decrease their volume, the immovable mucosa is a narrow strip on the top of the crests. Additional grade represents heavy atrophy with almost disappeared alveolar crests [25]. Kurlyanskiy's classification grades the atrophy in three types (**Fig. 1**) [29].

Resorptive processes can be considered from the length of incisive canal, which is a different value in dentulous and edentulous maxillary bone. The Y-morphology canal was most frequently observed at 60% in the dentulous maxilla and 55% in the edentu-

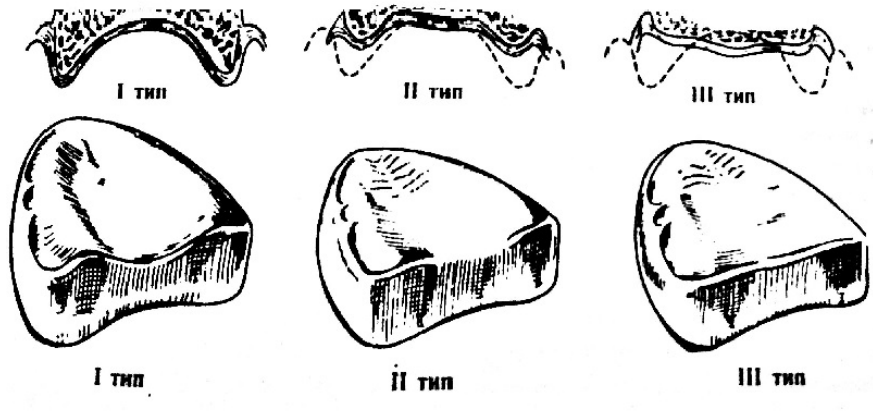

Fig. 1. Degrees of the atrophy according to Kurlyanskiy [4]

lous maxilla. Fukuda's study established mean length 10.75±1.70 mm in teeth presence, and 10.84±2.42 mm in teeth absence [8].

The purpose of Güncü's study was to identify the influence of gender and tooth loss on incisive canal characteristics and buccal bone dimensions in the anterior maxilla. Men had a significantly higher buccal bone dimension (length and width of the bone anterior to the canal) than women. Absence of teeth in the anterior maxilla decreased incisive canal length and buccal bone dimensions; however, the canal diameter remained unchanged [10].

In the literature there is little information for the connection between the residual height of the bone and its density. Monje identified a statistically significant, positive correlation between bone volumetric fraction and ridge height ($r = 0.417$, $p = 0.03$). A statistically significant negative correlation between trabecular pattern factor and ridge height was also found ($r = – 0.415$, $p = 0.03$) [19].

There are different investigations for evaluating the thickness of a facial alveolar bone in the frontal area. A thin bone contributes to risk of bone fenestration, dehiscence, and soft-tissue recession [9]. The thickness of a vestibular bone wall in edentulous maxilla is between 0.5 and 1 mm [14].

It has been suggested that a minimal width of 1-2 mm of buccal bone is necessary to maintain a stable vertical dimension of the alveolar crest. The mean width of the buccal and palatal bony walls was 1 and 1.2 mm, respectively ($p < 0.05$) [13]. In another survey it's ranged 1.0 to 1.3 mm because of the apparent fenestration occurrence (0 mm bone) within approximately 12% of teeth [20].

Edentulous maxillary first molar sites were analyzed on Cone Beam Computed Tomography. The alveolar ridge height (RH), widths at 1 and 3 mm from crest (RW1; RW3), and relative position of the bone crest (RR) were measured.Prevalence of patients with severe periodontal disease status was most frequent from 49.2% to 50.4%. The lower ridge heights were observed; 13.1% to 14%had RH < 2 mm, sites with both RH <8 mm and RW1 < 6 mm occurred at 59% to 68%. Gender and the adjacent teeth significantly affected RW [1].

To obtain successful treatment with complete dentures it is essential to appropriately plan the type of prosthesis (fixed or movable) and prosthetic design [15]. From the best available data, construction of technically correct dentures, a well-formed ridge and accuracy of jaw relations are also all positive indicators for success.There have been many attempts to relate the ridge form to prosthetic success. It is logical to assume that the better the alveolar ridge form is, the greater the chance of producing a stable, retentive denture with good support, which will be tolerated well by the patients. Patient negativity and a poorly formed alveolar ridges are both significant indicators for negative success rates. Other prognostic indicators have not been shown to be of significant value. There are afew patients who will never adapt to any conventional complete denture [5]. More failures are observed in the posterior maxilla, which is related with bone characteristics, local status and hygiene (smokers) [4].

Carlsson thinks that there is not strong evidence for an association between anatomical and technical prerequisites of a successful treatment with complete dentures, together, with the fact that psychological factors and personality are of great importance for the outcome of treatment [2].

Our investigation presents that the areas around Spina nasalis anterior and Tuber maxillaeare more conservative in the course of evolution and symmetrically changing. In the variable regions susceptible to evolutionary change are zones of canines, first and second premolars [23].

References

1. **Acharya, A., J. Hao, N. Mattheos, A. Chau, P. Shirke, N. P. Lang.** Residual ridge dimensions at edentulous maxillary first molar sites and periodontal bone loss among two ethnic cohorts seeking tooth replacement. – *Clin. Oral Implants Res*., **25**(12), 2014, 1386-1394.
2. **Carlsson, G. E.** Critical review of some dogmas in prosthodontics. – *J. Prosthodont. Res*., **53**(1),2009, 3-10.
3. **Chugh, T., S. V. Ganeshkar, A. V. Revankar, A. K. Jain.** Quantitative assessment of interradicular bone density in the maxilla and mandible: implications in clinical orthodontics. – *Prog. Orthod*., **14**(1), 2013, 38.
4. **Conrad, H. J., J. Jung, M. Barczak, S. Basu, W. J. Seong.** Retrospective cohort study of the predictors of implant failure in the posterior maxilla. – *Int. J. Oral Maxillofac.Implants*, **26**(1), 2011, 154-162.
5. **Critchlow, S. B., J. S. Ellis.** Prognostic indicators for conventional complete denture therapy: A review of the literature. – *J. Dent*., **38**(1), 2010, 2-9.
6. **Devlin, H., K. Horner, D. Ledgerton.** A comparison of maxillary and mandibular bone mineral densities. – *J. Prosthet. Dent*., **79**(3), 1998, 323-327.
7. **Fanuscu, M. I., T. L. Chang.** Three-dimensional morphometric analysis of human cadaver bone: Microstructural data from maxilla and mandible. – *Clin. Oral Implants Res*., **15**(2), 2004, 213-218.
8. **Fukuda, M., S. Matsunaga, K. Odaka, Y. Oomine, M. Kasahara, M. Yamamoto, et al.** Three-dimensional analysis of incisive canals in human dentulous and edentulous maxillary bones. – *Int. J. Implant Dent*., **1**(1), 2015, 12.
9. **Ghassemian, M., H. Nowzari, C. Lajolo, F. Verdugo, T. Pirronti.** The Thickness of Facial Alveolar Bone Overlying Healthy Maxillary Anterior Teeth. – *J. Periodontol*., **83**(2), 2012, 187-197.
10. **Güncü, G. N., Y. D. Yildirim, H. G. Yilmaz, P. Galindo-Moreno, M. Velasco-Torres, A. Hezaimi et al.** Is there a gender difference in anatomic features of incisive canal and maxillary environmental bone? – *Clin. Oral Implants Res*., **24**(9), 2013, 1023-1026.
11. https://en.wikipedia.org/wiki/Hounsfield_scale.
12. http://pocketdentistry.com/bone-density-for-dental-implants/.
13. **Huynh-Ba, G., B. E. Pjetursson, M. Sanz, D. Cecchinato, J. Ferrus, J. Lindhe et al.** Analysis of the socket bone wall dimensions in the upper maxilla in relation to immediate implant placement. – *Clin. Oral Implants Res*., **21**(1), 2010, 37-42.
14. **Januário, A. L., W. R. Duarte, M. Barriviera, J. C. Mesti, M. G. Araújo.** Dimension of the facial bone wall in the anterior maxilla: a cone-beam computed tomography study. – *Clin. Oral Implants Res.*, **22**(10), 2011, 1168-1171.
15. **Jivraj, S., W. Chee, P. Corrado.** Treatment planning of the edentulous maxilla. – *Br. Dent. J*., **201**(5), 2006, 261-279, quiz 304.
16. **Lindhe,J., E. Bressan, D. Cecchinato, E. Corrá, M. Toia, B. Liljenberg.** Bone tissue in different parts of the edentulous maxilla and mandible. – *Clin. Oral Implants Res*., **24**(4), 2013, 372-377.
17. **Manuscript, A.** Maxilla and Mandible. – *Int. J. Oral Maxillofac Surg*., **38**(10), 2010, 1088-1093.
18. **Martin, R., K. Saller.** Textbook of anthropology. Stuttgart, Germany: Fischer, 1957.
19. **Monje, A., F. Monje, R. González-García, F. Suarez, P. Galindo-Moreno, A. García-Nogales et al.** Influence of Atrophic Posterior Maxilla Ridge Height on Bone Density and Microarchitecture. – *Clin. Implant Dent. Relat. Res.*, **17**(1), 2015, 111-119.
20. **Nowzari, H., S. Molayem, C. Chiu, S. K. Rich.** Cone Beam Computed Tomographic Measurement of Maxillary Central Incisors to Determine Prevalence of Facial Alveolar Bone Width ≥2 mm. – *Clin. Implant Dent.*, **14**(4), 2012, 595-602.
21. **Parka, H. S., Y. J. Leeb, S. H. Jeongc, T. G. Kwond.** Density of the alveolar and basal bones of the maxilla and the mandible. – *Am. J. Orthod. Dentofac. Orthop*., **133**(1), 2008, 30-37.
22. **Peterson, J., Q. Wang, P. C. Dechow.** Material properties of the dentate maxilla. – *Anat. Rec. - Part A. Discov. Mol. Cell Evol. Biol*., **288**(9), 2006, 962–972.
23. **Shopova, D., T. Bozhkova, D. Slavchev, S. Muletarov, Z. Ivanova, E. Bozhikova.** Evaluation of maxillary bone dimensions in specific areas for removable dentures. – *J. of IMAB*, **23**(2), 2017, 1527-1531.

24. **Sogo, M., K. Ikebe, T. C. Yang, M. Wada, Y. Maeda.** Assessment of Bone Density in the Posterior Maxilla Based on Hounsfield Units to Enhance the Initial Stability of Implants. – *Clin. Implant Dent. Relat. Res*., **14**(1), 2012, 183-187.
25. **Боянов, Б., Б. Николов, В. Желязков, Ч. Ликов, Н. Попов.** *Клиника на ортопедичната стоматология*: *Учебник за студенти по стоматология*. (Ред. Б. Боянов). София: Медицина и физкултура, 1980, 238-245.
26. **Зубов, А.** *Одонтология: Методика антропологических исследований*. Изд-во Наука, 1968, 48.
27. **Йорданов, Й., К. Узунов, Х. Факих.** *Наръчник по анатомия и антропология за стоматолози*. София: Артграф, 2012, 233-234.
28. **Пеев,Т., А. Филчев.** *Клиника на Протетичната дентална медицина*. София: Еко Принт.2008, 234-235.
29. **Попов, Н.** *Клиника на протетичната стоматология*. София: Медицина и физкултура, 1999, 206-209.
30. **Славчев, Д.** *Пресъздаване дъгата на горна цяла протеза след анализ на фронтална телерентгенография*. Дисертация за присъждане на ОНС „Доктор“, Пловдив, 2005, 127.

Institute of Experimental Morphology, Pathology and Anthropology with Museum
Bulgarian Anatomical Society

Acta morphologica et anthropologica, 24 (1-2)
Sofia ● 2017

Ten Years National Anthropological Museum: Review

Atanas Katsarov[*]*, Diana Zlatkova, Maria Christova*

Institute of Experimental Morphology, Pathology and Anthropology with Museum, Bulgarian Academy of Sciences, Sofia, Bulgaria

[*]Corresponding author. e-mail: zanasko@gmail.com

National Anthropological Museum is a scientific, educational and cultural institution that presented anthropological studies of the Bulgarian population and the people who inhabited the Bulgarian lands in the past. These results known to a limited circle of specialists were not available to the general public. The creation of the permanent exhibition and the subsequent opening of the National Anthropological Museum on March 21 2007, contributing to the promotion of anthropological knowledge. Amid the data for the historic and cultural development and religious beliefs in different eras are presented physical types of people, knowledge about illnesses and injuries that have left marks on the bones, and medical and ritual influence on them. The museum is the youngest in the structure of BAS and it is an integral part of the Institute of Experimental Morphology, Pathology and Anthropology.

On March 21 2017 is the tenth anniversary of the opening of the permanent exhibition of the National Anthropological Museum. Designed to promote anthropological research in Bulgaria, the museum has become a center of attraction for those seeking answers to questions such as "Who are we?", "Where did we come from" and "What happens to us?"

The beginning of the museum is associated with the creation of a traveling exhibition "Man in the Past" at the Institute of Experimental Morphology and Anthropology (now the Institute of Experimental Morphology, Pathology and Anthropology), BAS realized by corresponding member of BAS prof. Yordan Yordanov. The interest shown by various groups of Bulgarian society as well by foreign experts and visitors of Bulgaria is a reason to proceed with the establishment of the National Anthropological Museum as a separate structure to IEMPAM, BAS.

The museum exposition is built in compliance with the two main principles in museology: the thematic and the chronological. At the same time it is in connection to the main exposition material - human bone remains found during archaeological excavations of necropolises, shrines, temples and settlements from the corresponding historical periods studied in the territory of modern Bulgaria [1].

Since its opening in 2007, ten years already, a team at the National Anthropological Museum, has been working in several directions. The first goal has been to make

Fig. 1. Book of impressions, responses and recommendations

the museum more accessible and attractive to visitors. The efforts in this direction can clearly be seen by those reflected in the "Book of impressions, responses and recommendations" (**Fig. 1**). This is a stimulus, necessary for the team to continue in the future in the promotion of anthropology as a science and of the National Anthropological Museum to the public as scientific, cultural and educational center.

In parallel with the permanent exhibition the museum realizes temporary exhibitions aimed at attracting wide public and promoting the possibilities of anthropology. Such exhibitions are *The monastery of Mostich* with guest professor Kazimir Popkonstantinov (2009), *Prominent Bulgarian anthropologists. Kadanov and Balan* (2010), *Modern Anthropology* (2014), and the latest dedicated to the tenth anniversary of the opening of the museum - *Anthropology in Bulgaria* and many others.

European *Night of Museums*, was born in France and became a tradition in Bulgaria, has become awaited event of the museum public. Despite its tender age and in competition with the leading museums in the capital, the National Anthropological Museum managed to establish itself as an attractive place for "The Night". The events which were organized in cooperation with scientists from the Department Anthropology and Anatomy of IEMPAM at BAS became desirable and sought in these ten years. Diverse program and submitted interesting facts and processes in the field of anthropology attract the attention of a large audience, and the established traditions of anthropological measurements have become an anticipated event in Night of Museums (**Fig. 2**).

In 2016, with the partial financing by the Ministry of Culture, National Anthropological Museum implemented a project with an educational focus "Funeral practices in our lands from Prehistory to the Middle Ages", including a temporary exhibition. This initiative has created new opportunities for collaboration with other museums and universities by presenting their material findings and research activities in the exhibition. Its main purpose is to acquaint the general public with the funeral practices from different historical eras and the significance of scientific research and analysis, as well as the promotion of results of the studies. The interdisciplinary approach set out in the project, allow to outline clearly the important components in the study of human – anthropo-

Fig. 2. Opening ceremony of the Night of Museums

logy and archeology. By visualizing the different burial practices from prehistory to the Middle Ages, the changes in our lands during the historical process – ethnic, religious, social stratification are illustrated. The educational program included in the project as a module to the temporary exhibition allowed the creation of sustainable product combining social and creative activities aimed at the promotion of anthropology as a science, on the one hand, and on the other, the inclusion of this type of museum in support of interactive learning in museums and schools. The exhibition caused serious interest among both the ordinary visitors and the specialized audiences. The inclusion of training modules proved to be the winning model to attract teenage audience, which wants to watch, co-experience, to participate in the process of acquiring knowledge and skills and to be widely informed.

Over the years, through good cooperation with various educational institutions (schools, universities), the National Anthropological Museum has become an educational center where the knowledge of history, biology and art are completed with the new knowledge in anthropology. This is the second major direction of development in which the museum team focuses its efforts. The museum lessons are combined with interactive sessions designed to engage the learner in the process of acquiring knowledge. This is possible thanks to the available copies of original exhibits and the good equipment, allowing various demonstrations and screenings of specially selected films. In interaction with schools through museum lessons and practical activities, the museum has the following targets:

– formation of permanent interest among youngsters to the museum as a source of knowledge in biology, history; anthropology;

– widening the knowledge of the material culture of different eras by studying the exposition;

– to stimulate analytical thinking and creative imagination.

The main museum educational programs conducted in the museum are:

1. Practical exercise: “The human body”.

The program is designed for students from grade 5th to 11th. Activities pass through clearly familiarizing students with the human anatomy on the model of the skeleton.

Conducting these exercises in an informal environment, such as the museum, the students more easily and affordable acquire knowledge about:

– What does the human body represent?
– How does it operate?
– What are the key elements of the human body?
– What is the bone?
– How are reflected injuries upon us?

2. Practical exercise: "Man and his environment" .

The program is designed for students of different ages and is bound to learn from these historical periods - Antiquity, Middle Ages, Renaissance and so on. For each historical period has developed its own terms of reference, consistent with the exhibition resources of NAM, which include:

– Information on particular individual including: sex, age, physical characteristics, ethnicity;
– Information on diseases and applied medical practices;
– Information on the applied specific ritualistic effects;
– Information on the funeral rites for the period.

In its work to attract new audiences National Anthropological Museum organizes lectures titled "Lesson from the Past" aimed at secondary school students. The cycle of lectures and exercises are based on educational programs for students in prehistory, medieval history and modern times. The smooth introduction of these periods contributes to the chronological order of exposure. Representing the past through the dynamics of societies and the world as well as people's perceptions of them, this course lectures reveals the main features of the past and modern eras. The emphasis in conducting "Lesson from the Past" is on the students to gain knowledge about basic historical problems and processes to master skills that allow them to orient in the huge flow of information that will help them in the process of building their own positions [2]

Since its inception in the spring of 2007 until now the National Anthropological Museum has passed a long way in becoming recognizable to the general public, but its development does not stop here. In the plans for the future of the museum stays the creation of a National Ossuary as an integral part of it. The purpose of this unique for Bulgaria repository is to preserve human bone remains of generations of people who lived in the Bulgarian lands from ancient times to the present day. The accumulated until now material and the findings from the upcoming archaeological studies will be subjected to specialized research. It includes systematization of data objects and periods and interdisciplinary research of the structure.

If necessary human bone remains will be preserved and restored. They will be stored for subsequent work of all Bulgarian and foreign experts dealing with anthropological issues. The provision, collection and storage of human bone remains from throughout the country in the National Ossuary have to be regulated by legislation and coordination with the institutes of the Academy and museum system in the country.

References

1. **Yordanov, Y., Br. Dimitrova.** Anthropological museum – concept, principles and implementation. – In: *The modern museum - models for adaptation*, 2003, 85-90.
2. **Mitova, D.** National Anthropological Museum – Lesson at museum. – In: *From regional to national*, 2010, 486-490.

Guidelines for Authors

Acta morphologica et anthropologica is an open access peer review journal and publishes original articles, short communications, reviews, letters to the Editors. The aim of the journal is to provide a forum for cytological, histological, anatomical and anthropological research community in life sciences, including cell biology, immunobiology, pathology, neurobiology, environmental and toxicological research, reproductive biology, pharmacology, physical development and medical anthropology; paleoanthropology, anatomy, paleoanatomy, etc.

Contact details and submission

Manuscripts should be in English with total length not exceeding 10 standard pages, line-spacing 1.5, justified with 2.5 cm margins. The authors are advised to use Times New Roman, 12 pt throughout the text. Pages should be numbered at the bottom right corner of the page. Manuscript submission is electronic only. The manuscripts should be sent to**: iempam@bas.bg.**

All correspondence, including notification for Editor's decision, requests for revision, is sent by e-mail. After acceptance of the manuscript a hard copy should be sent to Editorial Office address:

Institute of Experimental Morphology, Pathology and Anthropology with Museum
Bulgarian Academy of Sciences
Editorial Office of Acta morphologica et anthropologica
Acad. Georgi Bonchev Str., Bl. 25
1113 Sofia, Bulgaria

Article structure

The article should be arranged under the following headings: Introduction, Materials and Methods, Results, Discussion, Conclusion, Acknowledgements and References.

Title page – includes:

- **Title** – concise and informative;
- **Author(s)' names and affiliations** – indicate the given name(s) and family name(s) of all authors. Present the authors' affiliation addresses below the names. Indicate all affiliations with a lower-case superscript after the author's name and in front of the appropriate address. Provide the full postal address information for each affiliation, including the country name.
- **Corresponding author** – clearly indicate who will handle the correspondence for refereeing, publication and post-publication. An e-mail should be provided.
- **Abstract** – state briefly the aim of the work, the principal results and major conclusions and should not exceed 150 words. References and uncommon, or non-standard abbreviations should be avoided.
- **Key words** – provide up to 5 key words. Avoid general, plural and multiple concepts. The key words will be used for indexing purposes.

Introduction – state the objectives of the work and provide an adequate background, avoiding a detailed literature survey or summary of the results.

Materials and Methods – provide sufficient detail to allow the work to be reproduced. Methods already published should be indicated as a reference: only relevant modifications should be described.

Results – results should be clear and concise.

Discussion – should explore the significance of the results in the work, not repeat them. A combined *Results and Discussion* section is often appropriate. Avoid extensive citation and discussion of published literature.

Conclusions – the main conclusions of the study should be presented in a short section.

Acknowledgements – list here those individuals who provided help during the research and the funding sources.

Units – please use the International System of Units (SI).

Math formulae – please submit math equations as editable text, not as images.

Electronic artwork – number the tables and illustrations according to their sequence in the text. Provide captions for them on a separate page at the end of the manuscript. The proper place of each figure in the text should be indicated in the left margin of the corresponding page. **All illustrations (photos, graphs and diagrams)** should be referred to as "figures" and given in abbreviation "Fig.", and numbered in Arabic numerals in order of its mentioning in the manuscript. They should be provided in grayscale as JPEG or TIFF format, minimum 300 dpi. The illustrations should be submitted as separate files.

References – they should be listed in alphabetical order, indicated in the text by giving the corresponding numbers in parentheses. The "References" should be typed on a separate sheet. The names of authors should be arranged alphabetically according to family names, first the articles in Roman alphabet, followed by the articles in Cyrillic alphabet. In the reference list titles of works, published in languages with non-Latin alphabet, should be transliterated, original language must be indicated at the end of reference (e.g., [in Chinese, with English summary]). Articles should include the name(s) of author(s), followed by the full title of the article or book cited, the standard abbreviation of the journal (according to British Union Catalogue), the volume number, the year of publication and the pages cited, for books - the city of publication and publisher. In case of more than one author, the initials for the second, third, etc. authors precede their family names.

For articles: **Tuohy, V. K., Z. Lu, R. A. Sobel, R. A. Laursen, M. B. Lees.** A synthetic peptide from myelin proteolipid protein induces experimental allergic encephalomyelitis. – *J. Immunol.*, 141, 1988, 1126-1130.

For books: **Norton, W. T., W. Cammer.** Isolation and characterization of myelin. – In: Myelin (Ed. P. Morell), New York, Plenum Press, 1984, 147-180.

Page charges

Manuscript publication is free of charges.

Ethics in publishing

Before sending the manuscript the authors must make sure that it meets the Ethical guidelines for journal publication of Acta morphologica et anthropologica.

Human and animal rights

If the work involves the use of human subjects, the authors should ensure that work has been carried out in accordance with *The Code of Ethics of the World Medical Association* (Declaration of Helsinski). The authors should include a statement in the manuscript that informed consent was obtained for experimentation with human subjects. The privacy rights of human subjects must always be observed.

All animal experiments should comply with the *ARRIVE guidelines* and should be carried out in accordance with the U.K. Animals (Scientific procedures) Act, 1986 and the associated guidelines *EU Directive 2010/63/EU* for animal experiments, or the National Institutes of Health guide for the care and use of Laboratory animals (NIH Publications No. 8023, revised 1978) and the authors should clearly indicate in the manuscript that such guidelines have been followed.

Submission declaration

Submission of the manuscript implies that the work described has not been published previously, is not considered under publication elsewhere, that its publication is approved by all authors, and that if accepted, it will not be published elsewhere in the same form, in English or in any other language, including electronically, without the informed consent of the copyright-holder.

Contributors

The statement that all authors approve the final article should be included in the disclosure.

Copyright

Upon acceptance of an article, the authors will be asked to complete a "Journal Publishing Agreement". An e-mail will be sent to the corresponding author with the Journal Publishing Agreement Form or a link to the online version of this agreement.

Peer review

This journal operates a single blind review process. All contributions will be initially assessed by the Editor for suitability for the journal. All suitable papers are then sent to two independent expert reviewers to assess the scientific quality of the paper. The Editor is responsible for the final decision regarding acceptance or rejection of articles.

After acceptance

Proof correction

The corresponding author will receive proofs by e-mail in PDF format and will be requested to return it with any corrections within a week.

Offprints

The journal provides free access to all papers in each volume that can be downloaded from the following website: http://www.iempam.bas.bg/journals/acta.html

ISSN 1311-8773 (print)
ISSN 2535-0811 (online)